A STUDY OF MICROSTRIP TRANSMISSION LINES AND DISCONTINUITIES AT X-BAND

by

PETER RAYMOND DOUGLAS SCOTT

—·—

Ph.D. Thesis

University of Southampton

1974

*

CONTENTS

ABSTRACT

FACULTY OF SCIENCE

DEPARTMENT OF ELECTRONICS

Doctor of Philosophy

A STUDY OF MICROSTRIP TRANSMISSION LINES AND DISCONTINUITIES AT X-BAND

BY

Peter Raymond Douglas Scott

The problems of making accurate measurements on microstrip lines, and of observing the behaviour of discontinuities in microstrip are considered. The development of a microstrip standing wave indicator is described, but experiment showed that this instrument did not allow voltage standing wave ratio to be measured to a sufficiently high degree of accuracy owing to, among other things, substrate quality. The standing wave indicator was, however, used to make accurate measurements of wavelength.

The other measurement technique described is the use of coaxial probes above the substrate as a means of coupling to a microstrip resonator. The merits and demerits of this method are discussed, and experiments on line and ring resonators are described; line resonators were utilised in the study of losses, including radiation loss from an open-circuit, and of open-circuit end effect, and ring resonators primarily in the study of microstrip discontinuities. Results are given for the effect of a mitre on a right-angle corner in microstrip, and of an abrupt step in width of the top conductor.

The work is mainly concerned with standard microstrip lines on alumina substrates, but brief mention is also made of slot line and coupled microstrip lines. Measurement was confined to X-band frequencies.

Acknowledgement

The author is indebted to Mr. R. D. Stewart, who supervised the project and was a continual source of guidance and encouragement.

Thanks are extended to Mr. A. Purdy and the technicians responsible for the microstrip fabrication facility, to Mr. M. Carrington and the workshop staff who constructed much of the equipment, to Mrs J. Wright-Green who typed this thesis, and to the many members of the Department of Electronics and of the University who were of assistance in a multitude of ways.

The project was supported financially by the Admiralty Surface Weapons Establishment at Portsmouth, and the author is grateful for his financial support on the contract. Close liaison was maintained with Mr. E. Denison and Mr. J. Spilling of A. S. W. E., whose experience in the field of microstrip integrated circuits was of considerable value.

PRDS

January 1973

LIST OF FIGURES

LIST OF SYMBOLS

a	ground plane spacing in balanced stripline
b	normalised susceptance
B	susceptance; magnetic flux density; Bel
C'	capacitance per unit length of a TEM line
C_x	excess capacitance at an unmatched right angle corner
D	displacement
E	electric field
f	frequency
g	coupling coefficient of probes in resonator measurements
G'	conductance per unit length
h	height of dielectric in microstrip line
H	magnetic field; Henry
I	inductance at abrupt impedance step
J	Joule; current density
k	wave number
L	geometric length of microstrip line
L'	electrical length of microstrip line
m	depth of mitre at right angle corner (%); metre
M	number of wavelengths on a ring at resonance
N	number of half-wavelengths on a line at resonance
p	undisturbed width of microstrip substrate
P	Poyntingvector; power density
q	width of section of infinite parallel plate waveguide
Q	Q factor
Q_c	Q factor associated with conductor and dielectric losses
Q_m	measured Q factor
Q_o	unloaded Q factor (in absence of coupling probes)

Q_r Q factor associated with radiation loss

r height of parallel plate waveguide

R' resistance per unit length of line

R_s surface resistivity.

s separation of parallel coupled microstrip lines

S length of one side of square ring resonator (measured to inside corner); Siemen

t thickness of top microstrip conductor; time

T transmitted power; reference planes

u effective length of right angle corner

U energy stored in electromagnetic fields

v velocity of TEM propagation

v_g group velocity

v_o velocity in free space, = 2.9979×10^8 m/sec.

v_p phase velocity

w width of microstrip line

W watt

W_{eff} effective width of parallel-plate microstrip model

x co-ordinate direction

X reactance

X'' normalised reactance

y co-ordinate direction

Y admittance

Y_o characteristic admittance

z co-ordinate direction

Z_o characteristic impedance

α	line attenuation
α_c	line attenuation due solely to conductor loss
α_d	line attenuation due solely to dielectric loss
β	phase constant, $= 2\pi/\lambda$
γ	propagation coefficient, $=\alpha + j\beta$
Γ	reflection coefficient of taper
δ	skin depth; $\tan^{-1}(\varepsilon''/\varepsilon')$
$\Delta\ell$	end correction at open circuit
ΔF	equivalent width of fringing field at corner
ε	permittivity (dielectric constant), $= \varepsilon_o\varepsilon_r$
ε'	real part of complex relative permittivity
ε''	imaginary part of complex relative permittivity
ε_{eff}	effective permittivity
ε_o	permittivity of free space, $= 8.854 \times 10^{-12}$ Fm^{-1}
ε_r	relative permittivity
η	intrinsic impedance
θ	electrical length of a structure
λ	wavelength
λ_g	microstrip wavelength
λ_o	wavelength in free space
μ	permeability, $= \mu_o\mu_r$
μ_o	permeability of free space, $= 4\pi \times 10^{-7}$
μ_r	relative permeability
ρ	reflection coefficient
σ	conductivity
ω	frequency in radians, $= 2\pi f$
Ω	ohms

1. INTRODUCTION

Guided transmission of electromagnetic waves at microwave frequencies has conventionally been achieved by means of either coaxial line or waveguide. The second World War saw many advances in the field of microwave electronics, and one of these was the development of planar transmission lines consisting of dielectric and conducting strips in some form of sandwich structure.[1] Immediate applications of these lines were not forthcoming, but in the years after the war some of the advantages of planar lines came to be recognised. The greatest advantage was their ease of manufacture in both the prototype and production stages, compared to the complex machining operations required in the manufacture of coaxial or waveguide components. In addition planar lines offered broadband characteristics approaching those of coaxial line. In the early 1950's there was a good deal of work done on planar lines and a number of different configurations evolved; the configuration that proved most successful was the triplate form of balanced stripline, with polystyrene, glass fibre or later PTFE as the dielectric. Components such as circulators and directional couplers using stripline became available commercially, but further development was held back by the relatively high losses of planar lines, and by the difficulty of making a suitable transition from the existing power sources (e.g. the Klystron).

It was some years before progress in other fields of technology reached a stage where the potentialities of planar lines could be fully exploited. Two factors were of particular importance: one was the development of semiconductor devices capable of operating at microwave

frequencies, and the other was the high permittivity, low loss dielectric materials which became available, and which allowed the open forms of planar line, hitherto neglected owing to high radiation loss, to be employed. The concept of a microwave integrated circuit (M.I.C.) now became a reality. Immediate applications existed for M.I.C's in military and aerospace systems - one such application being phased array radar - which required the mass-production of circuits. As a result the microstrip form of planar line came to the fore, since microstrip is one of the simplest forms of line to manufacture; it also permits semiconductor devices to be easily mounted on the line. To date most M.I.C's have been hybrid in nature; monolithic M.I.C's are presently held back by technological problems, but in any case do not offer the same flexibility as do hybrid circuits.

This project was instigated in 1969 when a number of M.I.C's were on the market, but when in spite of the sophistication of some of these circuits there was very little information on the basic properties of the line or on common discontinuities. One reason for this dearth was the aforementioned ease of manufacture of microstrip circuits, which made it a simple matter to use 'cut and try' techniques at the design stage in order to achieve the desired performance. The broad aim of the project was to investigate those properties of microstrip relating to the needs of the circuit designer, and to attempt to provide information on the behaviour of discontinuities in the region of X-band. There was no intention to fabricate complete circuits or components, although an awareness of the problem in so doing was naturally important.

For microwave circuit design in any transmission system the impedance, attenuation factor and phase constant of the line are required, together

with their behaviour over the frequency band in question. For microstrip, theoretical predictions by Wheeler[2] for line impedance had been verified experimentally by a number of workers[3,4] and could be relied upon. It had been found however that typical microstrip lines exhibited measurable dispersion at X-band[5] and that calculations on the basis of Wheeler's work increasingly over-estimated the phase velocity as the frequency increased. At the time there was very little published experimental information as to the extent of this effect, and it was intended to investigate the topic further, as precise knowledge of wavelength is vital in circuit design. Precise knowledge of the attenuation factor is of less importance, and some theoretical work on losses in microstrip had been published, together with a large number of experimental results[6] which it was intended to duplicate and verify.

The types of discontinuity encountered in microstrip circuit design are the counterparts of those that occur in any high-frequency line: the open- and short-circuit terminations, for which the position of the electrical defining plane must be accurately known in order to design stubs of exact electrical length; the change in impedance, realised in microstrip by an abrupt step in width in the centre conductor; and the matched right angle corner - an alternative to circular bends which leads to more compact, rectilinear circuitry. In order to set about measuring any of these discontinuities it was necessary to devise a measurement technique which would allow their effect to be observed. All existing techniques were based on measurements in coaxial line or waveguide connected to the microstrip circuit via some form of transition, but this transition was the source of reflected signals which masked any small reflections from the microstrip discontinuity.

The solution was to make measurements on the substrate itself rather than via a transition, and experiments to this end are described in Sections 5, 6, and 7. Before this, however, consideration is given to the technology of microstrip (Section 3) and to the physical properties of microstrip lines (Sections 2 and 4).

Note 1

There is still a lack of standardisation in the nomenclature of planar lines, and therefore the definitions used in this report are given below, with reference to Figure 1.

Microstrip is the structure shown in Figure 1(a) - a dielectric slab supporting a narrow conducting strip on top and with a wide ground plane: this structure is occasionally referred to as standard microstrip to differentiate it from the embedded microstrip of Figure 1(b). The triplate lines (c) and (d) are referred to as dielectric supported stripline and balanced stripline respectively. The structure in Figure 1(e) is slot line and that in (f) coplanar waveguide.

Note 2

On graphs showing experimental results, the following convention is adopted: a curve fitted through a set of experimental points is shown by a broken line; a theoretical curve is shown by a solid line.

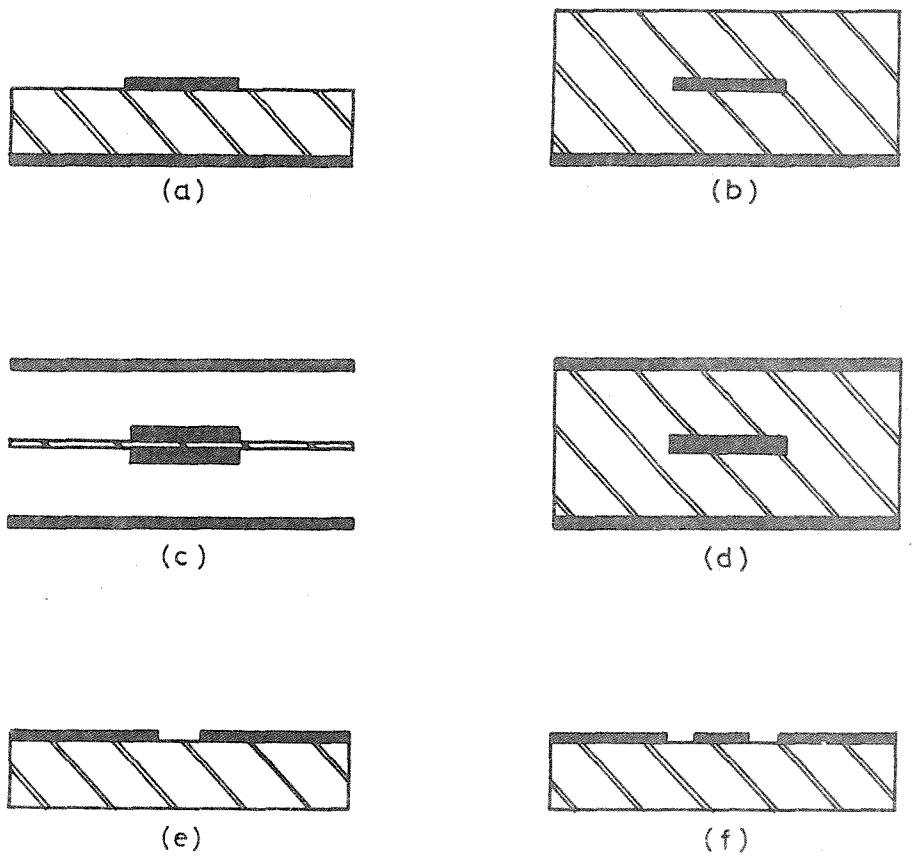

Figure 1. PLANAR TRANSMISSION LINES

(a) Standard microstrip.

(b) Embedded Microstrip.

(c) Dielectric supported stripline.

(d) Balanced stripline.

(e) Slot line.

(f) Coplanar waveguide.

2. PROPAGATION IN MICROSTRIP

2.1 Basic electromagnetic theory

Electromagnetic wave propagation is described by Maxwell's equations, and for a wave travelling through a perfect dielectric of permittivity ε and permeability μ the wave equations are

$$\nabla^2 \bar{E} = \varepsilon\mu \frac{\partial^2 \bar{E}}{\partial t^2} \tag{1}$$

and

$$\nabla^2 \bar{H} = \varepsilon\mu \frac{\partial^2 \bar{H}}{\partial t^2} \tag{2}$$

A uniform plane wave has no longitudinal (z) field components, and the transverse field components can be taken to have a sinusoidal variation with z without loss of generality. Equation 1 now has a solution of the form

$$E_x = E_1 e^{j\omega(t - \frac{z}{v})} + E_2 e^{j\omega(t + \frac{z}{v})} \tag{3}$$

where v is the velocity of propagation of the wave and is equal to $(\varepsilon\mu)^{-\frac{1}{2}}$. This solution implies waves travelling in the positive and negative directions, and similar solutions exist for E_y, H_x, H_y.

The intrinsic impedance η of the medium is given by

$$\eta = (\mu/\varepsilon)^{\frac{1}{2}} \tag{4}$$

and it relates the transverse electric and magnetic field components:

$$\frac{E_x^{\pm}}{H_y^{\pm}} = -\frac{E_y^{\pm}}{H_x^{\pm}} = \pm\eta \tag{5}$$

If the dielectric is not perfect and supports a conduction current, then Maxwell's equations are

$$\nabla \times \bar{E} = -\frac{\partial \bar{B}}{\partial t} = -j\omega\mu\ \bar{H}\ e^{j\omega t} \tag{6}$$

$$\nabla \times \bar{H} = \frac{\partial \bar{D}}{\partial t} + \bar{J} = (\sigma + j\omega\varepsilon)\bar{E}\ e^{j\omega t} = j\omega\varepsilon\ (1 + \sigma/j\omega\varepsilon)\bar{E}\ e^{j\omega t} \tag{7}$$

and equation 1 becomes

$$\nabla^2 \bar{E} = \mu\varepsilon\ (1 + \sigma/j\omega\varepsilon)\frac{\partial^2 \bar{E}}{\partial t^2} \tag{8}$$

A solution to this equation is

$$E = E_1\ e^{-\gamma z} + E_2\ e^{+\gamma z} \qquad (e^{j\omega t} \text{ omitted}) \tag{9}$$

where $\gamma = \alpha + j\beta = j\omega \left[\mu\varepsilon\ (1 + \sigma/j\omega\varepsilon) \right]^{\frac{1}{2}}$ (10)

Thus $\alpha = \omega \left[\frac{\mu\varepsilon}{2} \{(1 + \sigma^2/\omega^2\varepsilon^2)^{\frac{1}{2}} - 1\} \right]^{\frac{1}{2}}$ (11)

$\beta = \omega \left[\frac{\mu\varepsilon}{2} \{(1 + \sigma^2/\omega^2\varepsilon^2)^{\frac{1}{2}} + 1\} \right]^{\frac{1}{2}}$ (12)

The new dielectric constant $(1 + \sigma/j\omega\varepsilon)\varepsilon$ can be written

$$(\varepsilon' - j\varepsilon'') \tag{13}$$

where $\frac{\varepsilon''}{\varepsilon'} = \frac{\sigma}{\omega\varepsilon}$

$\varepsilon''/\varepsilon'$ is the ratio of conduction current to displacement current in the dielectric, and is often quoted as the loss tangent, $\tan\delta$, of the medium. For a good dielectric $\tan\delta \ll 1$, and thus equation 11 becomes

$$\alpha = \frac{\omega}{2}\sqrt{\mu\varepsilon}\ \tan\delta \tag{14}$$

The above discussion has concerned a uniform plane wave propagating far from conducting boundaries, but such a wave can also be supported

by two parallel conducting planes embedded in a uniform dielectric medium. The wave is then known as a Transverse Electromagnetic (TEM) wave, and is characterised by a frequency independent propagation velocity ($v_{phase} = v_{group} = \text{constant}$). This mode is equivalent to the classical transmission line mode, and the following identities may be derived.

$$\beta = \omega \sqrt{\mu\varepsilon} \tag{15}$$

$$Z_o = \frac{\eta r}{q} = \frac{1}{vC'} \tag{16}$$

where r is the separation of the parallel plates

C' is the capacitance per unit length between plates of width q.

Transmission line formulae allow the line attenuation α to be calculated;

$$\text{thus } \alpha = \frac{R'}{2Z_o} + \frac{G'Z_o}{2} \tag{17}$$

where R' is the resistance per unit length of the line

and G' is the conductance per unit length of the line.

For a good dielectric $G' \ll 1$ and

$$\alpha \simeq \frac{R'}{2Z_o} \tag{18}$$

2.2 Microstrip

Microstrip is basically a parallel-plate form of line, and thus may be expected to manifest TEM-like properties. It was found at an early stage that this was indeed the case, with microstrip lines exhibiting constant phase velocity over a wide frequency range. The mixed dielectric in microstrip makes pure TEM propagation impossible, but if a high permittivity substrate is employed most of the field is confined to the substrate, and this is the reason for the 'quasi-TEM' behaviour of the line. This 'quasi-TEM' propagation is described in

terms of an effective relative permittivity, ε_{eff}, such that $v = v_o/\sqrt{\varepsilon_{eff}}$ where $\varepsilon_r > \varepsilon_{eff} > 1$, and this is found to be valid up to frequencies for which the dimensions of the line are small in comparison with the microstrip wavelength. For example, a 50 ohm line on an alumina substrate 0.64 mm thick exhibits constant phase velocity up to approximately 4GHz[7]. A sketch of the microstrip field distribution is shown in figure 2. The impedance of the line is a function of the width of the top conductor, w , the thickness of the substrate h, and the relative permittivity of the substrate, ε_r, (the ground plane being assumed infinitely wide). Normally alumina substrates are 0.4 - 1.25mm. thick, and for a 50 ohm line $w \simeq h$. An introductory discussion on some of the other forms of planar line is given in reference 8.

The nature of the microstrip mode discourages exact analysis, and until recently the quasi-TEM assumption has been used almost exclusively in analyses of microstrip : the problem is then one of determining the static capacitance per unit length of the line in the presence of the dielectric. Numerous solutions have been proposed, only a few of which are discussed in this report. An extensive microstrip bibliography appeared in 1969/1970[9] but there has been considerable published work since then, particularly on dispersion in microstrip. References 10-15 list some of the more recent and wide-ranging contributions. There follows an outline of the way in which analysis of microstrip has progressed, which will also facilitate subsequent discussion of some of the properties of microstrip lines.

In 1953, Assadourian and Rimai [16] analysed embedded microstrip - not a very practical form of line but one amenable to rigorous analysis. Their results approximated to the behaviour of standard microstrip, but it was not for some considerable time that a more accurate treatment

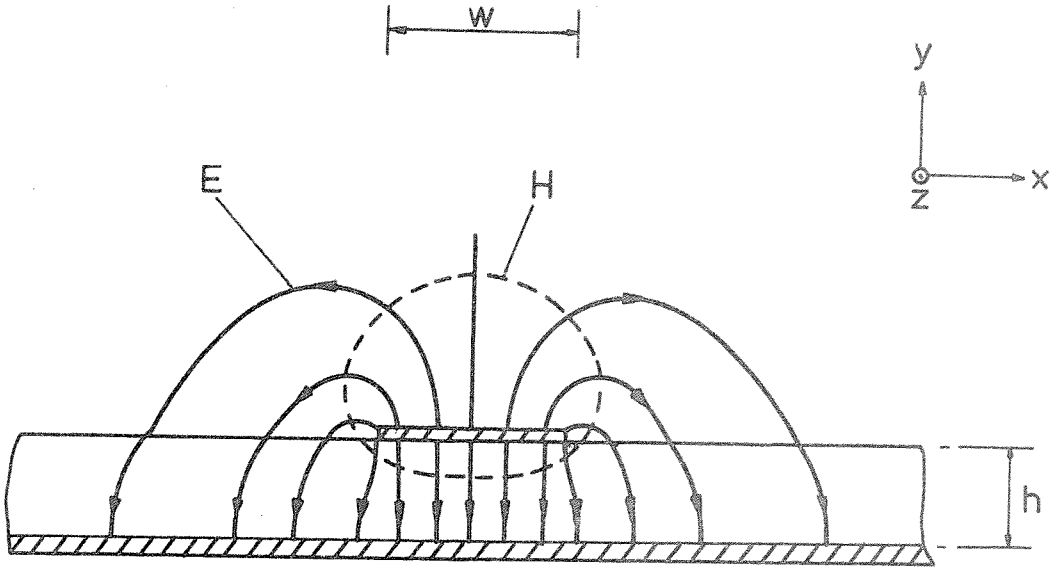

FIGURE 2. STATIC FIELD DISTRIBUTION IN MICROSTRIP

of microstrip was given. It was in 1964 that Wheeler[2,17] considered the problem of the mixed dielectric using an approximate conformal-mapping procedure. He introduced a 'filling fraction' related to the proportion of the field inside the dielectric, and was able to predict impedance and effective relative permittivity to an accuracy of a few percent for a wide range of line geometries. The analysis was based on 'thin' conducting strips, but by making a correction to the linewidth the results were applicable to lines of finite thickness. Wheeler's work remains one of the most significant contributions in the field, and it has provided the basis for much of the more recent work on microstrip.

Rigorous analysis of the microstrip problem, even assuming TEM propagation, results in often impossibly complex mathematics, but with the advent of the computer it became feasible to use numerical techniques to tackle these complexities. Silvester[18] used the classical method of images to derive the Greens function characterising the dielectric/air boundary, and solved the resulting integral equation numerically. Shortly afterwards, Bryant and Weiss[19] presented results for even and odd mode propagation in coupled microstrip using a similar approach. The alternative to rigorous analysis is to adopt numerical methods at the outset to solve Laplace's equation in the region of interest. A solution is only possible if the region is bounded, and it is therefore necessary to consider the microstrip line to be in a shielding enclosure or 'box', but if the dimensions of the box are large with respect to the linewidth the results are equally applicable to open microstrip. Standard finite difference techniques have been used successfully[20], but attempts to minimise computation time have led to the development of faster techniques[21].

The true nature of the propagating mode in microstrip is a hybrid mode which degenenerates to a pure TEM mode only a zero frequency. It is known that an arbitrary field can be represented by a set of transverse electric (TE) and transverse magnetic (TM) modes, and Denlinger[22] has applied this principle to obtain a solution comprising a set of TE and TM surface waves which together satisfy the microstrip boundary conditions. TE and TM surface waves modes can be supported on a dielectric-coated ground plane, and are characterised by an exponential field decay away from the dielectric surface[23]. The TM_o mode has zero cut-off frequency, but all other modes have a lower cut-off frequency given by

$$f_c = \frac{n\, v_o}{4h(\varepsilon_r - 1)^{\frac{1}{2}}} \qquad (19)$$

where for TE_n modes n = 1,3,5,..... and for TM_n modes n = 2,4,6,..... For an alumina substrate with ε_r = 9.8, h = 0.64mm the TM_o mode has a phase velocity approximately equal to the free space velocity until well above X-band, and the next lowest-order mode, the TE_1, has a cut-off frequency of ~40 GHz. In fact the presence of the top conductor in microstrip imposes boundary conditions which cannot be satisfied by any pure surface wave mode, but just as the quasi-TEM assumption provides a useful model at low frequencies, so the model of a quasi-TEM mode coupled to a TM_o surface wave can be used at frequencies where dispersion becomes significant[24,25]. In practice microstrip is always used in some form of enclosure and at higher frequencies it is also necessary to take into account modes supported by the enclosure[24].

Theoretical microstrip analyses have not yet yielded comprehensive accessible data on phase velocity variation, but a number of empirical

formulae are available covering the common ranges of impedance and permittivity. The formulae due to Arnold[7] and to Jain et al[25] have been found to agree within 1% of each other for lines around 50 ohms on alumina, and show that for such a substrate at 10 GHz the phase velocity has decreased by about 3% from its low frequency value. Arnold's formula was based on measurements on 35-80 ohm lines on alumina, and in a second paper Jain et al[26] have shown that its accuracy outside this range is poor. It has been found in the course of this investigation that the relative permittivity required in either Arnold's or Jain's[25] formulae to provide a good fit to experimental points can differ markedly from the manufacturer's quoted value. Discrepancy between the measured and quoted values for the permittivity of alumina has also been noted elsewhere[27].

3. MICROSTRIP TECHNOLOGY

The properties of microstrip are closely linked to the technology, and in any programme of work involving microstrip the quality of materials and the manufacturing process play an important role.

3.1 Fabrication

Thin-film fabrication techniques are normally used for M.I.C's and have been used in this work in conjunction with standard photo-mechanical methods. The substrates are coated on both sides with an evaporated nichrome/gold film which is then plated up through a resist layer; after plating, unwanted areas of evaporated metal are removed by selective etching, leaving only the required conductor pattern. The process is described in detail in the Appendix, (12.1).

The choice of thin-film rather than thick-film techniques is due to the lower losses and better definition possible with this method[28], although thick-film techniques offer distinct advantages in large scale production and as their technology advances are likely to be used increasingly for M.I.C's. In thin film processing it is possible either to plate up the substrate selectively or to plate up the whole substrate and then etch away unwanted areas of plated-up metal. The former method requires two photoresist stages and it is necessary to be able to accurately re-register the substrate with the photomaster, but the method has the advantage of reducing undercutting in the finished conductors since the final etching is only of the thin evaporated film, and not the whole thickness of the plated layer. Narrow lines plated up through resist may exhibit inferior conductivity to those formed by etching back, but the effect of undercutting on the line width

is most severe for narrow lines: an etched-back line is undercut at each side a distance approximately equal to the line thickness. The difference in undercut between the two methods is not in fact as large as might be expected since the plated layer etches at a faster rate than the evaporated layer, but the plating-up method still has the advantage in this respect. The etch-back method may also prove expensive unless steps are taken to reclaim the gold from the etching solution.

On balance the 'plating-up' process appeared the most suitable and it was known that satisfactory alignment of the photomasters could be achieved using a mechanical jig[29]; this process has been used for all circuits fabricated in the course of this project.

3.2 Materials

3.2.1 Substrate

There is now a huge variety of materials suitable for use as substrates for microstrip, and the relative permittivities of these materials extend over a wide range. The ideal dielectric for a microstrip substrate possesses the following properties:

(i) Low loss tangent and high resistivity,

(ii) Homogeneity, good surface finish and dimensional tolerance,

(iii) Temperature stable relative permittivity, of a value suited to the thicknesses available and to the frequency and impedance ranges required.

For particular applications other factors such as cost, tensile strength or thermal conductivity may also be important.

In the early days low permittivity dielectrics such as polystyrene, glass fibre and quartz were common, but today most circuits at X-band

employ higher permittivity materials such as sapphire, alumina ($\varepsilon_r \simeq 10$) rutile ($\varepsilon_r \simeq 16$) or one of the rare earth compounds. In the lower gigahertz frequencies the polyolefins ($\varepsilon_r \simeq 2.3$) have to a great extent replaced previously used materials. Alumina is popular for work at 1 - 12 GHz: the microstrip wavelength is $\sim\lambda_o/3$, which leads to circuits of a suitable size, and it has no great disadvantages in any of the categories above. Sapphire is an expensive alternative to alumina with superior qualities; it is single crystal alumina and is thus homogeneous but anisotropic. Use of very high permittivity substrates leads to increased losses and to reduced component size. Above X-band even components on alumina become small, and fused quartz ($\varepsilon_r = 3.78$) has been used for frequencies up to 20 GHz[30].

In this project, 99.5% alumina has been employed almost exclusively, since it is the most widely used material for M.I.C's; it is readily available and can be supplied in relatively large substrate sizes. Two types have been used: a medium quality substrate made by Coors (ADS-995), and a higher quality material from Materials Research Corporation (M.R.C. 'Superstrates').

3.2.2 Conductors

Good conductivity is of primary importance in choosing a metallisation for microstrip, but the metals which satisfy this criterion - gold, copper, silver, aluminium - do not, in general, adhere well to dielectrics. (Aluminium is an exception to this but is avoided because of its surface passivity). In order to deposit these metals it is necessary to first deposit a very thin adhesion layer, of nichrome, chromium, tantalum or titanium. The combination of metals employed is usually determined by the type of circuit being fabricated or by the conditions under which the circuit will operate.

For example, a titanium film can be oxidised to form capacitors and titanium/gold is stable at high temperatures; alternatively a nichrome adhesion layer can be used to form resistors. In this project these factors were of secondary importance since the work was concerned with transmission lines and not complete circuits, and extreme operating conditions were not envisaged. A nichrome/gold system was in use at A.S.W.E. and it was decided to adopt the same system for this work.

The process consists of an evaporation stage to deposit the nichrome adhesion layer and the gold seed layer, followed by electrolytic gold plating in a neutral gold/cyanide solution. Keister[31] had recommended a similar process in an evaluation of processes and materials for microstrip. Gold has a slightly lower conductivity than copper but is less prone to chemical attack and provides a good surface for soldering or bonding.

3.3 Limitations and Imperfections in Alumina/Gold microstrip lines

Although alumina is a perfectly acceptable material for the commercial production of M.I.C's, in the measurement of fundamental properties one is often faced with limitations of the material. In order to understand how these arise it is necessary to outline the manufacture and composition of alumina substrates.

Alumina occurs naturally in the hydrated form, as bauxite. The ore is purified to give up to 99.9% pure alumina, the remaining impurities being sodium and iron oxides, and it is then finely powdered and thoroughly mixed with a plasticiser, a binder of magnesium oxide, and small quantities of other compounds to aid the manufacturing process. At this stage the mixture is a viscous slurry; it is dropped onto a horizontal moving belt and carried under a blade whose height above the belt governs the thickness of the emerging 'tape' of material. The tape

cures to become soft and flexible and substrate shapes are stamped out prior to the material being fired at high temperature. During firing the plasticiser evaporates and the finished, hardened substrate is produced. It is now referred to as an 'as fired' substrate and is approximately 99.5% pure alumina, the remainder being the magnesium oxide binder. Further trimming to size, or grinding and polishing to improve the surface finish, may follow. The process is a batch process, and this is the main reason for the variable quality of alumina substrates. Material from different manufacturers varies, batches from the same manufacturer vary, and individual substrates vary. Figures for the relative permittivity of different samples of nominal 99.5% alumina have revealed variations of 3% in batches from the same manufacturer[32], of 1% in a typical batch of 100 substrates, and of 0.2% over a single 51x51 mm substrate[33]. This variability can lead to errors in experiments involving measurements on several substrates and allowances must be made. One technique is to place a test pattern - a small resonator for example - on each substrate, by means of which the permittivity of the substrate can be calculated. Alternatively the same substrate can be reprocessed several times; this avoids any problem with permittivity variation but also prevents subsequent checking of a particular measurement. The first method has been used in this work.

'As fired' substrates are available in two purities: 96% and 99.5%. The 96% material contains a glass phase which leads to inferior surface finish,and these substrates are normally used for thick-film circuits where the conductors require a good mechanical bond to the substrate. The 99.5% alumina is used for thin-film circuits since its better surface finish allows the higher definition possible with thin-film

techniques to be realised. Closer control of its composition is maintained during manufacture and this leads to less variability in substrate quality.

Alumina is a polycrystalline structure, and the most important factors governing the quality of the substrate are size and variation in size of the crystallites. A high quality 99.5% alumina such as the MRC Superstrates has crystallites with diameters from 0.6 - 1.5μm and a surface finish (as fired) of 0.1μm C.L.A. A medium quality substrate like the Coors ADS 995 alumina may have crystallites 1-20μm in diameter and a surface finish of 0.3μm. Substrates normally exhibit a slightly better surface finish on one side than the other, the good side being the one in contact with the belt when the tape is cast. The surface finish of as-fired substrates can be improved by grindingand polishing but in this process crystallites are plucked out of the body of the material leaving deep pits in an otherwise smooth surface. Lower loss can be achieved on polished substrates, but the polishing process is expensive and stresses at the pluck-out pits lead to poorer adhesion of metallic films. Figure 3 shows four scanning electron micrographs of different alumina samples. Plates I and II show the two sides of a Coors substrate, with a quoted surface finish of 0.25μm on the top and 0.6μm on the underside. Difference in the two sides is clear; also evident is the wide range of crystallite diameters in the substrate. Plate III is of an MRC 'Superstrate', with a surface finish of 0.1μm. This sample showed little variation between top and bottom surfaces, and the crystallites can be seen to be smaller and more uniform in size. Plate IV shows the edge of a plated up line on a polished substrate in which the pluck-out pits are clearly visible. (The definition at the

Scanning Electron Micrographs of alumina substrates

Plate I

'As fired' Coors ADS 995

top surface

Plate II

bottom surface

Plate III

'As fired' MRC 'Superstrate'®

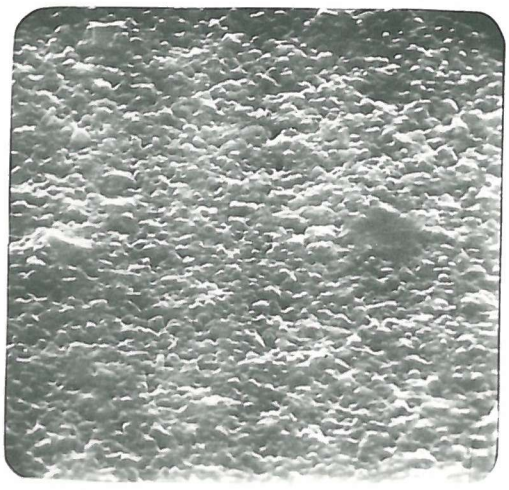

Plate IV

Polished alumina

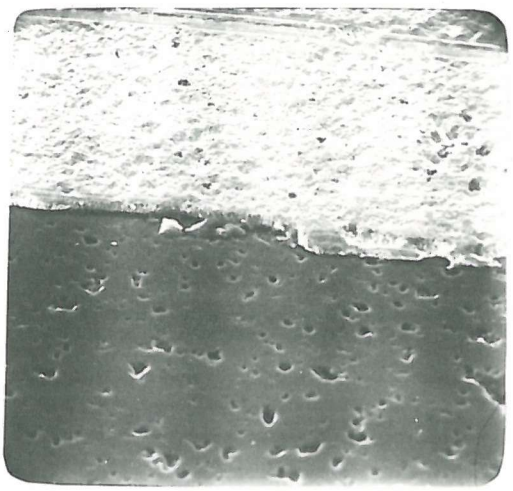

Figure 3

edge of this line is not particularly good). Large variations in crystallite diameter have other disadvantages: crystallites have a preferred degree of orientation and this effect can become significant for large crystals and lead to anisotropy. (Sapphire is the extreme case of this phenomenon, with permittivities 8.6, 8.6, 10.6). Another disadvantage is that stresses are set up during casting which lead to warping of the substrate at the firing stage. The gradient of this warp or camber may be 30μm per linear centimetre in the finished substrates. Figure 4 (a) and (b) shows surface profiles of an alumina substrate 25 x 51 mm, in directions perpendicular and parallel to a plated-up line running centrally down the length of the substrate. A similar profile, made by drawing a dial gauge across the surface, is shown for a sapphire substrate in Figure 4 (c); it exhibits much less warp than the alumina substrate. Profiles on both sides of each substrate confirmed that the undulation was due to the camber of the substrate and not to variations in thickness.

The differences in thickness that do occur in alumina substrates is another factor which contributes to the variability in performance of microstrip circuits. The histograms in Figure 5 show the measured thicknesses of one batch of Coors ADS 995 substrates and two batches of MRC Superstrates, and the accompanying table gives details of the thickness variation over a single substrate. Thickness measurements were made at twelve points on each substrate using a micrometer. For the majority of substrates the average thickness fell within the manufacturers' tolerances.

The two factors of thickness and permittivity variation across an alumina substrate lead to a degree of uncertainty in measuring very

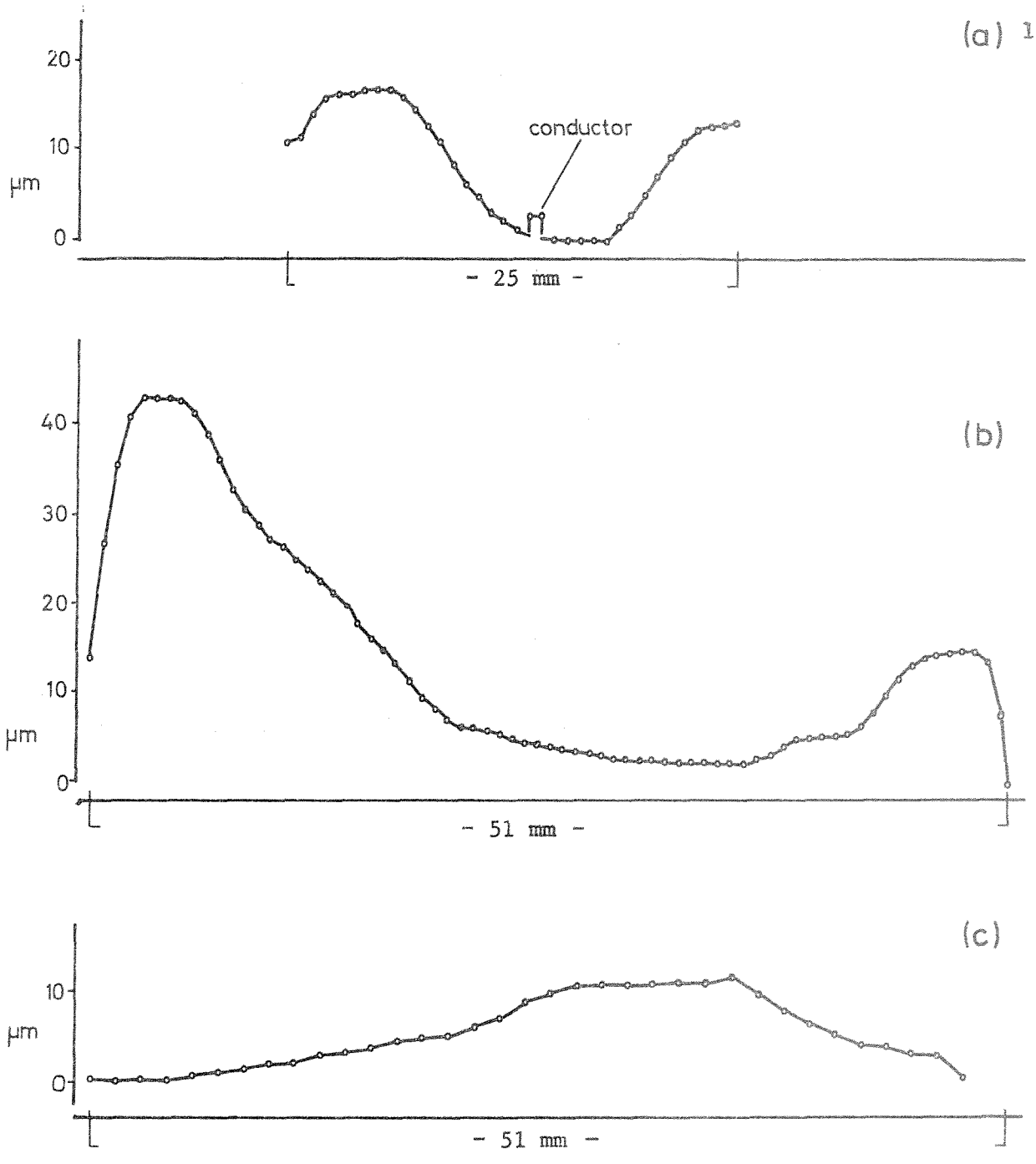

FIGURE 4. SURFACE PROFILES OF MICROSTRIP SUBSTRATES

(a) Profile across a 25 x 51 x 0.64 mm alumina substrate.

(b) Profile along the alumina substrate in (a).

(c) Profile along a 13 x 51 x 0.64mm Sapphire substrate.

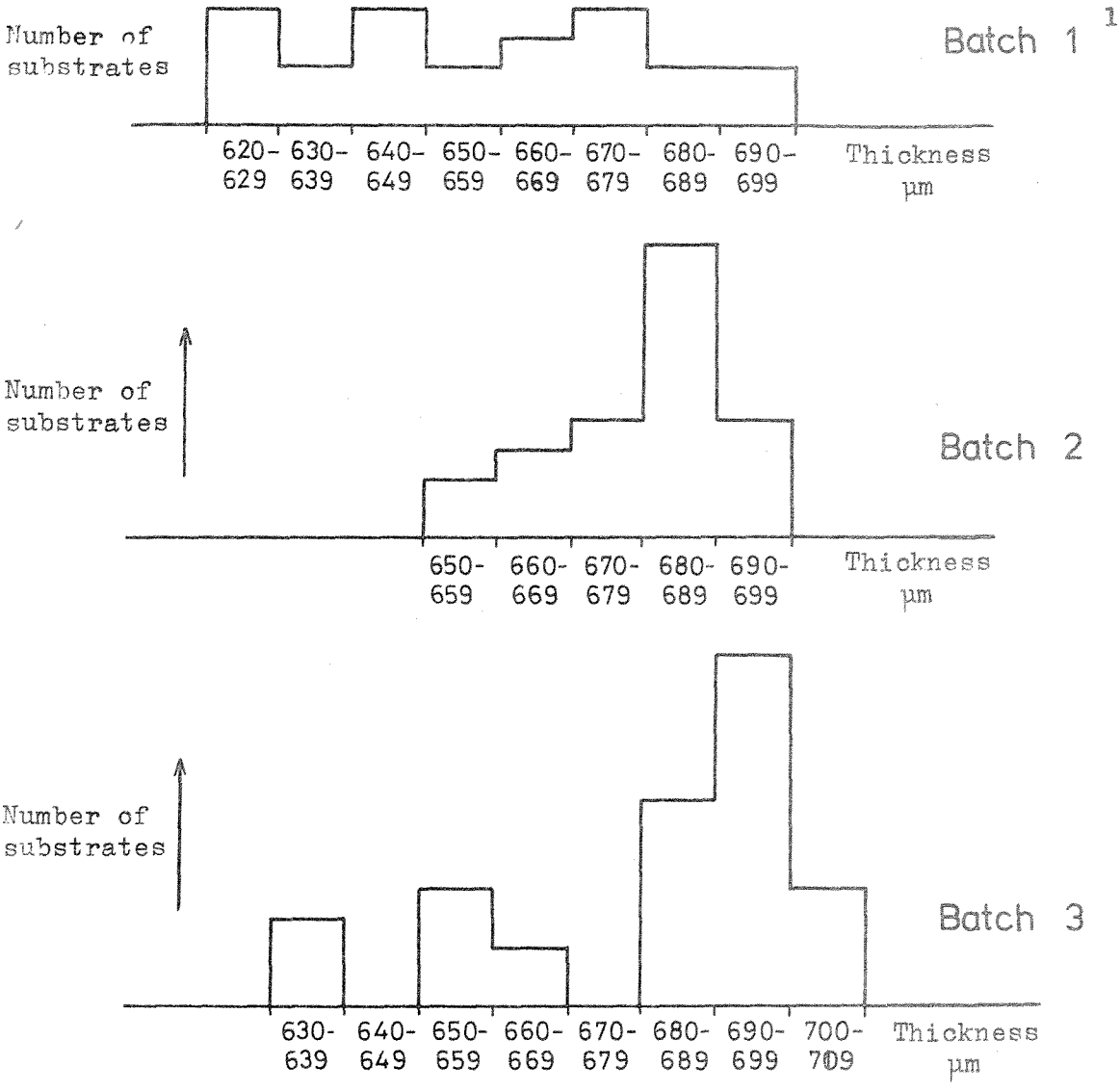

Batch & no.of substrates	Manufacturer & substrate size	Manufacturer's thickness specification	Average thickness of batch	Average variation in thickness over one substrate
1 (23)	Coors 25 x 76 mm	635 ± 64 µm	656	± 15 µm
2 (23)	MRC 51 x 51mm	686 ± 38	679	± 10
3 (32)	MRC 51 x 51mm	686 ± 38	681	± 16

FIGURE 5. DIMENSIONS OF ALUMINA SUBSTRATES

small discontinuities. Nevertheless work in this project has been confined almost exclusively to 'as fired' alumina for two reasons: firstly, alternatives such as sapphire are expensive, especially in large sizes, and secondly, whatever the substrate, other manufacturing tolerances on for example linewidth, are likely to have an influence of the same order of magnitude.

Imperfections in the conductors can in part be due to faults in the substrate. The warping already discussed can prevent intimate contact between the substrate and the photomaster during resist exposure, and this may lead to 'spreading' of the conductors in certain areas. Ideally the top conductor should be of constant, rectangular cross-section to maintain constant impedance, and free from burrs which lead to high field concentrations and increased losses. Protrusions of alumina above the surface[34] lead to non-uniformity if they occur underneath a narrow conducting stripe; occasionally they become dislodged between evaporation and plating and this leads to pinholes in the conductor. Any abrasion prior to evaporation to remove these protrusions impairs adhesion to the substrate. Uneven build-up of the plated gold layer is another common manufacturing fault. Figure 6(a) shows a Tallysurf measurement on a line exhibiting substantial edge build-up; the small central hillock was a localised fault but the build-up extended along the whole length of the line. Profiles across a more normal line are shown in Figure 6(b) for two positions on the line; there is a very slight build-up of gold at the edges and also a difference of about 25% in the average line thickness at the two positions.

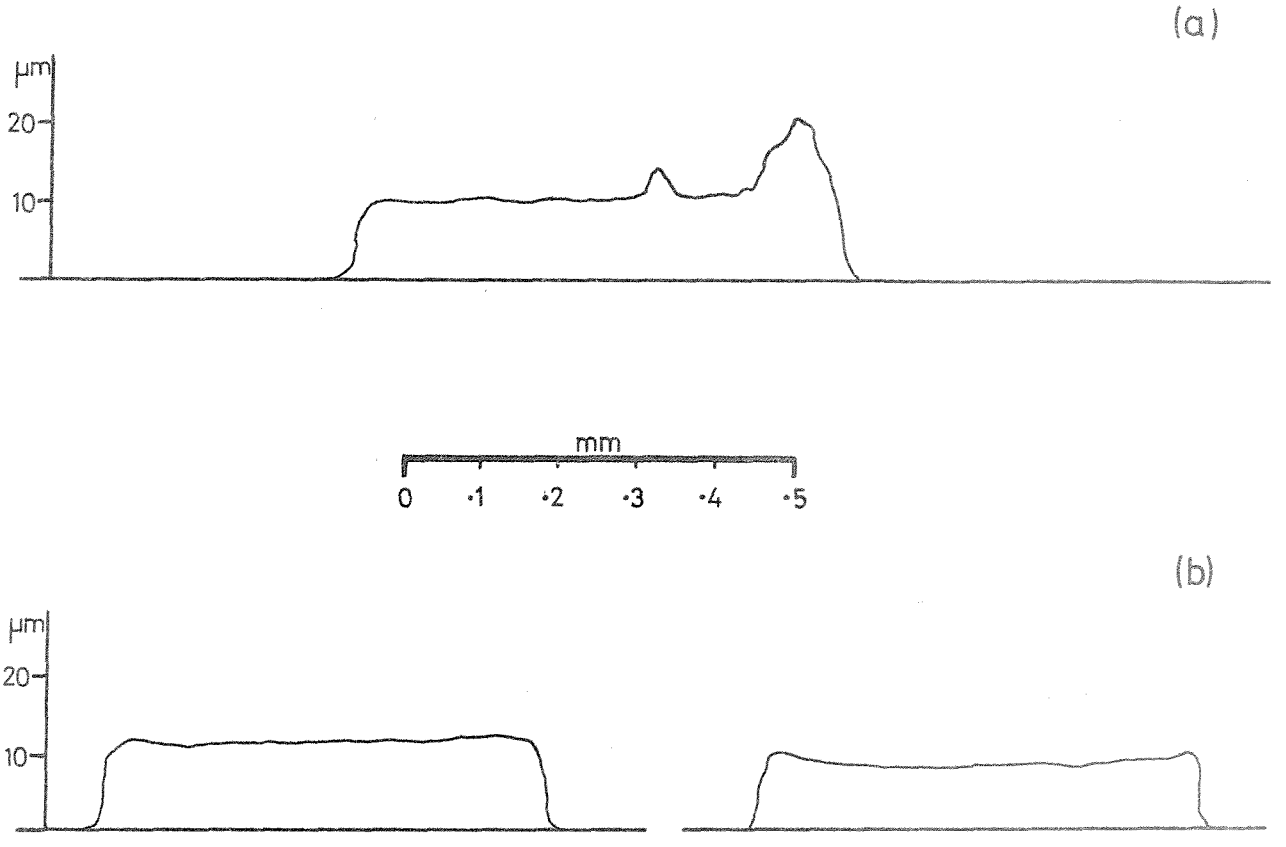

FIGURE 6. TALLYSURF PROFILES OF PLATED-UP CONDUCTORS

(a) Profile of a line exhibiting a local fault and considerable edge build up.

(b) Profile at two places on a normally plated-up line, (10 mm long).

(Tip radius 0.0001", Cut-off 0.003").

4. LOSSES IN MICROSTRIP

In general there are three loss mechanisms which may be present in any guiding system: dissipation in the conductors, in the dielectric, and radiation loss. Frequently one of these factors predominates, and for microstrip on alumina this is conductor loss. Dielectric loss in alumina at X-band is an order of magnitude lower than conductor loss, and radiation loss only becomes important at discontinuities. These three loss mechanisms will now be considered in more detail.

4.1 Dielectric Loss

The permittivity of an isotropic medium is a complex scalar which may be written $\varepsilon = \varepsilon' - j\varepsilon''$. The loss tangent, tan δ, is $\varepsilon''/\varepsilon'$ and is the inverse of the Q factor of the dielectric. For a TEM wave propagating in a homogeneous medium, the dielectric loss is given approximately by equation 14 (Section 2.1), repeated below:

$$\alpha_d \simeq \frac{\omega}{2}(\mu\varepsilon)^{\frac{1}{2}} \cdot \tan\delta \quad \text{np/unit length} \qquad (20)$$

For microstrip it is possible, providing the loss tangent of the dielectric is low, to make use of Wheeler's concept of a filling fraction, q, to give [35]

$$\alpha_d \simeq \frac{\pi}{\lambda_g} q \sqrt{\frac{\varepsilon_r}{\varepsilon_{eff}}} \tan\delta \quad \text{np/unit length} \qquad (21)$$

Manufacturers of alumina do not always quote tan δ at microwave frequencies, but since it is not strongly frequency dependent in this region the use of the V.H.F. value does not lead to serious error. Taking a typical value of tan δ for alumina of 10^{-4}, $\alpha_d = 0.2$ dB/m.

4.2 Conductor Loss

Conductor loss in microstrip is influenced by the conductor material and by the substrate. Loss arises from longitudinal and transverse currents in both the top conductor and the ground-plane, but at X-band the effect of transverse currents is sufficiently small to be ignored[37]. Thus, assuming TEM propagation, the conductor attenuation is given approximately by

$$\alpha_c \simeq \frac{R'}{2Z_o} \quad \text{neper/unit length} \qquad (22)$$

from equation 17, where R' is the total resistance per unit length of the line.

Because of the skin effect, the resistance of a thin plane conducting layer varies significantly with the thickness of the layer. Figure 7 shows the variation in resistance of a thin plane conductor (relative to the high frequency value) with the normalised line thickness t/δ [δ-skin depth]. The curve is based on the formula[36]

$$\frac{R}{R_{(hf)}} = \frac{\sinh(2t/\delta) + \sin(2t/\delta)}{\cosh(2t/\delta) - \cos(2t/\delta)} \qquad (23)$$

and it can be seen that for certain values of t/δ the resistance drops below the high frequency resistance. Horton[37] has found that for common types of microstrip line minimum attenuation occurs at a conductor thickness of between 2 and 4 skindepths.

If the longitudinal current is assumed to be uniform in both conductors and, in the ground-plane, to be confined to that area immediately beneath the top conductor, then $R' = 2R_s/w$ (where R_s is the surface resistivity of the conductors) and

$$\alpha_c \simeq \frac{R_s}{Z_o w} \quad \text{neper / unit length} \qquad (24)$$

This expression is strictly true in the limit as $w/h \to \infty$, and

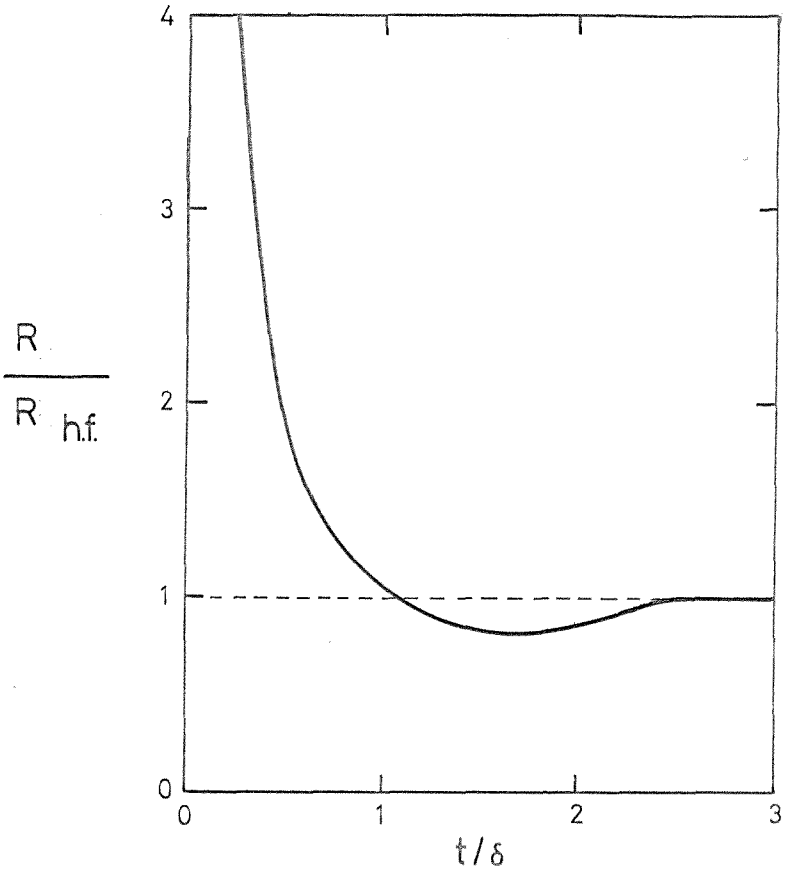

FIGURE 7. VARIATION IN RESISTANCE OF A THIN CONDUCTING PLANE RELATIVE TO THE HIGH FREQUENCY VALUE (R/R_{hf}) AS A FUNCTION OF NORMALISED CONDUCTOR THICKNESS (t/δ) (from equation 23).

experiment has shown that it is within the range of measurement accuracy for strips with $w/h > 2$. The surface resistivity R_s is given by $(\sigma\delta)^{-1}$, [σ conductivity]. Microstrip conductors are often a composite metal - in the case of this work a thin nichrome adhesion layer underneath a thick layer of gold; the nichrome can be ignored in calculating the surface resistivity[12] since the skin depth in nichrome is $\sim$ 5μm at 10 GHz and greatly exceeds the thickness of the nichrome layer ($<$ 50nm). (It is possible at high temperatures for the nichrome to migrate into the gold layer and to degrade its conductivity, but the effect is only significant if the gold layer is thin[13]; in the work reported here the plated gold layer was two to three orders of magnitude thicker than the nichrome adhesion layer).

In TEM propagation the microstrip current distribution is simply related to the charge density on the strips, and its form resembles that sketched in Figure 8; there is very high current density at the edges of the top conductor, and the current in the ground plane extends for its full width. Pucel[6] has calculated conductor loss in microstrip supporting a TEM wave, but avoided having to know the exact form of this current distribution by calculating the series skin resistance from the internal inductance of the conductors, relying on the equality of surface resistance and surface reactance at a given frequency. His derivation is based on an extension of Wheeler's work and leads to straightforward, if long, expressions for α_c. The work includes a large number of experimental results, but in comparing theory and experiment a substantial correction for additional loss due to surface roughness is introduced, which amounts to 33% in some cases. It appears probable that this factor is excessively large, in which case there is a discrepancy between Pucel's calculated and measured losses. Gopinath[38] has

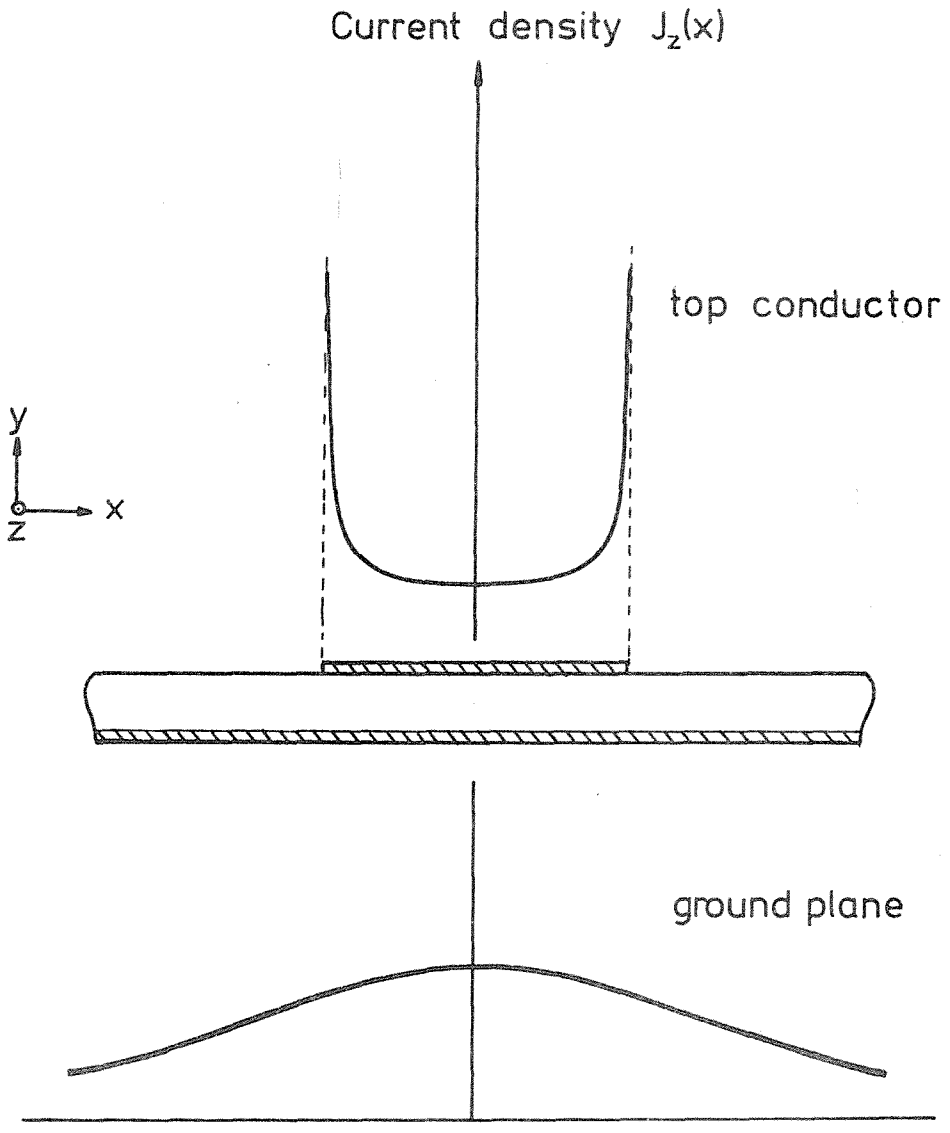

FIGURE 8. APPROXIMATE DISTRIBUTION OF LONGITUDINAL CURRENT IN MICROSTRIP

calculated conductor loss using Silvester's method of images to calculate the form of the current distribution, and his results for thick and thin conductors, including the effects of transverse current, bracket Pucel's experimental results but exceed Pucel's theoretical results.

Little published theoretical work exists on the effect of surface roughness on conductor loss, but Sobol[12] has drawn attention to results derived for waveguide, in which eddy current losses due to grooves transverse to direction of current flow were calculated[39]. Grooves running parallel to the current flow were found to have a much smaller effect and to a first order approximation could be neglected. Sanderson[40] has also considered the effect of surface roughness on TEM propagation, in coaxial line, and uses the concept of a displacement of the conductor surface to account for the roughness. Results show that the important factor is the periodicity of the grooves and their depth in relation to the skin depth, but that the actual shape of the groove has only a minor effect. According to Sobol, for a gold line on a substrate with a surface finish of 250nm C.L.A. the required correction factor is about 1.1 at 10 GHz.

Gopinath used numerical methods in his derivation, and there remains the need for a simple analytic expression for conductor loss. Caulton and Sobol[41] have proposed a model in which uniform current density in both strips is assumed, but in which the current in the ground-plane extends a distance $w/2+h$ either side of the centre line. Equation 24 now becomes

$$\alpha_c = \frac{R_s}{Z_o}\left[\frac{1}{w} + \frac{1}{2h+w}\right] \qquad (25)$$

The origin of the width (2h+w) for which the current in the ground-plane extends is not made clear, and appears to be a semi-empirical value.

Experimental determination of line attenuation, which is predominantly conductor loss, is discussed in Section 8.3 and results are compared to the theoretical values of Caulton and Pucel.

4.3 Radiation Loss

Radiation loss from microstrip is a flow of energy away from the line and occurs at any non-uniformity in the line such as transitions or terminations. In normal use microstrip circuits are completely enclosed so that radiation from the circuit is eliminated, but radiation from components of the circuit can lead to unwanted coupling, and in order to attenuate this lossy material is often used to line the inside surfaces of M.I.C. enclosures.

One method of calculating the energy radiated from a microstrip source is to form the Poynting vector for the particular field configuration and then to integrate this over a hemisphere. Lewin[42] used this approach in studying various forms of microstrip discontinuity, and derived analytic expressions for the power fraction radiated (relative to the power incident) by terminations, transitions and a right-angle corner. The power fraction radiated is found to be proportional to $Z_o(h/\lambda_g)^2$, and it is also found that radiation from an open-circuit is significantly greater than radiation from a short circuit. Easter et al[43,44,45] have studied radiation from various forms of microstrip resonator and calculated the energy loss numerically. In references 43 and 44 it is found that conventional forms of microstrip resonator can exhibit considerable loss if their dimensions are small with respect to the wavelength. For example, a circular ring resonator of circumference λ_g is shown to radiate to the same extent as a $\lambda_g/2$ open-circuit resonator;

radiation from large rings is shown to be negligible, as had already been verified experimentally. A novel type of open-circuit line resonator in the shape of a narrow U is proposed as a form of low loss resonator. Discussion of radiation from open-circuit line resonators is deferred until section 8.4 where the experimental results are also given.

Assumptions common to both Lewin's and Easter's work are TEM propagation with a uniform relative permittivity ε_{eff}, and that cross-sectional line dimensions are small with respect to the free space wavelength.

5. MEASUREMENTS IN MICROSTRIP

5.1 General microwave measurement techniques

It has already been established that the parameters of interest are the impedance, phase constant and attenuation factor of the microstrip line, and the behaviour of discontinuities in the line. Traditional microwave measurement techniques based on coaxial line or waveguide have relied to a great extent on standing wave measurements at fixed frequency, and a variety of well-known techniques suited to different circumstances have evolved from the fundamental method. Single-point measurements are in general accurate but laborious, and have been superseded to a large extent by swept frequency measurements, which give a much clearer insight into the characteristics of a component over a wide frequency range. Either reflection or transmission measurements can be made, and with the more sophisticated equipment a pre-programmed series of tests can be carried out; once a calibration run has been made results can be automatically corrected for errors in the measuring system before presentation.

The alternative approach is to make measurements in the time domain using a fast voltage step to 'interrogate' the system. The technique is known as Time Domain Reflectometry (T.D.R.) and has the advantage that reflections from different parts of the system being analysed remain segregated in time and can be displayed and measured separately. This is a great advantage over reflection measurements made in the frequency domain, where only the total reflected power from all components in the system is observed.

5.2 Measurement Techniques for Microstrip

In using conventional coaxial line or waveguide test equipment to investigate microstrip it is necessary to have some form of transition between the two systems. The best currently available transitions are 3mm coaxial line to microstrip 'launchers' with a V.S.W.R. of around 1.1 at X-band; this is sufficiently large to preclude any direct measurement of microstrip properties in the frequency domain, since reflections from the launcher mask any small reflections emanating from beyond it. A computerised network analysis system would allow reflections from the microstrip line to be extracted from the overall reflected signal, and results would be accurate provided the reproducible behaviour of the launcher could be guaranteed, but such a system is really only justified where a large number of similar measurements are to be made; otherwise a disproportionate amount of time is liable to be spent in calibration and programming.

Measurements in the time domain do allow the effects of the line and the launcher to be separated, as can be seen in Figure 9, which is a T.D.R. display of a 51mm length of 50 ohm microstrip line inserted in a matched 50 ohm coaxial system. The limitations of T.D.R. are also evident from Figure 9, and are a result of the finite rise-time of the voltage step, which prevents resolution of closely spaced discontinuities. Thus it is only possible to locate the ends of the microstrip line within the limits shown, and an accurate determination of phase velocity on the line is impossible. T.D.R. makes the nature of a discontinuity - whether inductive or capacitive - immediately obvious, and the amplitude of its reflection coefficient can be read directly from the display (although it is necessary to exercise caution with small discontinuities). In

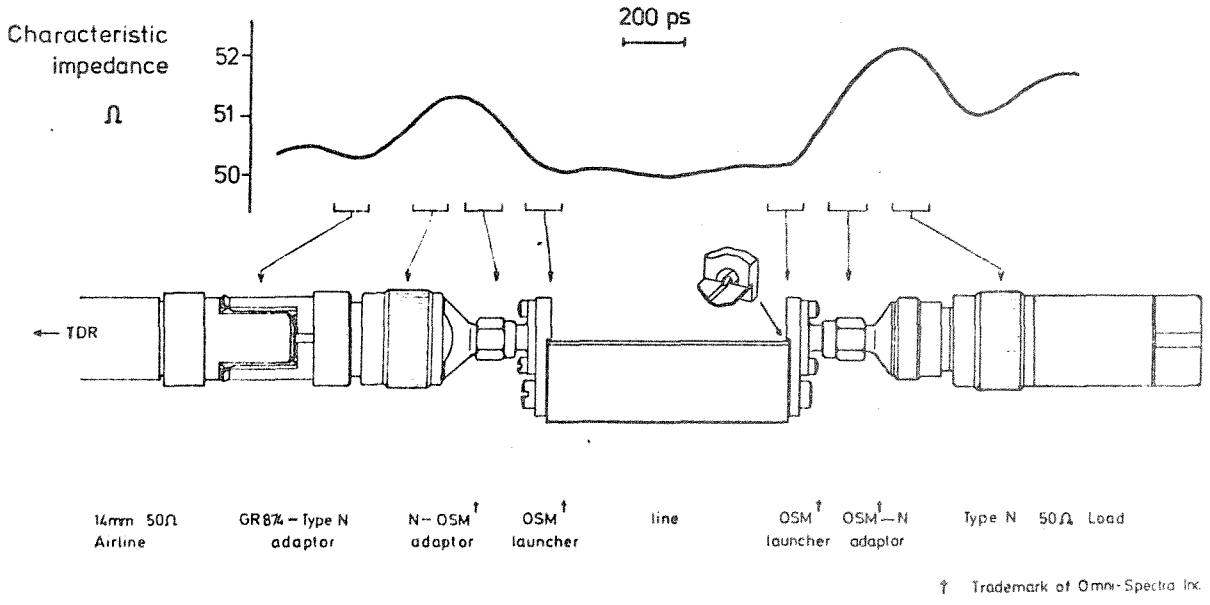

FIGURE 9. TIME DOMAIN REFLECTOMETRY TRACE OF SECTION OF MICROSTRIP LINE, 51mm LONG, INSERTED IN A 50 ohm SYSTEM

(Pulse Risetime = 128 ps).

principle it is also possible to calculate the numerical value of components from the decay time of the pulse, but this is inconvenient and lacks accuracy. T.D.R. is best suited to qualitative checking of overall systems or to quantitative measurement of impedance, especially in the region of the instrument's own impedance (usually 50 ohms). Figure 10 shows the approximate accuracy achieved in T.D.R. impedance measurements given a good 50 ohm standard. The curve is only approximate because factors such as the type of connector used and the length of the unknown line also influence the accuracy. T.D.R. has been used throughout this project for impedance measurement, using an instrument with a rise time of 128 ps, equivalent to an upper frequency of 2.3 GHz.

There remains the problem of measuring the other parameters of a microstrip line, and clearly in order to minimise the effect of the transition this is best accomplished by making measurements on the actual line. The open structure of microstrip lends itself to direct coupling into the electric and magnetic fields, and a standing wave indicator above the line is an attractive proposition. Such an instrument has the potential of yielding line wavelength directly, and of enabling discontinuities and losses to be studied by normal V.S.W.R. techniques. A typical microstrip line has cross-sectional dimensions which are small with respect to the line wavelength, and thus the properties of the line are unlikely to be strongly frequency dependent. Because the line is open, displacement of the probe from the reflecting interface can be measured directly, and there is no need for a microstrip counterpart to the short-circuit termination used to determine phase change in waveguide standing-wave measurements. The effect of the launcher cannot be completely eliminated, since any signal incident on the launcher from the microstrip side will be partly reflected,

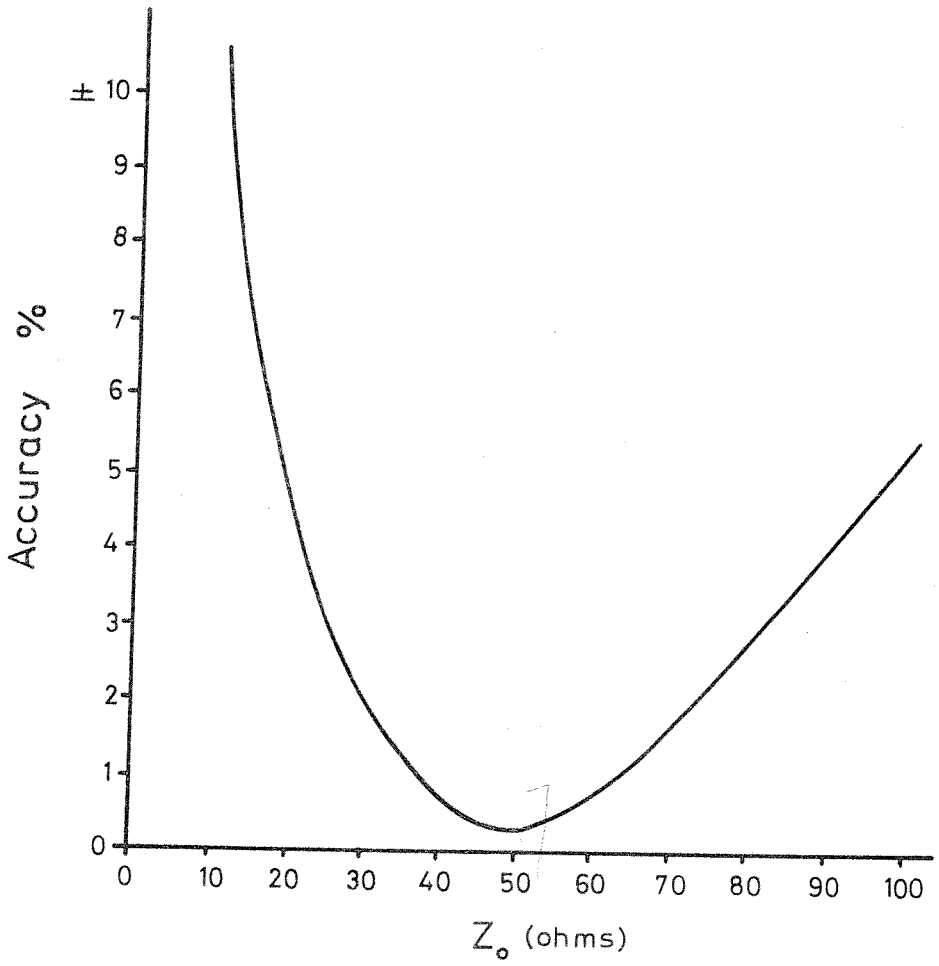

FIGURE 10. APPROXIMATE ACCURACY OF TIME DOMAIN REFLECTOMETRY FOR IMPEDANCE MEASUREMENTS

but these reflections will be small and if necessary could be attenuated further by introducing additional padding. In view of the apparent simplicity of a microstrip standing wave indicator, it was surprising that the only references to such an instrument appeared to be by Kostriza[46] and Bowness[47] in 1956, although in balanced stripline a standing wave indicator had been used with success in the study of discontinuities[48].

6. THE MICROSTRIP STANDING WAVE INDICATOR

6.1 Development

Preliminary work in the department[49] had demonstrated the feasibility of a standing wave indicator on a microstrip line and the instrument used for that work is shown in Figure 11. It was found that standing waves were readily detected, and voltage standing waves observed on an open-circuit microstrip line are shown in Figure 12, for two heights of the probe above the substrate. Close to the line the pattern had a wavelength of $\sim\lambda_o/\sqrt{\varepsilon_{eff}}$, but some distance above the line a standing wave of wavelength $\sim\lambda_o$ was also noted. Both these patterns exhibited irregularity in the amplitude and separation of the maxima and minima.

It was decided to develop a more sophisticated form of this instrument, which was to have superior mechanical performance and the minimum of metallic structures in the vicinity of the microstrip line. In this way it was hoped to remove the irregularity in the standing waves noted with the Mark I instrument. The Mark II design was based on a commercially available travelling microscope, with the substrate fixed in place of the viewing stage and the standing-wave probe replacing the eyepiece. The final form of this instrument is shown in Figure 13. The probe is a length of miniature coaxial cable, and has vernier adjustment in the vertical (y) and longitudinal (z) planes, and a preset adjustment in the transverse (x) plane. The substrate is mounted on a parallel-sided block clamped to a ground steel baseplate which is carefully aligned with the microscope bed.

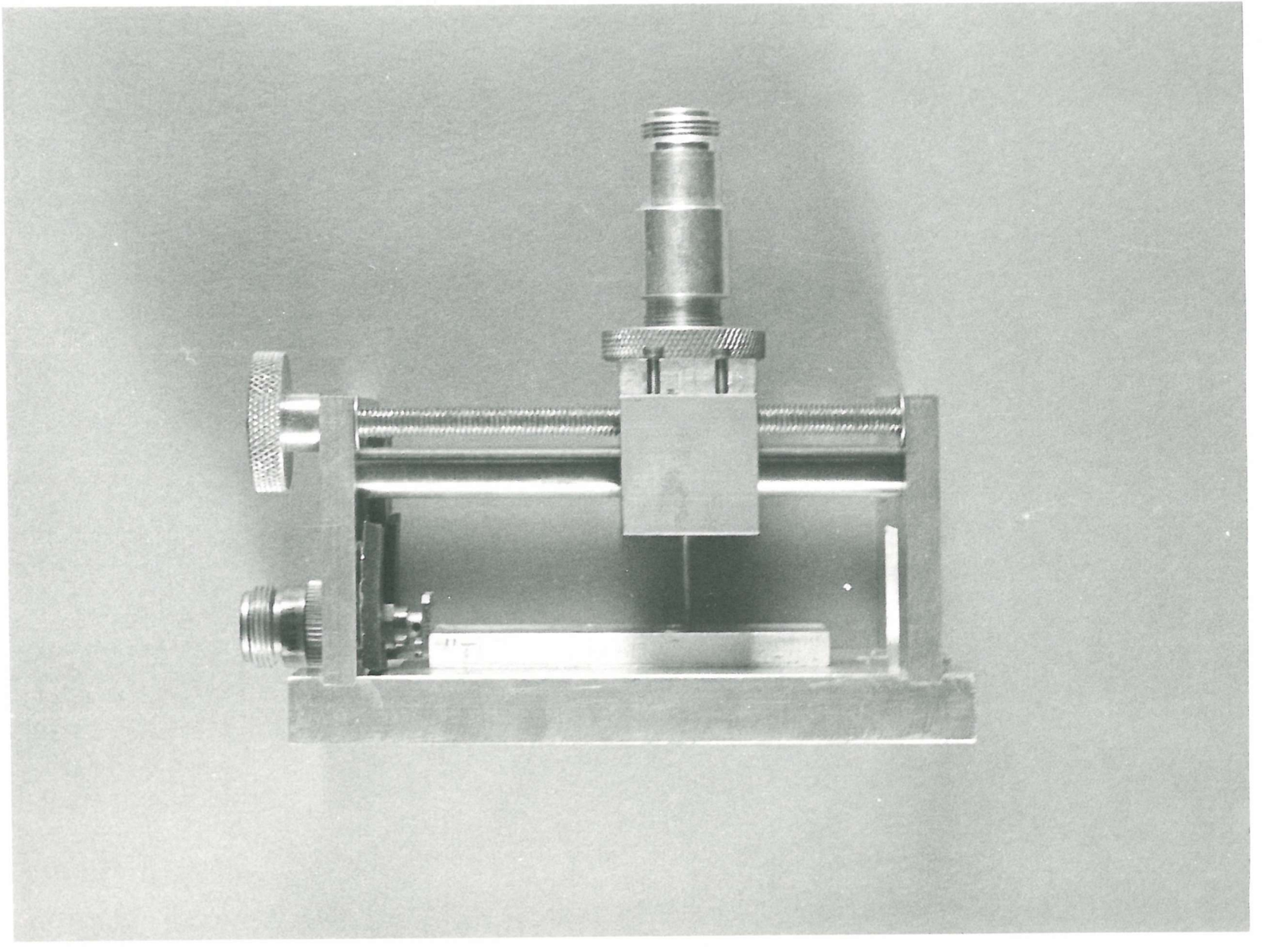

Figure 11. The Mk. I Microstrip Standing Wave Indicator

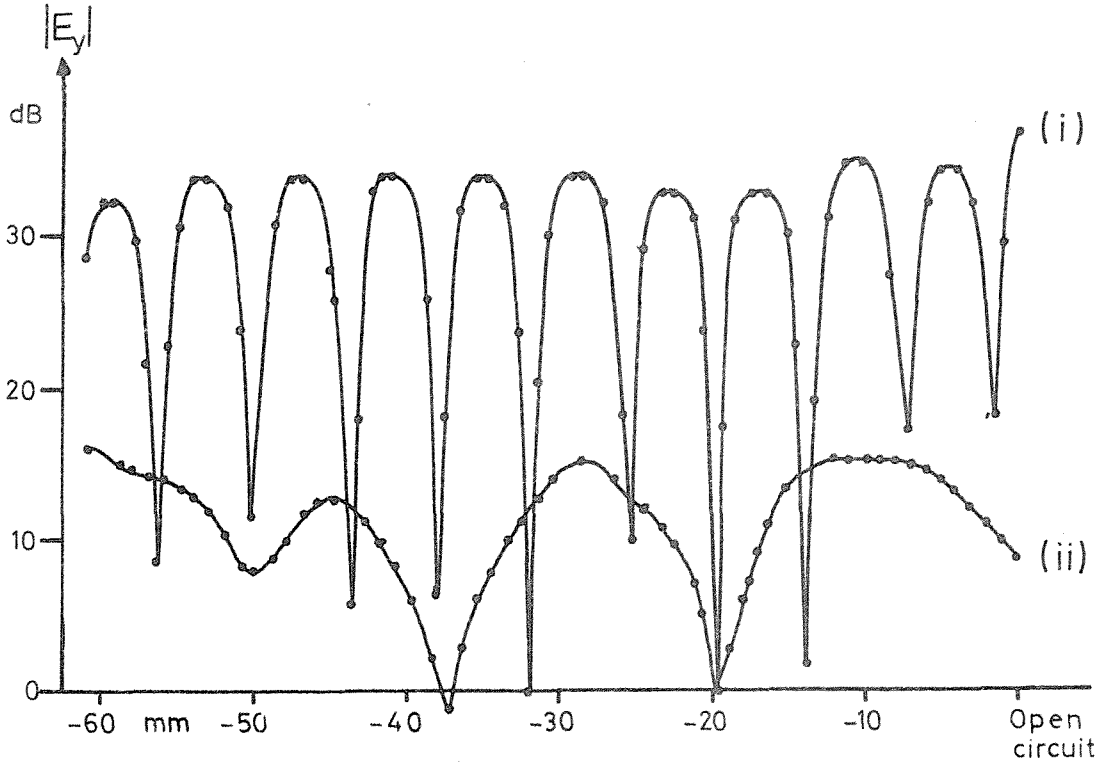

FIGURE 12. STANDING WAVES DETECTED USING THE MK. I. S.W.I.

(Sampling the vertical component of electric field above an O/C 50Ω line on alumina) 9.38 GHz

(i) Probe ~1mm above substrate

(ii) Probe ~15mm above substrate.

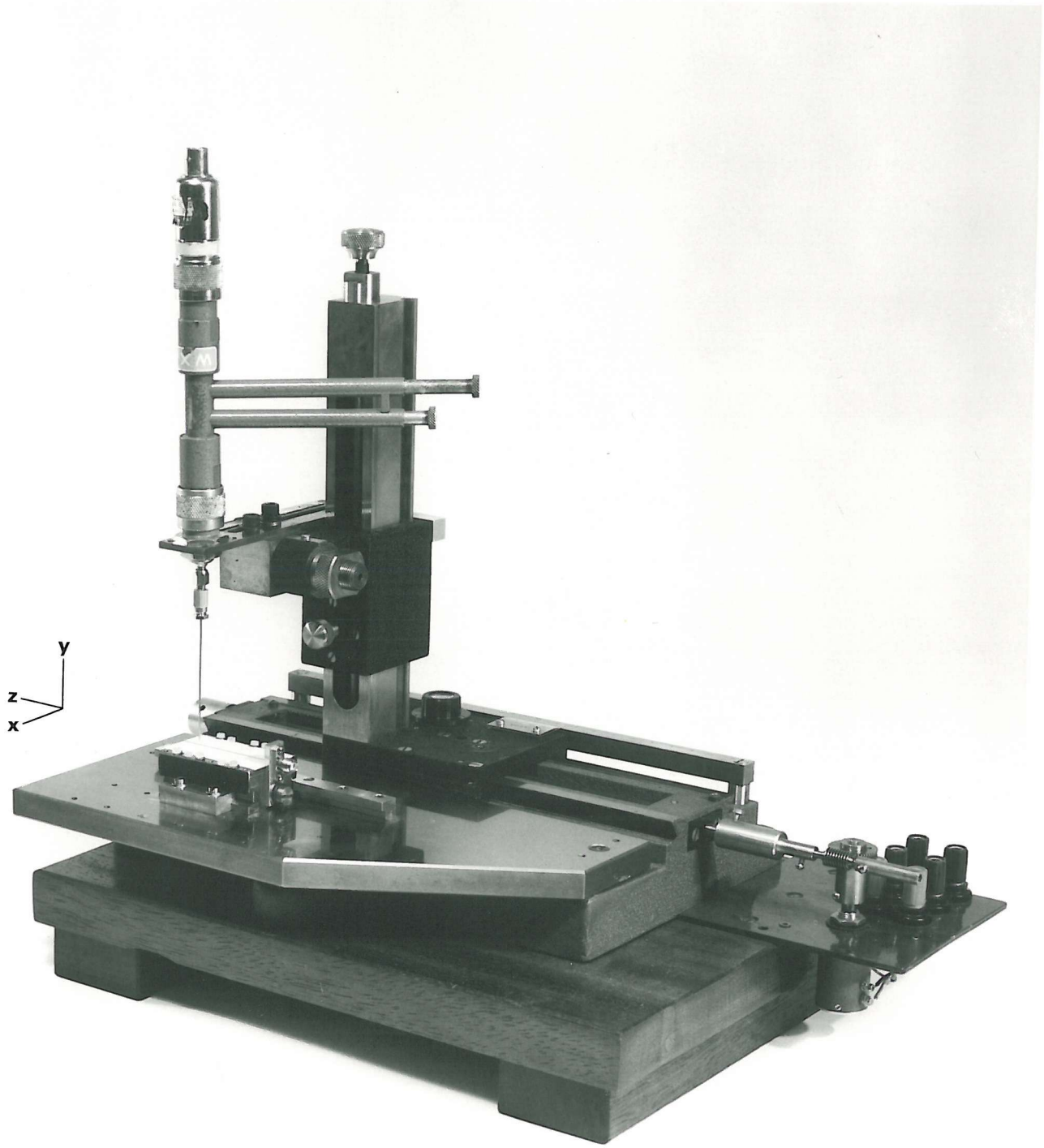

Figure 13. The Mk.II Microstrip Standing Wave Indicator

The substrate is held down by nylon screws overlapping along each edge – a method which allows fine positional adjustments to be made in order to set the microstrip line parallel to the line of travel of the probe. A fine lead-screw is used to drive the probe carriage in the z direction, and a potentiometer geared to this shaft provides a proportional voltage suitable for input to an X-Y plotter, which allows a standing wave pattern to be recorded directly. Detection is by means of a square-law crystal detector; a 2-stub tuner was used in conjunction with the probe to minimise probe reflections. The probes used consisted of 034† semi-rigid cable with Sealectro 'Conhex' connectors. The connectors were designed for a larger diameter cable but were the smallest coaxial connectors available at the time. They were found reasonably easy to mount on the small diameter cable, and T.D.R measurements indicated a V.S.W.R. for the connection comparable to that quoted for a pair of mated connectors (1.06 at 2 GHz and 1.18 at 10 GHz). The test procedure was to mount a connector on each end of a length of 034 cable and to examine this cable terminated in a 50 ohm load; Figure 14 shows a typical T.D.R. trace of the connector at one end of such a cable. If the test proved satisfactory the cable was cut up to form a pair of probes.

6.2 Standing Wave Indicator Measurements

Initial results obtained with the Mark II standing wave indicator showed similar irregularities in the standing wave patterns as had the previous model, in spite of the precautions taken in its design, but

---

† 034 cable : 50 ohm coaxial cable with an outer diameter of 0.034 in. or 0.86 mm.

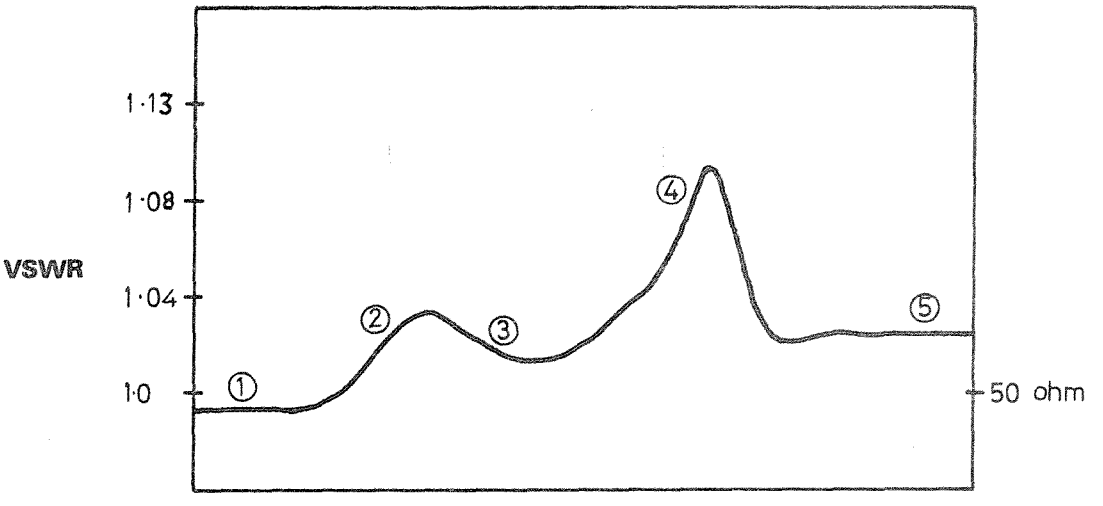

FIGURE 14. TIME DOMAIN REFLOMETER TRACE IN S.W.I. PROBE TEST

1 GR 14mm coaxial air line

2 GR - Type N adaptor

3 Type N - Conhex adaptor

4 Junction of 034 cable to Conhex connector

5 034 cable

experiments on alumina and sapphire substrates quickly showed that the irregularity was electrical and not mechanical in origin. Possible causes lay with the probe itself or else with radiation from either the launcher or the end of the line. T.D.R. measurements at an effective frequency of 2.3 GHz had shown that the probe had negligible effect unless it was actually touching the line, as Figure 15 illustrates. This behaviour was confirmed by standing-wave measurements at X-band using two probes; a static probe was used to monitor the signal on the generator side of the moving probe and showed a variation of less than $\pm$ 0.25 dB for all positions of the moving probe. Radiation as a cause of the irregularity in the standing wave pattern was at first ruled out, since experiments over a blank substrate had revealed a rapid decay of signal in front of the launcher, with no detectable signal over most of the substrate. A microstrip open-circuit does radiate, but radiation only from the end of the line could not explain the existence of the standing wave detected some distance above the substrate, the amplitude of which was also found to be frequency dependent. It later transpired that radiation from the launcher was the cause of the contamination, but until this became apparent work continued towards a fuller understanding of the fields associated with the microstrip line, and this will now be discussed.

Most of the following standing wave patterns were made on nominal 50 ohm, open-circuited lines on (Coors) alumina substrates, 0.64mm thick, and usually 25 x 51mm. The vertical component of the electric field along the centre of the line is shown in Figure 16 at 7,8,9,10 and 11 GHz, and it can be seen that measurement of standing wave ratio is completely impossible, although many of the minima are close to zero indicating little attenuation on the line. On this figure, and on several of those to follow, no vertical scale is shown; typically the maxima of the

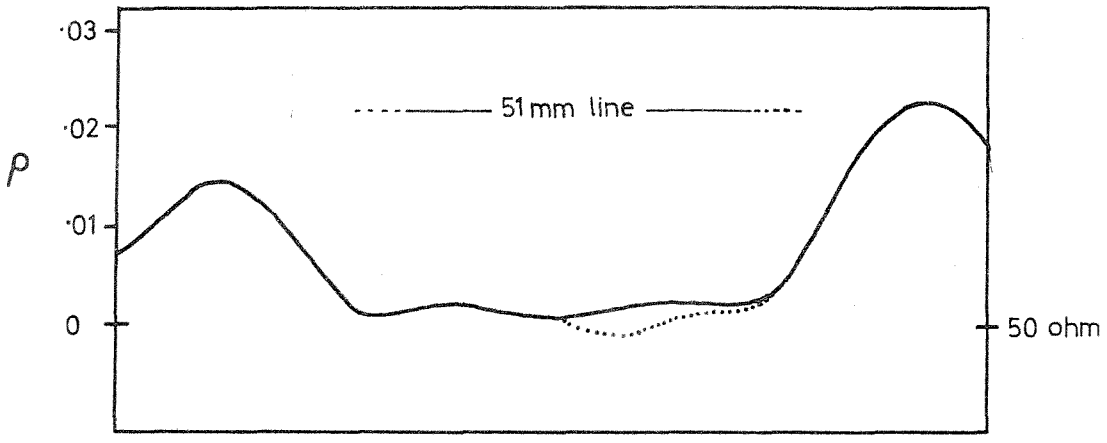

FIGURE 15. TIME DOMAIN REFLECTOMETER TRACE SHOWING EFFECT OF S.W.I. PROBE TOUCHING TOP CONDUCTOR

..... probe in contact with line

—— probe close to, but not in contact with line

(the same trace is observed when the probe is completely removed from the vicinity of the line)

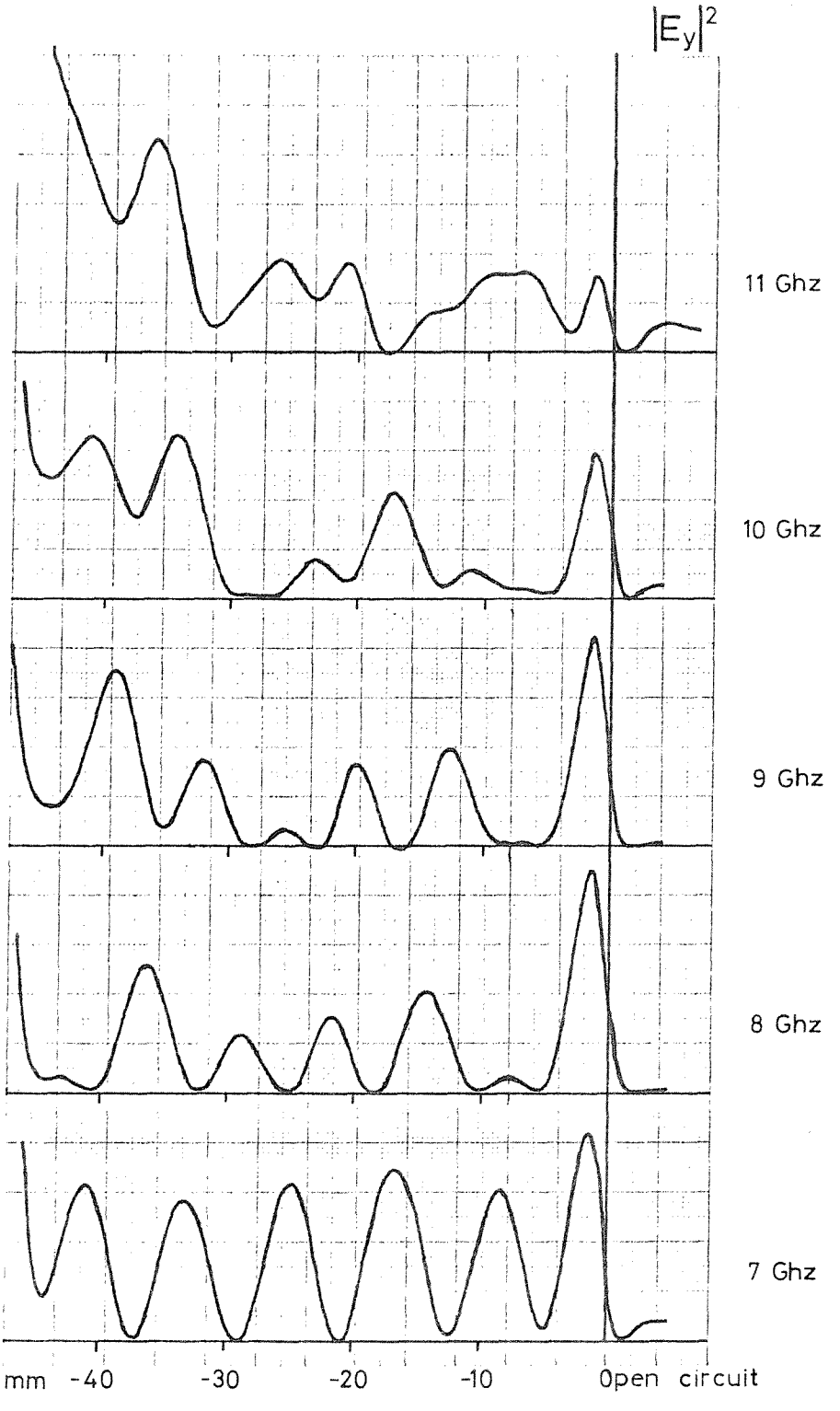

FIGURE 16. VERTICAL ELECTRIC FIELD COMPONENT OF STANDING WAVES ON OPEN-CIRCUIT LINE AT 7, 8, 9, 10, 11 GHz

(50 ohm line on alumina substrate, Mk.II. S.W.I).

standing wave patterns are 20-30dB above noise level. A more complete picture of the vertical electric field component above the substrate is seen in Figure 17; the shape of these curves arises from the field distribution shown in Figure 2, and thus it varies slightly with the height of the probe above the substrate. A standard height of 1.0 mm was used for these measurements. The existence of longitudinal electromagnetic field components in microstrip had been noted at much lower frequencies by Grüneberger[50], and these are readily observable at X-band. A vertical probe with its foot bent through a right-angle was used to detect the longitudinal component of electric field, and the measured field distribution above the substrate is shown in Figure 18; the large fringing field at the open circuit is very noticable, and as discussed in a later section this leads to uncertainty in the exact position of the electrical plane defining the open circuit. [The peripheral signal which is detected in certain positions either side of the centre peak, and which would appear to indicate a longitudinal electric field above the dielectric, was in fact due to spurious signals picked up by this probe as a result of its shape.] As expected, the longitudinal electric field is maximum at positions where the vertical (and transverse) fields are minimum.

The spatial relationship of the magnetic field components to the vertical electric field are shown in Figure 19. The magnetic fields were sampled using a vertical probe with a small magnetic loop at the tip, orientated to detect the desired field component. At zero frequency, the magnetic field forms single loops around the microstrip line, but at high frequency adjacent loops interact to give saddle-shaped loops with a longitudinal component, as sketched in Figure 20. This

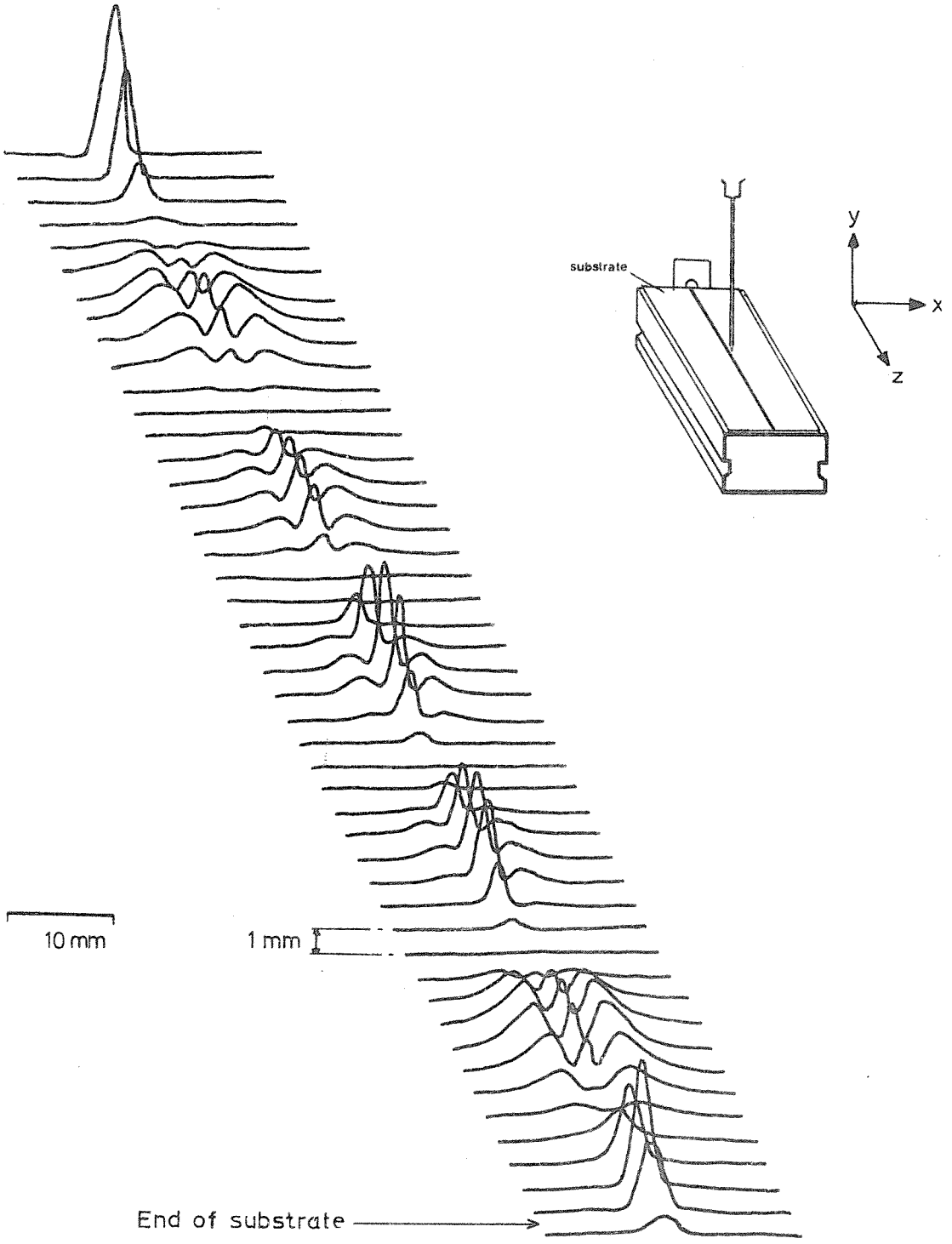

FIGURE 17. VERTICAL ELECTRIC FIELD AMPLITUDE $|E_y|^2$ ABOVE ALUMINA SUBSTRATE SUPPORTING O/C LINE. 7 GHz

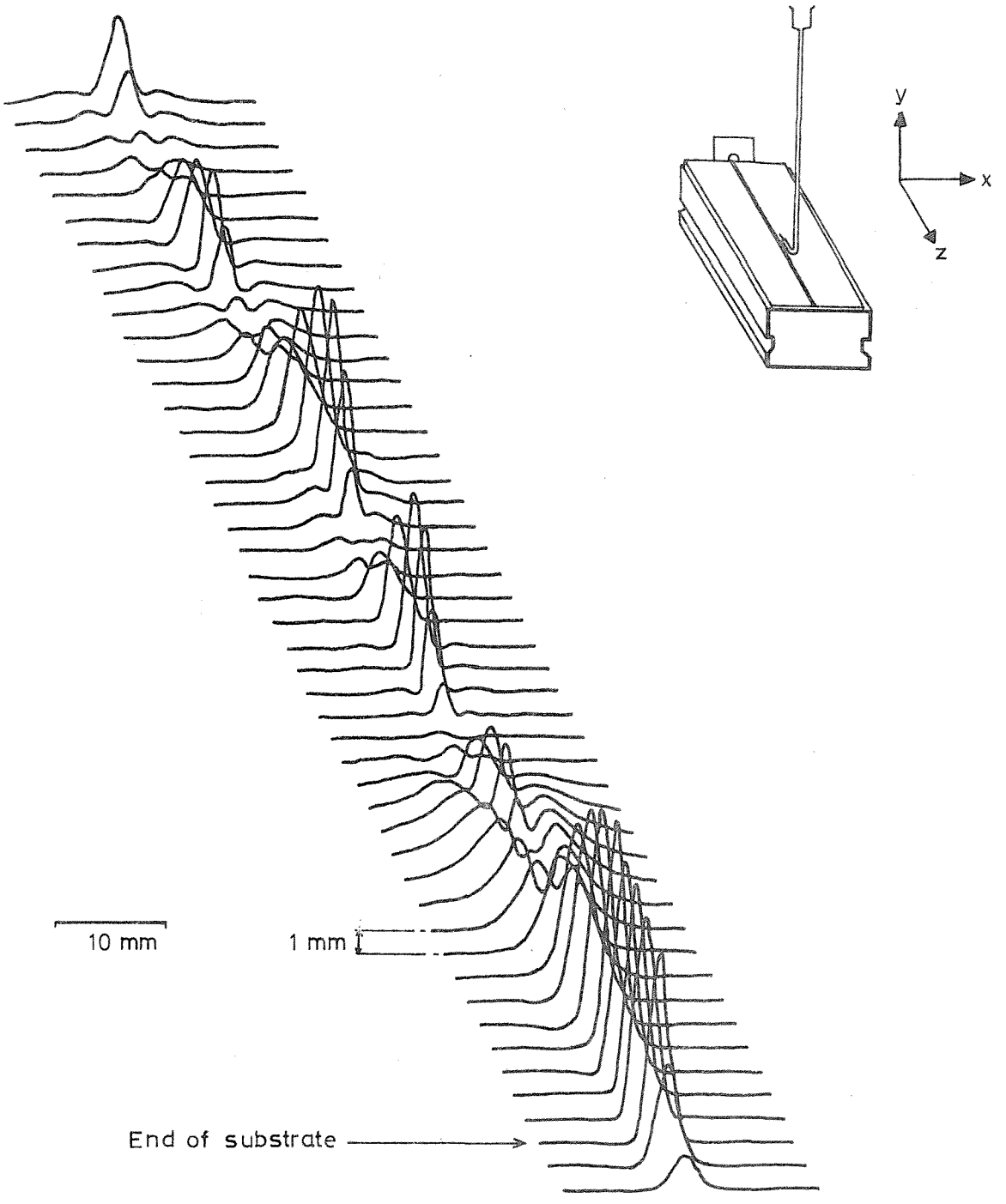

FIGURE 18. LONGITUDINAL ELECTRIC FIELD AMPLITUDE $|E_z|^2$ ABOVE ALUMINA SUBSTRATE SUPPORTING O/C LINE. 7 GHz

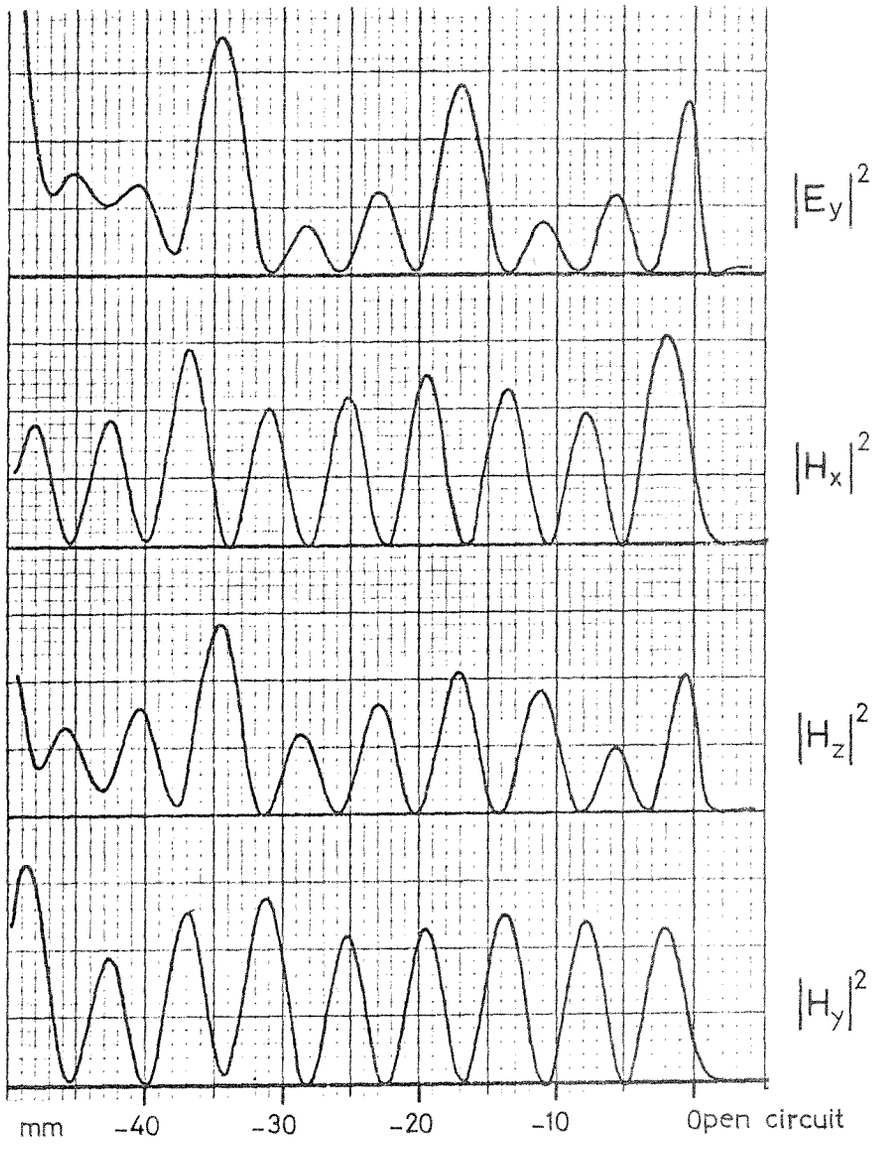

FIGURE 19. MAGNETIC FIELD COMPONENTS IN RELATION TO VERTICAL ELECTRIC FIELD. 10 GHz

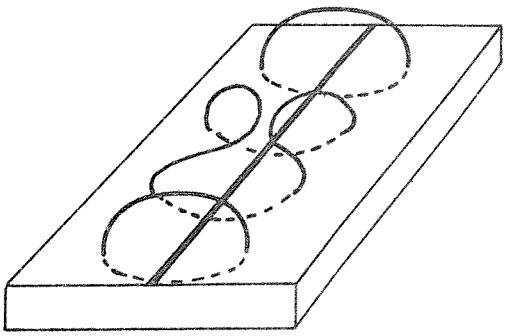

FIGURE 20. SKETCH OF LINKED MAGNETIC FIELD LOOPS WITH LONGITUDINAL COMPONENTS

explains the relationship between the magnetic field components shown in Figure 19: the vertical (H_y) and transverse (H_x) field components are in phase with each other, but out of phase with the longitudinal component (H_z). The magnetic probes had previously been checked in the known field at the end of a waveguide to ensure that they were not responding to the electric fields, and that this was the case is confirmed by Figure 19 where minima of the magnetic field patterns are detected in regions of high electric field.

The irregularity in amplitude of the standing wave patterns like those in Figure 19 has only a second order effect on the separation of adjacent minima in the standing wave, and thus it was possible to determine wavelength to within the limits set by this variation. Figure 21 is a graph of inverse microstrip wavelength ($\beta/2\pi$) versus frequency ($\omega/2\pi$) and shows the results of wavelength measurements on a number of nominal 99.5% alumina substrates from different manufacturers. For clarity error bars have been omitted, but it was found that for a particular substrate the average deviation of points from the best fit curve through the points was just over 1%. The overall spread of points in Figure 21 is approximately 6%, and this implies a variation in relative permittivity between the different substrates of 1-2%. Calculation of ε_r from the resonator measurements discussed later show a similar variation; substrates of relative permittivities between 9.5 and 11.1 have been measured.

In many of the standing wave patterns a periodicity of approximately $3\lambda_g$ was evident, which corresponds to the wavelength in air. Further experimental work using a signal generator capable of delivering higher output power allowed the amplitude of the standing wave minima to be

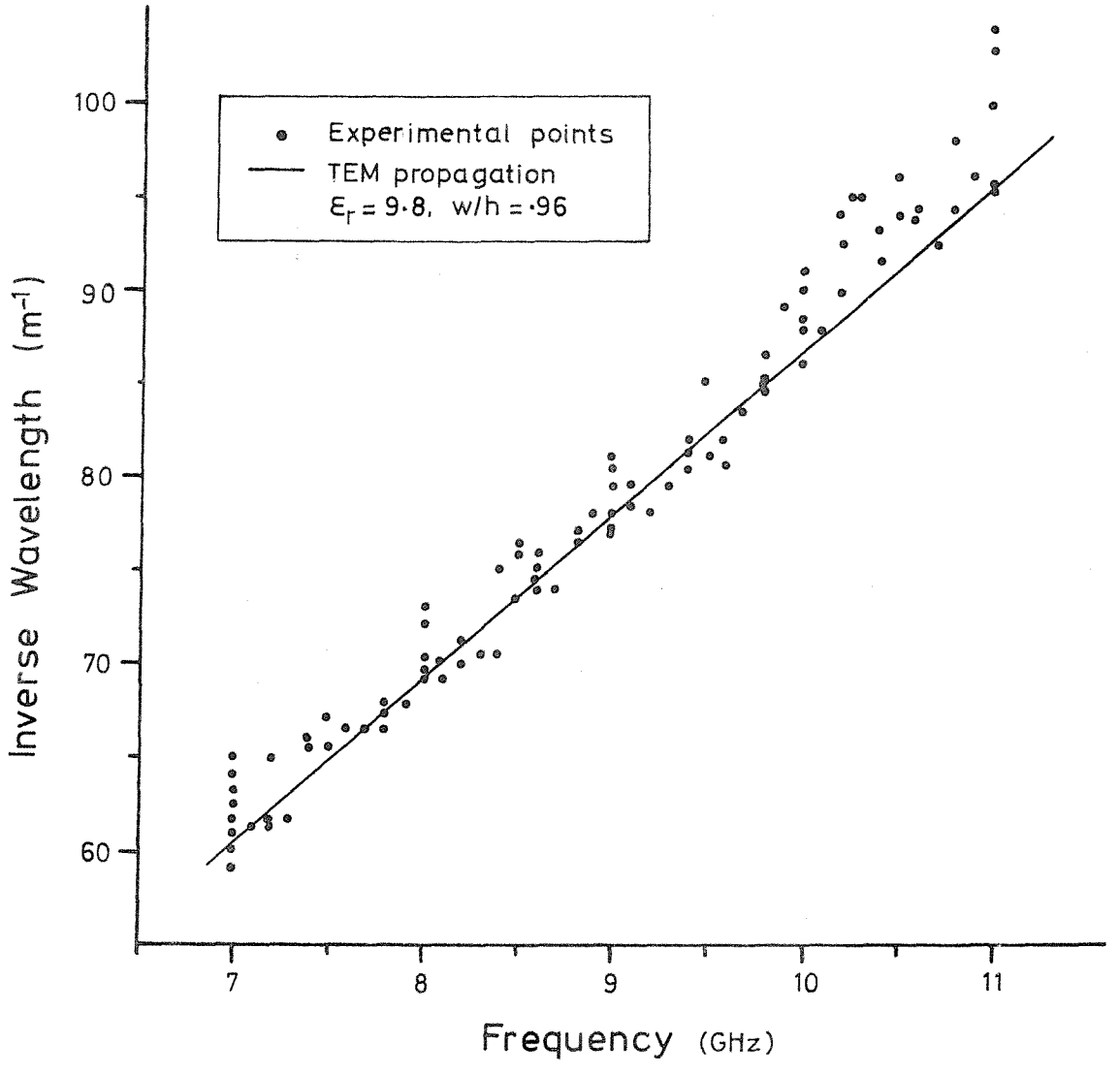

FIGURE 21. GRAPH OF INVERSE WAVELENGTH vs. FREQUENCY FROM MEASUREMENTS ON NOMINAL 99.5% ALUMINA SUBSTRATES.

The line is a calculated value based on Wheeler's theory.

studied more closely, and revealed that a second signal was indeed present. Figure 22 (a) shows a normal standing wave pattern on an open-circuited line, with evidence of the exponential decay of the field close to the launcher. Figure 22 (b) is a repeat of the first plot except that maximum generator power was used. (The signal amplitude has been deliberately limited in the detection stage). The variation in amplitude of the minima in Figure 22 (b) points to the existence of a low amplitude standing wave of wavelength approximately $3\lambda_g$. The signal detected beyond the end of the substrate is due to radiation from the open-circuit, which takes the form of almost symmetrical lobes front and rear, and clearly this radiation cannot account for the observed phenomenon. Assuming that the irregularity in the standing wave patterns was merely due to the superimposition of two standing waves of different wavelengths and amplitudes, there existed the possibility of simulating the experimental standing wave pattern by a function of the form

$$f(z) = \left| A \cos(\beta_1 z) + B \cos(\beta_2 z + \zeta) \right| \qquad (26)$$

with $\beta_1 / \beta_2 = \sqrt{\varepsilon_{eff}}$ and z the distance along the line.
Trial and error methods were used to determine value of the ratio A/B and the phase difference ζ which gave the best match to one of the measured standing wave patterns, that shown in Figure 23. The dotted curve is the theoretical curve which has been superimposed on the measured curve, and it can be seen that there is very close agreement between the two. Thus the assumption appeared to be valid.

The origin of this standing wave of wavelength λ_o was still in doubt; the fact that it was a standing wave with zero minima ruled

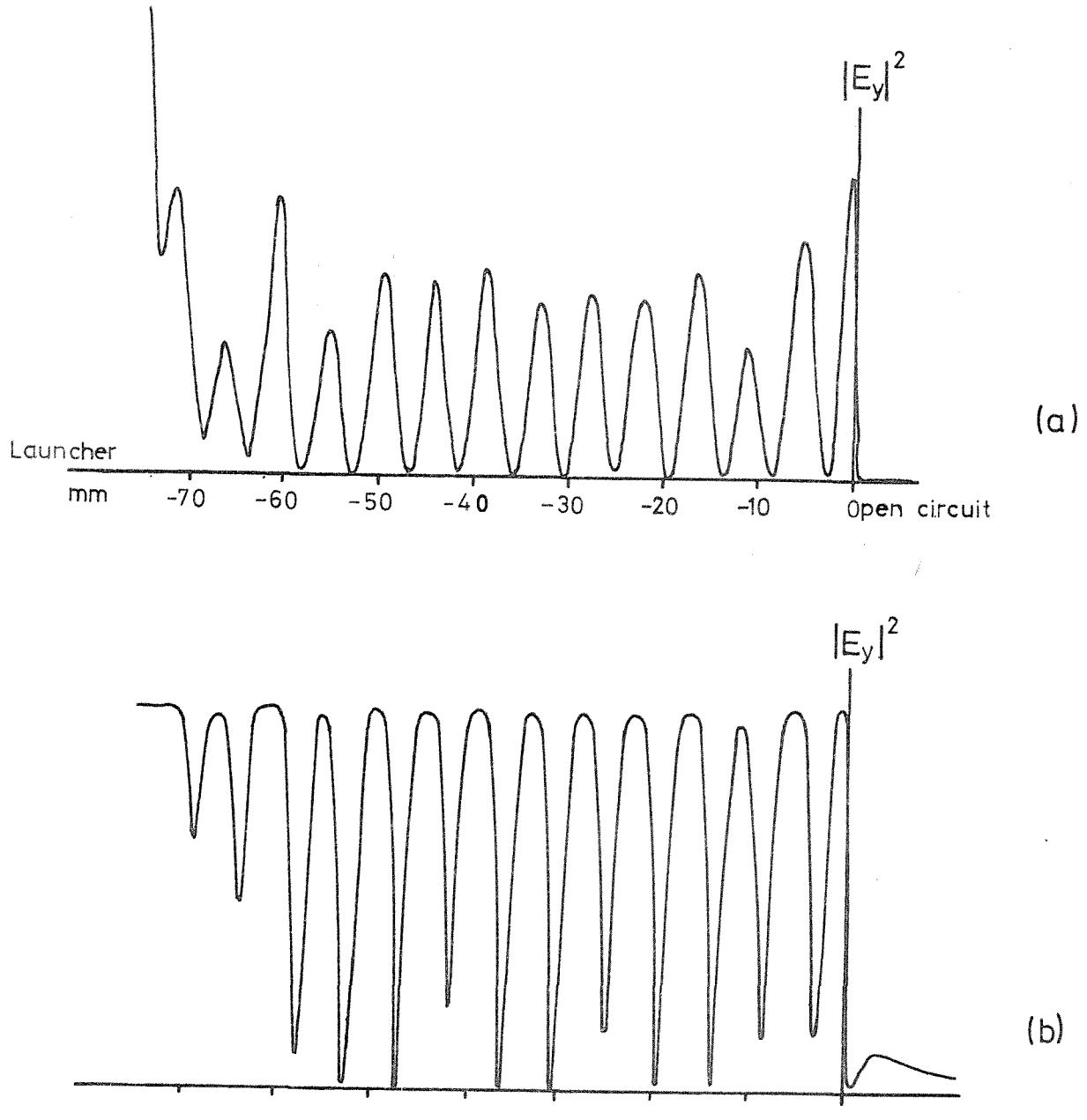

FIGURE 22. (a) NORMAL STANDING WAVE PLOT ON O/C LINE

(b) AS (a) BUT WITH INCREASED POWER INPUT (the detector is limiting at the maxima)

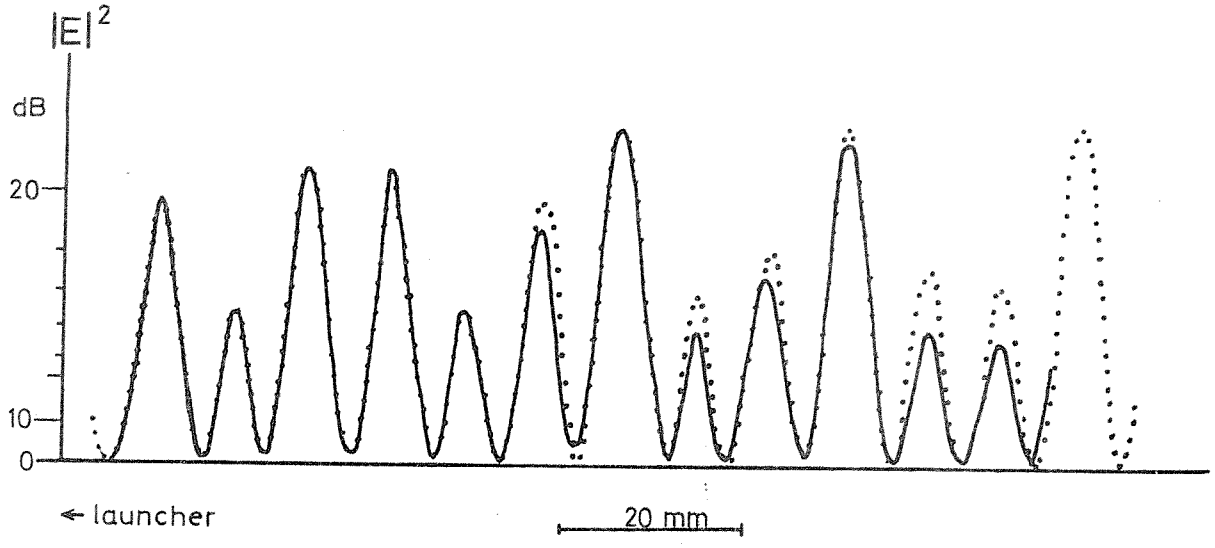

FIGURE 23. CALCULATED ELECTRIC FIELD AMPLITUDE (DOTTED CURVE) GIVEN BY

$$f(z) = \left| A \cos \beta_1 z + B \cos(\beta_2 z + \zeta) \right|$$

SUPERIMPOSED ON OBSERVED STANDING WAVE PATTERN, (SOLID CURVE)

$A/B = 5 \qquad \beta_1 / \beta_2 = 2.7$

out the existence of any wave supported by the dielectric alone, since any such wave was unlikely to undergo 100% reflection at the end of the substrate. As more standing wave plots were made, it became apparent that the observed pattern depended on the probe used. This can be seen by comparing the $|E_y|$ plot at 10 GHz in Figure 16 with that in Figure 19 - two plots made with different probes as the standing wave indicator evolved.

Experiments were therefore carried out using a separate probe, 100 mm long,

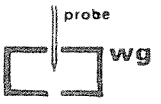

which could be inserted right through a section of rectangular waveguide with slots in the centres of the broad faces. As the probe was inserted slowly into and on through the waveguide, signal was detected in the probe not only when the tip was at the centre of the guide but also at other positions regularly spaced along the length of the probe. This showed that the outer conductor of the probe was supporting a standing wave, which was found to be of wavelength λ_o. Here then was the contaminant of the standing wave patterns. Further work was carried out to determine whether the microstrip launcher was the source of standing waves on the probe. A microstrip line on the SWI was terminated in a coaxial sliding short circuit, and by this means it was found that the electric field strength measured with the probe some distance above the substrate was dependent on the voltage and current conditions at the launcher; radiation was detected only when a current antinode occurred at the launcher, and this explained the negative result obtained previously on a blank substrate. As a further check on this finding, a second experiment was carried out on a blank substrate, but this time with and without a small piece of foil short-circuiting the centre-pin of the launcher to ground. The results are

shown in Figure 24: with the foil in place current at the launcher is maximum and a large radiation field is observed; without the foil the radiation is negligible. The frequency dependence of the observed radiated field was now also explained; with an open-circuited microstrip line, a current antinode occurs at the launcher whenever the line is an odd number of quarter wavelengths long, which for a 51mm line is every 1.1 GHz.

The problem now was to minimise the effect of this radiation on the probe. This was achieved by using a sheath of Polyiron (a solid epoxy/iron microwave absorber) in the form of a 12mm diameter rod machined out to take the probe and connector, which left only the tip of the probe unshielded. This, together with a piece of polyiron in front of the launcher, resulted in standing waves of greatly improved uniformity. A further improvement was achieved by reducing the height of the probe above the substrate, thereby increasing the relative strength of the microstrip field. Standing wave patterns observed with this new method are shown in Figure 25, in which the improvement is immediately apparent (c.f. Figure 16). Figure 25 actually shows results obtained on a sapphire substrate, but the improvement is entirely due to the shielding of the probe, and not to the substrate.

Further measurements of wavelength were made from standing wave patterns in which the full gain of the generator was used to sharpen the position of the minima and thus increase the measurement accuracy. An example of one of these plots is shown in Figure 26; it can be seen that some of the minima are not quite zero which indicates that the radiated wave has not been completely attenuated. As a result the wavelength measurements taken from these standing wave patterns show a slight periodic fluctuation, as can be seen in Figure 27. The fluctuation is, however, small and within the $\pm 1\%$ accuracy of the measured points, which are found to follow closely the expirical curve

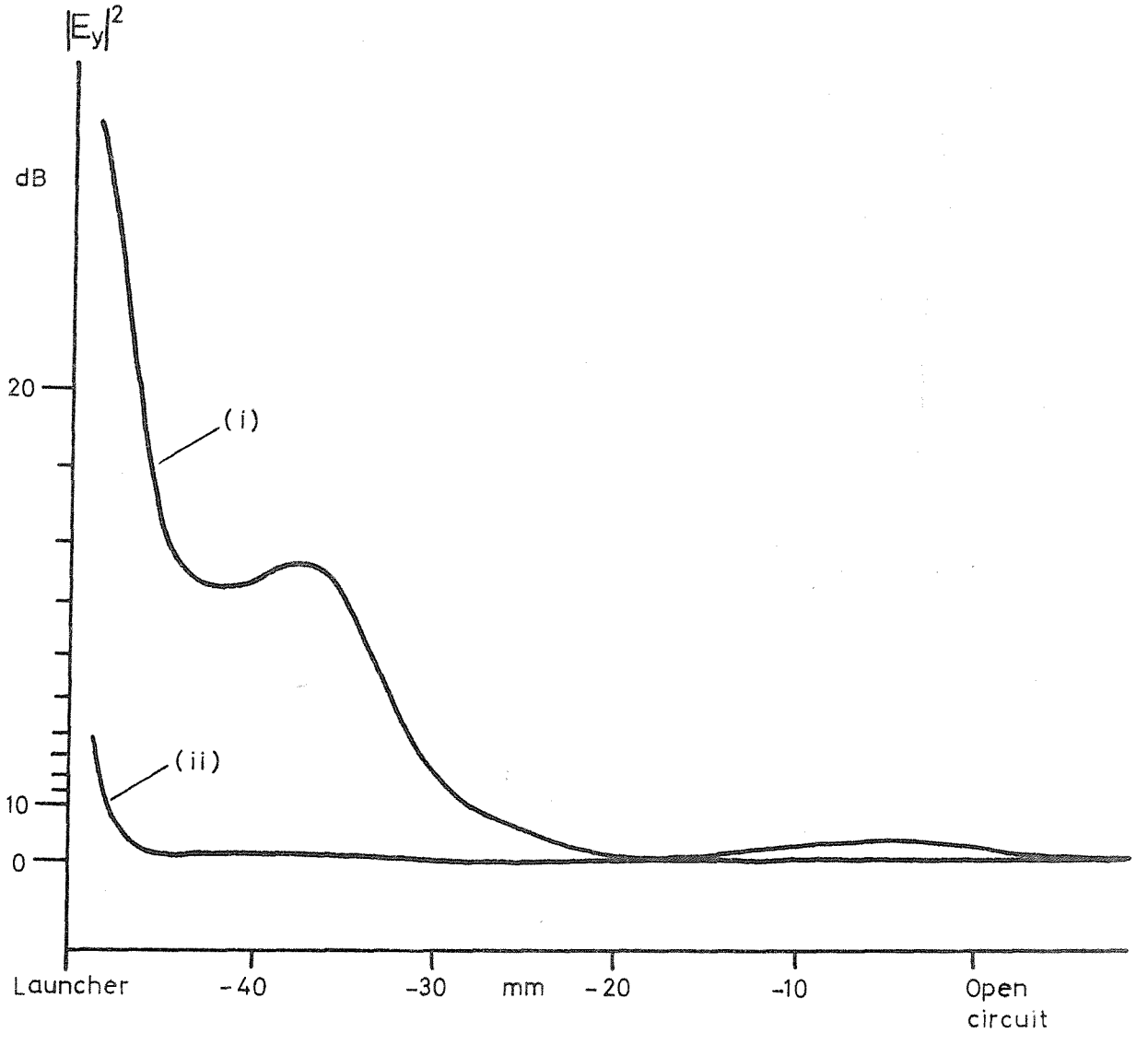

FIGURE 24. RADIATION FROM MICROSTRIP LAUNCHER.

AMPLITUDE OF VERTICAL ELECTRIC FIELD ABOVE BLANK SUBSTRATE WITH

(i) foil used to create short-circuit at launcher

(ii) launcher used normally

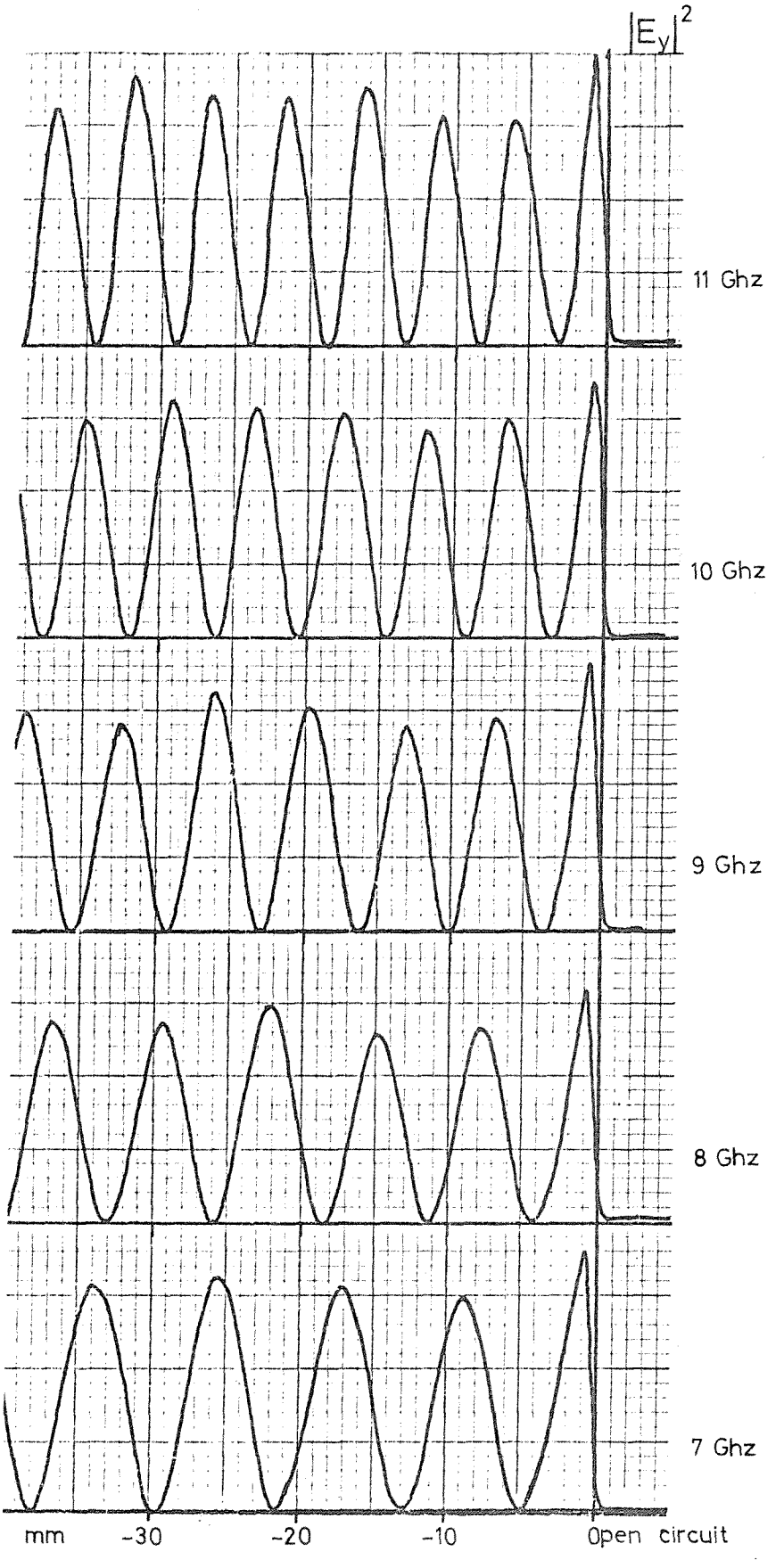

FIGURE 25. IMPROVED STANDING WAVES PATTERNS AFTER SHIELDING PROBE AND REDUCING PROBE HEIGHT TO 0.2mm. Vertical electric field component at 7,8,9,10,11 GHz, 50 ohm line on sapphire.

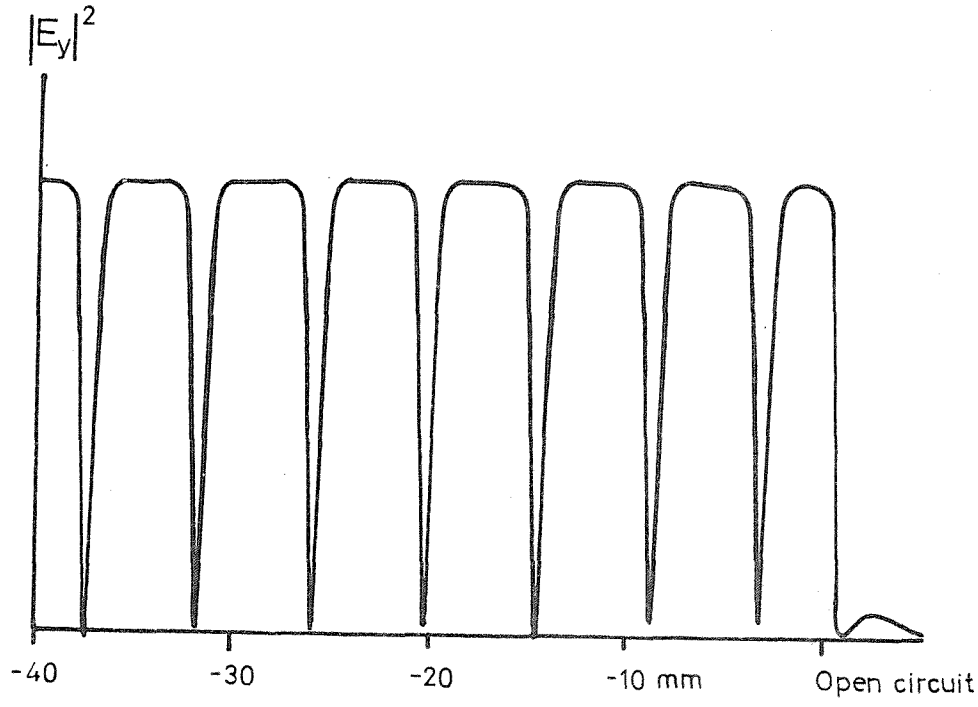

FIGURE 26. IMPROVED STANDING WAVE PATTERNS ON ALUMINA, USING MAXIMUM SYSTEM GAIN

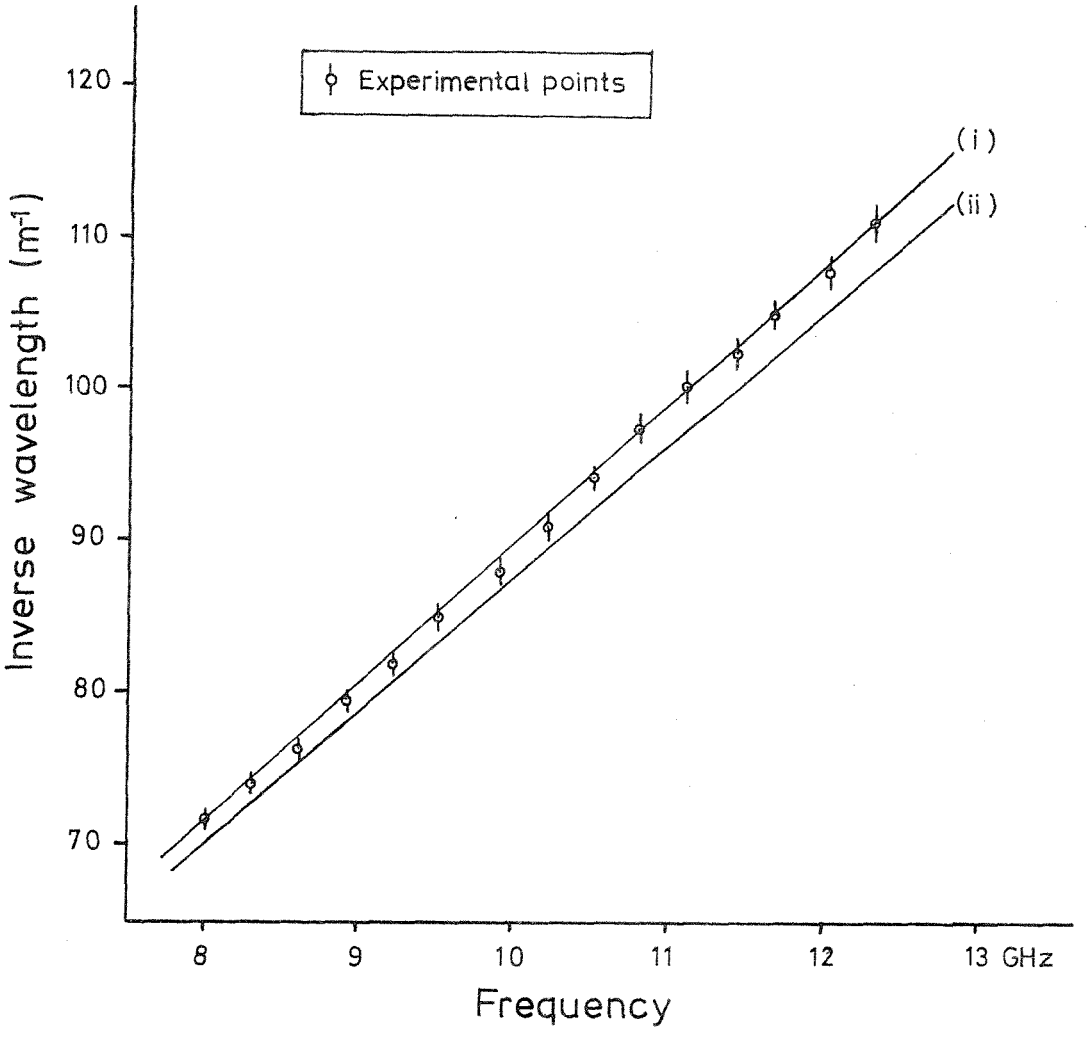

FIGURE 27. INVERSE WAVELENGTH vs. FREQUENCY FOR COORS ADS 995 ALUMINA, FROM MEASUREMENTS ON PLOTS SIMILAR TO FIGURE 26

(i) Curve based on empirical expressions of Jain/Arnold with $\varepsilon_r = 10.1$

(ii) Line based on Wheeler's results, $\varepsilon_r = 10.1$

of Jain et al[25] for $\varepsilon_r = 10.1$.

One disadvantage incurred with the improved system was that undulations in the substrate surface now had a noticeable effect on the standing wave pattern. At the previous probe height of 1.0mm the detected signal varied at a rate of 1dB per 0.1mm change in height, but at the new height of 0.2mm the signal varied at about twice this rate. Using a sapphire substrate, which exhibits less surface irregularity than alumina, some correlation was noted between the surface profile of the substrate and the measured standing wave pattern. In Figure 28(a) the amplitude of each maximum in the standing waves of Figure 25 has been normalised and plotted in its correct position relative to the end of the line; Figure 28(b) shows the surface profile of the substrate just to one side of the line, and its similarity to the distribution of points in Figure 28(a) is clear. The same procedure was attempted for an alumina substrate, but the irregular nature of the surface made any correlation impossible.

At this stage it was decided to review the situation over the standing wave indicator, and the salient points are summarised below.

6.3 Summary of standing wave indicator measurements

(1) It had proved possible to obtain reasonably uniform standing wave patterns from which the microstrip wavelength could be determined to within $\pm$ 1%.

(2) For measurements of low V.S.W.R's it would be necessary to correct these patterns for variations in substrate profile, and to do this successfully sapphire substrates would be required.

(3) The effects of the increased bulk of the probe and the Polyiron in front of the launcher on the standing wave patterns had yet to be assessed.

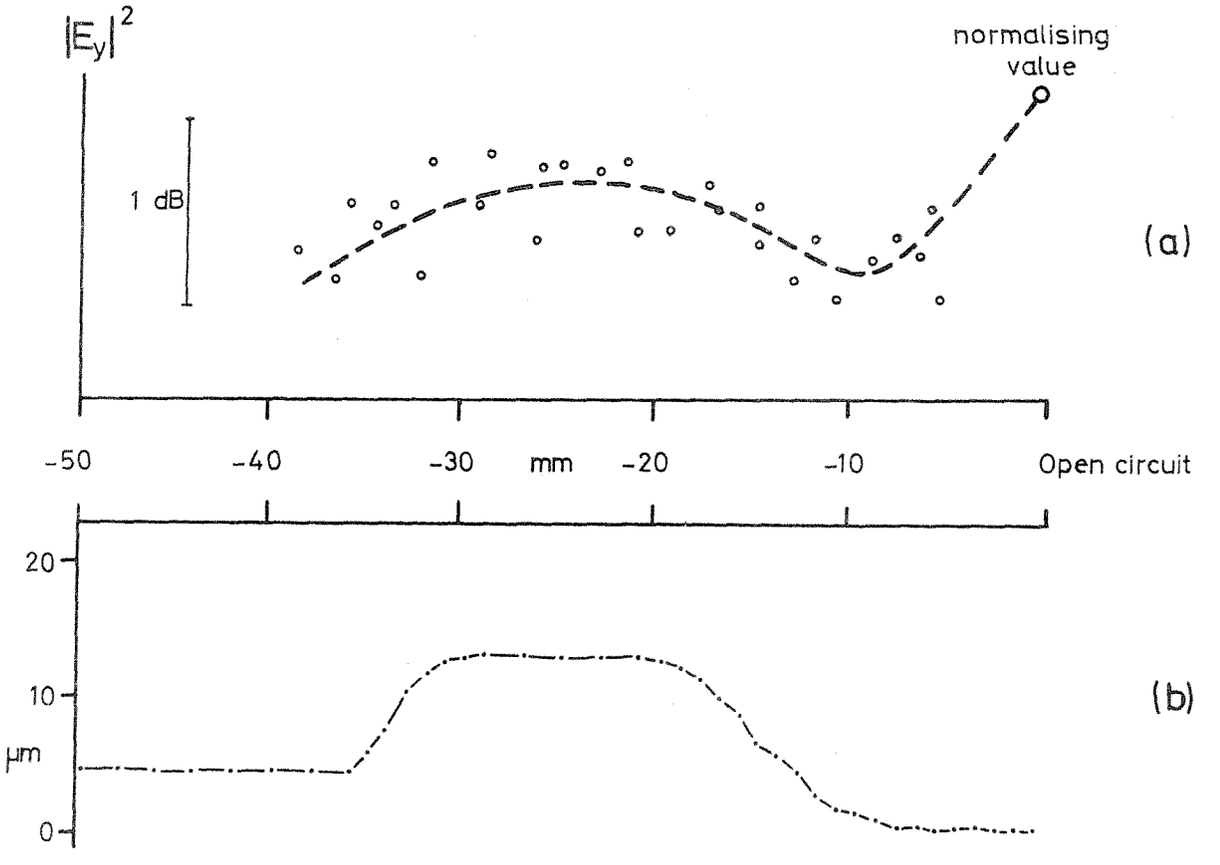

FIGURE 28. (a) Amplitude of standing wave maxima (∘) of Figure 25, normalised and plotted in their correct position. The dotted line illustrates the trend.

(b) Surface profile of the sapphire substrate on which the standing waves of Figure 25 were observed, parallel to the top conductor.

(4) An appreciation of the physical distances involved in determining the reference planes of microstrip discontinuities showed that the sheer size of the probe would pose limitations. For example, the electrical plane of an open-circuit is ~200μm beyond the end of the line on a 0.64mm substrate, but the diameter of the inner conductor of the probe was 125μm. Even using the smallest semi-rigid cable available, with an outer diameter of 125μm, the inner conductor would still be 50μm in diameter.

These factors, together with an awareness of the simplicity and accuracy of resonator measurements, and of the possibility of using coaxial probes for coupling to them, led to work on the standing wave indicator being dropped in favour of further study of resonant structures in microstrip.

7. MICROSTRIP RESONATORS

The use of resonant cavities in waveguides as a microwave measurement technique led to similar methods being applied to planar lines[51]. Measurement of the resonant frequency of a line of known length allows the phase velocity to be calculated (assuming the wavelength is known approximately), and measurement of the Q factor enables losses to be determined. Difficulty arose in applying these techniques to microstrip since a good short-circuit termination is difficult to manufacture and an open-circuit is not located at the geometric end of the line, and both types of termination are lossy. Accurate calculations can be made using several lines in order to eliminate the effect of the termination, but a better solution was proposed by Troughton[52] in 1968, namely the use of ring resonators. There are no terminations to introduce error in a ring resonator, and with a large ring there is negligible radiation loss and the curvature of the ring can be ignored. The advantage of resonator methods of either type is that apart from physical length, the only measured quantity is frequency. For Q measurements it is also necessary to be able to accurately detect a 3dB change in the transmitted power, but the method is unaffected by reflections from the launcher provided these are constant over the narrow frequency band of the resonance curve, wherein lies its superiority over other methods. The use of resonators allows the phase velocity and line attenuation to be found directly, and it is a valuable technique in the study of small discontinuities, since any disturbance introduced into a resonator can cause a shift in resonant frequency which yields quantitative information on the discontinuity.

7.1 Coupling techniques for Microstrip Resonators

Experience with the standing wave indicator led to the investigation of coaxial probes above the substrate as a means of exciting microstrip resonators. Troughton[52,53] and others had used microstrip probes either side- or end-coupled, and trial and error techniques were required initially to set the probes for optimum coupling. It was found that coaxial probes did behave satisfactorily, and that they had certain advantages over microstrip probes.

The greatest advantage was the flexibility of movement which they allowed: with the probes in manipulators above the substrate both the degree of coupling and the point of excitation could be altered with ease, and the whole of the substrate was accessible. At the present state of the art when basic microstrip characteristics are still under investigation these advantages are considerable.

One problem with the coaxial probes was standing waves on the outer conductor of the probe caused by radiative coupling - an effect noted previously with the standing wave indicator. In practical terms it was found that, with the probes close together in the absence of a substrate, the swept frequency response showed broadband resonances related to the length of the probes. The solution adopted for the standing wave indicator of completely shielding the probe and its connector was not suitable in these circumstances, as the bulk of the shielded probes would counteract all the advantages inherent in the method. Experiments showed that this coupling could be reduced by using magnetic loops sampling the vertical magnetic field component and by maintaining the probes at least 10mm apart. The use of a small cylinder of flexible absorber threaded onto the probe also helped to attenuate the directly coupled signal, and with care in carrying out measurements it was quite

possible to ensure that this coupling normally had no significant effect. It is known that a small dipole above a grounded dielectric can lead to the excitation of surface waves[23], but no transmission across a blank substrate has been observed using either E or H coupling probes. It is interesting to note, however, that coupling probes sampling the vertical magnetic field are found to behave most satisfactorily, and that the only non cut-off surface wave - the TM_o mode - has no vertical magnetic field component.

In order to couple into a resonator at all the coupling probes must introduce some loading, but it is possible to ensure that the loading is small or even negligible by using very loose coupling. If the measured Q factor is designated Q_m, and the coupling coefficients of the probes are g_1 and g_2 then

$$Q_o = Q_m (1 + g_1 + g_2) \qquad (27)$$

where Q_o is the Q factor of the resonator, whether a line or a ring, in the absence of coupling probes. For a resonator with no radiation loss Q_o is equal to Q_c, the Q factor associated solely with line attenuation (mainly conductor loss); for a resonator which does radiate, Q_o is related both to Q_c and to Q_r, the Q factor associated solely with radiation loss. Normally with coaxial probes the coupling coefficient is set the same for each probe ($g_1 = g_2 = g$) and can be found from the transmitted power loss through the resonant system, T, since[54]

$$T = \frac{4 g^2}{(1 + 2g)^2} \qquad (28)$$

T as a function of g is shown in Figure 29. It was found experimentally that a transmission loss > 30 dB could be tolerated, and hence the measured Q factor, Q_m, is within 3% of Q_o.

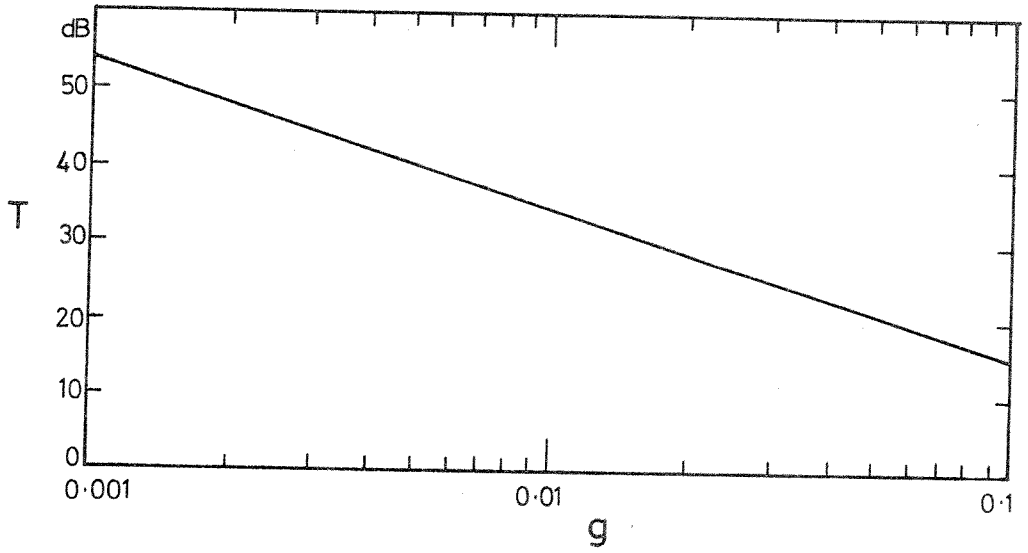

FIGURE 29. RELATIONSHIP BETWEEN THE TRANSMITTED POWER THROUGH A RESONATOR (T) AND THE COUPLING COEFFICIENT (g) OF SYMMETRICALLY COUPLED PROBES. (eqn.27)

7.2 Procedure for resonator measurements

Transmission measurements have been made on microstrip resonators, using a swept frequency source for qualitative assessment of the resonance curve and a single frequency source for quantitative measurement. At resonance the transmitted power is a maximum; the Q factor is found by noting the two frequencies at which the transmitted power falls by one half - the so-called 3 dB points. Figure 30 is a block diagram of the equipment.

The input probe is connected directly to the directional coupler to avoid the use of flexible cables in the r.f. line, and the substrate and output probe are mounted on XYZ manipulators. Figure 31 shows the arrangement. Care was taken to isolate the probes and substrate from excessive vibration which can affect the coupling.

Using a swept frequency signal a resonance is located and the curve of transmitted power vs. frequency is displayed on the oscilloscope, on whose screen an ideal Q curve is permanently outlined. Comparison of the two reveals any gross distortion in the experimental curve and allows the positions of the probes to be optimised. Figure 32 (a) shows the response of a ring resonator over 8-12 GHz, for which the probes were not optimally set. The first resonance peak is shown expanded in Figure 32 (b), and resembles closely the ideal resonance curve. The effect of direct coupling between the probes is seen at the bases of the second and fourth resonance peaks in (a), and results in a mis-shapen resonance curve as in the upper part of (c). By suitably adjusting the positions of the probes, direct coupling between them may be reduced and an improved curve obtained, as shown in the lower part of Figure 32 (c). The resonance splitting at the third peak in (a), shown magnified in (d), is discussed further in section 9.2;

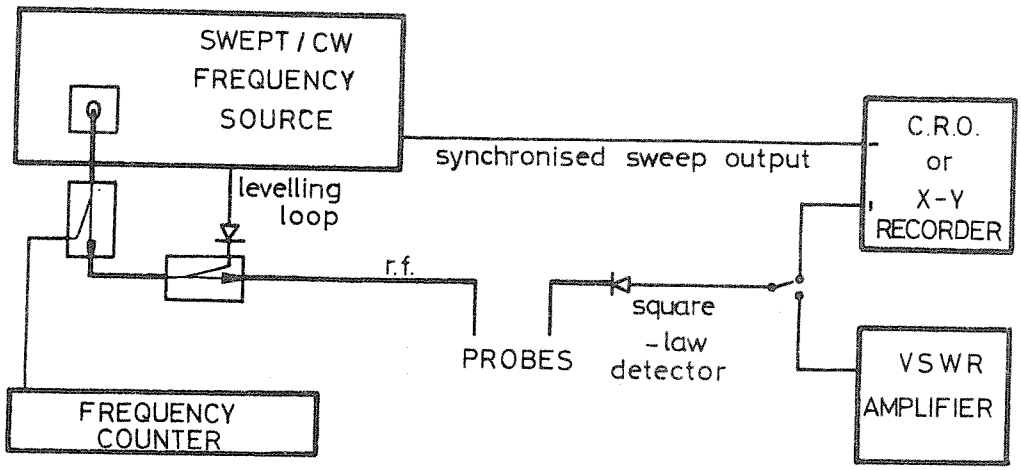

FIGURE 30. BLOCK DIAGRAM OF EQUIPMENT USED FOR RESONATOR MEASUREMENTS

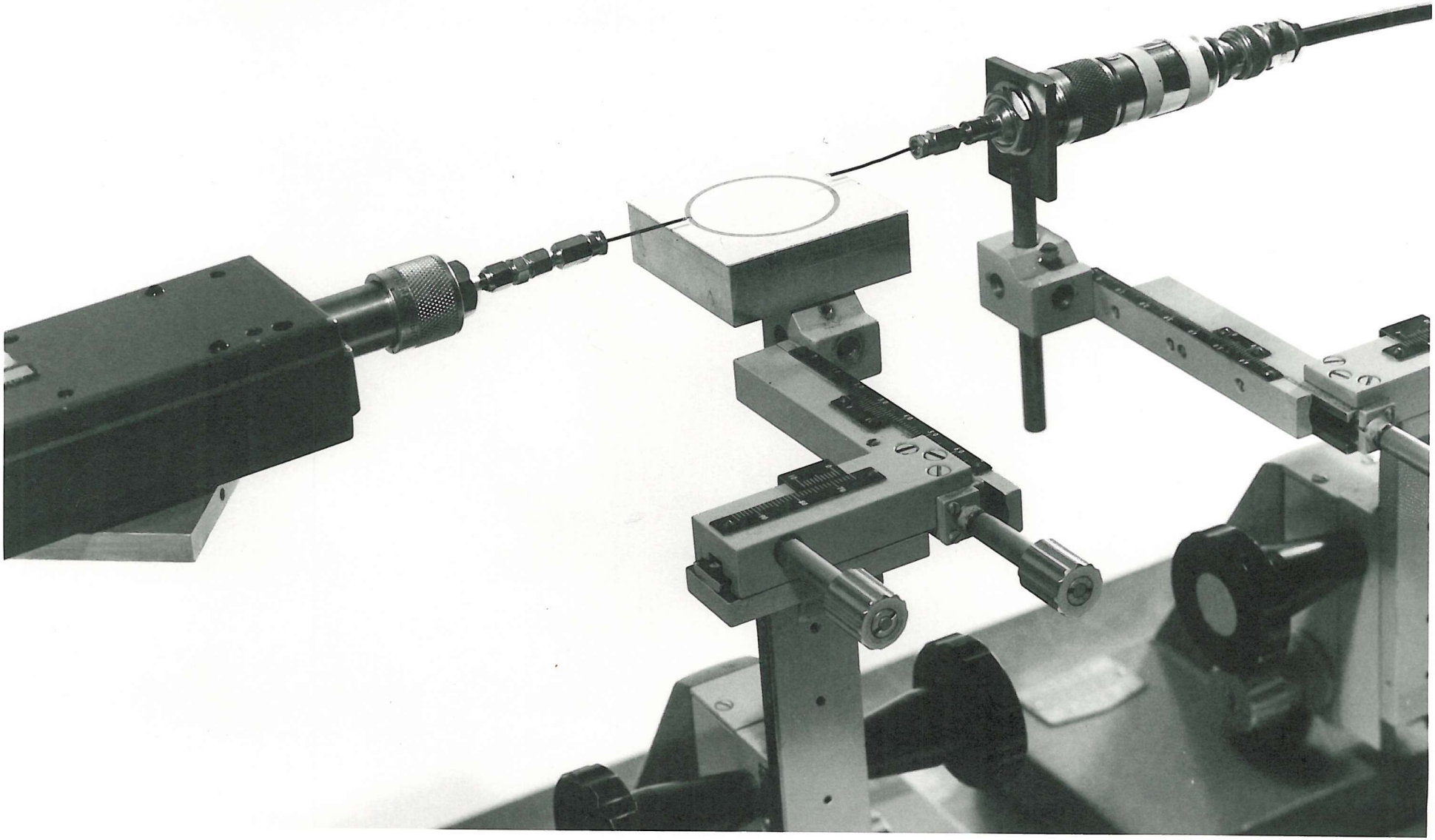

Figure 31. Arrangement of coaxial coupling probes above a resonator

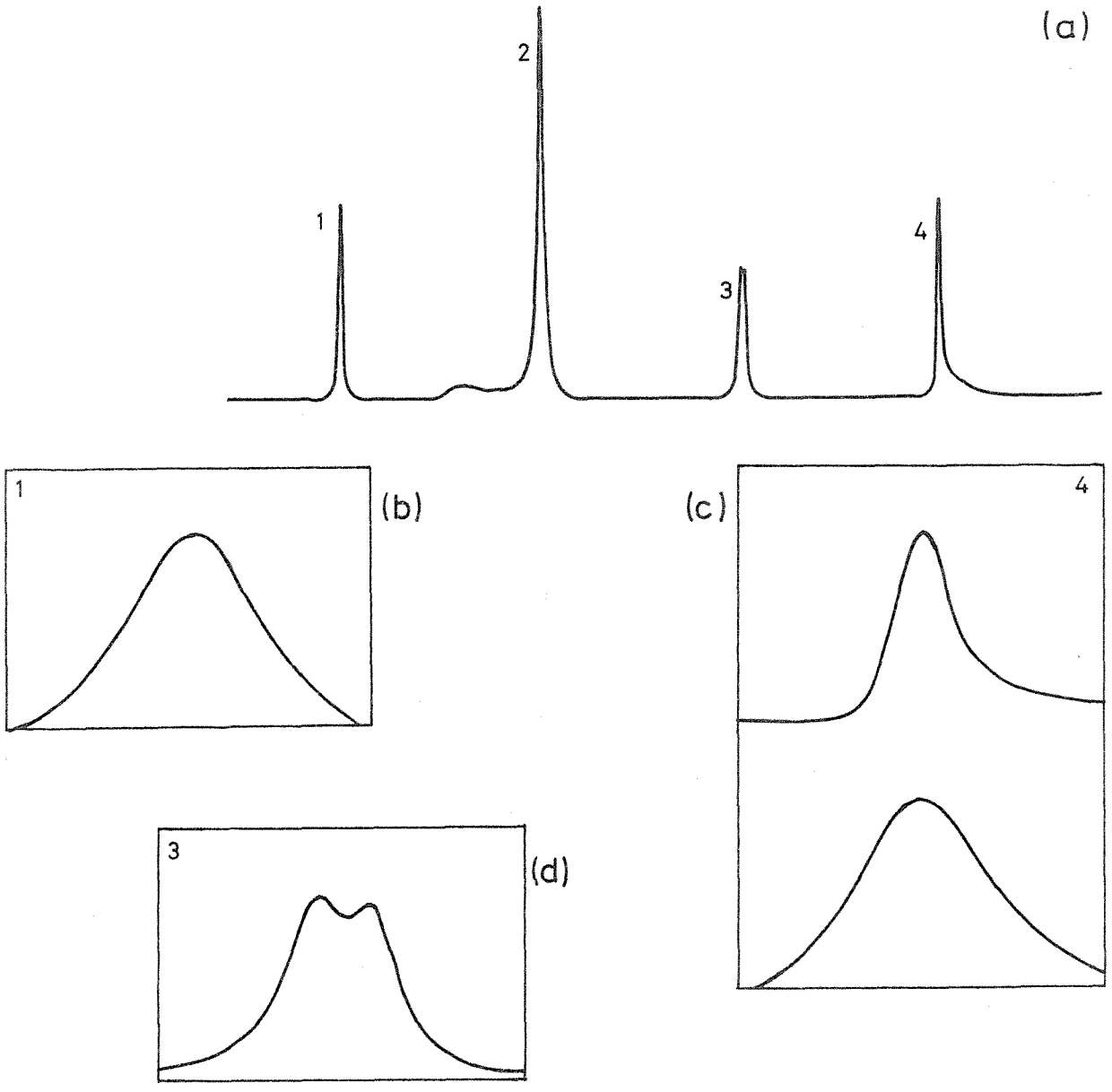

FIGURE 32. (a) Broadband response of microstrip resonator, with coupling probes not optimally placed

(8 - 12.4 GHz sweep)

(b) Expanded view of resonance peak 1.

(c) Expanded view of resonance peak 4 before (top) and after (bottom) probes were optimally positioned.

(d) Expanded view of resonance peak 3 showing resonance splitting.

it is usually possible to adjust the positions of the coupling probes to detect only one of the two peaks. Once the best resonance curve has been obtained, the generator is switched to C.W. and modulated at 1 kHz, and the output of the detector switched to the VSWR amplifier. This allows the 0 and 3 dB power levels to be set, at which the frequency is measured using a digital counter.

In considering the accuracy of this or any other system, it is necessary to differentiate between errors inherent in the measuring apparatus and errors associated with the quantity being measured. Ideally errors in the measuring instrument should be an order of magnitude lower than other errors in the system, but this is not always the case. The frequency counter is accurate to better than one part in 10^9, and in measuring resonant frequency the only errors arise from the flatness of the resonance curve and the slight frequency pulling due to the probe loading. It has been found in a large number of resonant frequency measurements that the average deviation from the mean resonant frequency is 1 MHz and that the actual deviation from the mean only rarely exceeds 2 MHz. This error was considered sufficiently small to obviate the need to resort to bracketing techniques to determine the centre frequency. The repeatability of the Q factor of a particular resonance curve is $\pm$ 2%; this arises from the error in the centre frequency discussed above, a very much smaller error in the 3 dB frequencies, and in the setting of the VSWR meter to the 0 and -3 dB levels. The 3 dB points are taken to be where the meter deflection is half that at 0 dB, and there is also an absolute error in these readings arising from the linearity of the square law crystal detector and the power levelling performance of the signal generator. The response of the crystal detector was checked using a precision attenuator; the output power of the signal generator was found to vary a maximum

of 0.2 dB over any 50 MHz bandwidth. These two factors lead to an additional error of ± 3% in Q, giving an overall error in the measured Q factor of ± 5%. The known 3% decrease in Q due to probe loading is not included in this figure, since it is constant and can be easily accounted for. The error of ± 5% represents the worst error in an ideal Q curve, and two further points should be borne in mind: firstly individual Q values may be more accurate than this since the generator power levelling varies over X-band, and the error could drop to ± 3% at certain frequencies; secondly, although a good match can usually be obtained between the ideal and experimental resonance curves, there are occasions when this is not the case and the error could then exceed ± 5%. The best guide to the accuracy of a particular measurement is to note how it relates to other similar measurements, and to treat with caution any reading well outside the normal range.

8. MEASUREMENTS ON LINE RESONATORS

Losses in microstrip have already been discussed, (p20). Measurements of line attenuation and open-circuit radiation loss have been made using open-circuit 50 ohm line resonators; these experiments also yielded information on open-circuit end-effect in 50 ohm lines, and the results have been extended to predict the end correction for lines of other impedances. Further work has been carried out on the effect of reducing the size of the substrate supporting a resonant line, and that of bringing up grounded conductors close to a line at resonance.

8.1 Line Resonators

A microstrip line resonates when its electrical length L' is a whole number of half wavelengths, i.e.

$$L' = \frac{N\lambda_g}{2} = \frac{Nv}{2f} \qquad (29)$$

where v is the phase velocity, and N is integer.

It can be shown (Appendix, Section 12.2) that the Q of a typical line resonator with radiation loss at each end is given approximately by

$$Q_o = \frac{\beta L'}{2\alpha L' - 2\ell n\rho} \qquad (30)$$

where $\beta = 2\pi/\lambda_g$, α is the line attenuation in nepers per unit length, and ρ is the reflection coefficient of the open circuit and is real. The Q factor of a line resonator increases as the length of the resonator increases since radiation loss becomes a smaller fraction of the total losses, but because line attenuation increases as $\sqrt{f}$, whereas radiation loss increases as f^2, a given line will exhibit

maximum Q at a particular frequency.

Equation 30 can be rearranged to give

$$\frac{1}{Q_o} = \frac{2\alpha}{\beta} - \frac{2\ell n\rho}{\beta L'} \tag{31}$$

Writing $$\frac{1}{Q_c} = \frac{2\alpha}{\beta} \tag{32}$$

and $$\frac{1}{Q_r} = \frac{-2\ell n\rho}{\beta L'} \tag{33}$$

we have $$\frac{1}{Q_o} = \frac{1}{Q_c} + \frac{1}{Q_r} \tag{34}$$

8.2 Experimental Method

One set of substrates was used for the measurements on line attenuation, open-circuit radiation loss and open-circuit end effect. Eleven 76 x 25 mm substrates were involved, each supporting five open-circuit line resonators whose lengths were different multiples of $\lambda_g/2$ at a particular frequency. In this way five Q measurements were made at each of eleven frequencies throughout X-band, and by assuming that the radiation loss was independent of the resonator length it was possible to separate the effects of radiation loss and line attenuation. This can be seen by combining equations 29 and 30 to give

$$\frac{N}{Q} = \frac{2\alpha L'}{\pi} - \frac{2\ell n\rho}{\pi} \tag{35}$$

A graph of N/Q vs L' has gradient $(2\alpha/\pi)$ and an intercept on the N/Q axis of $(-2\ell n\,\rho/\pi)$. One such graph was drawn from measurements on the five lines on each substrate, and the gradient and intercept were

computed using a least squares technique. One substrate exhibited an unacceptably wide variation in N/Q, and loss calculations for this substrate have been omitted.

8.3 Line Attenuation

Line attenuation includes losses due to conductor loss and to dielectric loss, and Q measurements on line resonators reveal nothing of the relative contributions of each, but since both factors are always present it is this overall attenuation which is important practically. The attenuation is found from the gradient of the N/Q vs. L' graphs which, together with the standard deviation in the gradient due to the spread of experimental points, was computed for each of the eleven substrates. The calculated values of α were then adjusted for variations in linewidth arising from tolerances in the processing and normalised to a width of 0.61 mm (assuming α is proportional to w). The results are shown in Figure 33 where the vertical bars indicate $\pm$ one standard deviation. Also shown on Figure 33 are three theoretical curves for overall line attenuation based on the bulk conductivity of gold (4.17×10^7 Sm^{-1}). Curve (i) is with the conductor loss calculated according to the simple uniform current distribution model of equation 24; curve (ii) is with the conductor loss calculated on the basis of Caulton's[41] expression, equation 25, and includes a correction factor of 1.1 for surface roughness; curve (iii) is with the conductor loss calculated on Pucel's[6] theory, and also includes a roughness factor of 1.1. At first sight the results appear to agree reasonably well with Caulton's model, but when the d.c. conductivity of the plated lines was measured using a four point probe method, it was found that the values lay between 80 and 100% of the bulk value for gold. This

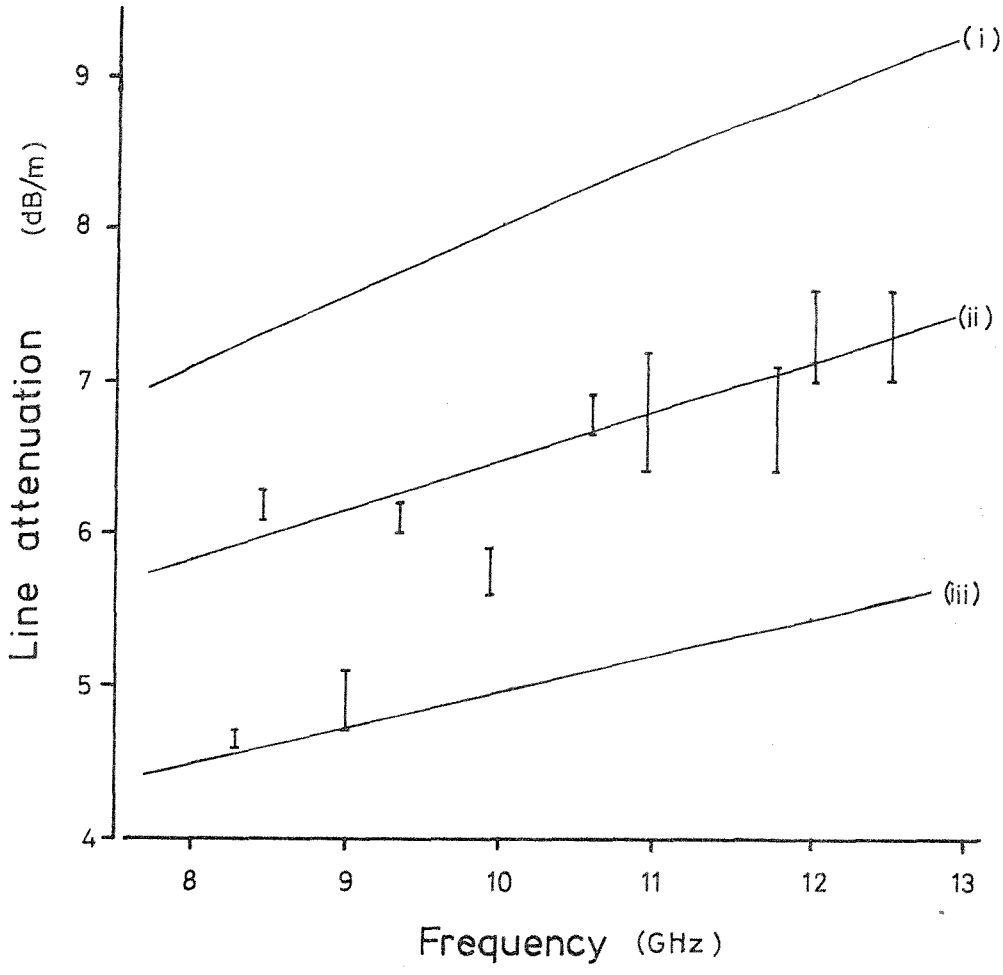

FIGURE 33. Attenuation vs. frequency for nominal 50 ohm lines on alumina substrates (Coors ADS 995) from Q measurements on line resonators. The vertical bars are ± one standard deviation of the 5 experimental values at each frequency.

Curves are calculated attenuation, including dielectric loss, from

(i) uniform current theory, eqn. 24

(ii) Caulton & Sobol expression, eqn 25.

(iii) Pucel expression, reference 6.

Curves (ii) and (iii) include a surface roughness factor of 1.1

$w = 0.61$, $h = 0.65$, $\tan \delta = 10^{-4}$.

suggests that Caulton's theory overestimates the losses, and the existence of points on Figure 33 significantly lower than Caulton's prediction tends to confirm this. The reason for the spread in experimental points is variation in quality of the plated gold layer on different substrates. This was due to the policy adopted for the plating bath by which the solution was used in batches and discarded when exhausted, with the result that before adequate monitoring facilities were installed substrates produced towards the end of the life of the solution tended to be of inferior quality. [In a production environment with a uniform throughput of substrates and continuous replenishment of the plating bath this problem is unlikely to occur.]

The varying error bars on the experimental points also arise in part from variations in line quality; it has been noted on occasions that lines on a single substrate have not plated up to a uniform thickness, and have also exhibited some edge built-up, apparently at random. The error bars derive from the standard deviation of the gradient of the N/Q vs L' graphs, and thus only partly account for error in the measurement procedure; they do not include the systematic errors such as crystal calibration, which introduce a further error of approximately $\pm$ 1%.

Other results on line attenuation have been acquired from Q measurements on ring resonators from which it is assumed that there is no radiation loss, so that α is found directly from equation 32. Figure 34 shows the calculated losses from a number of circular rings of different diameters. There is a preponderance of measurements on rings $3\lambda_g$ and $4\lambda_g$ in circumference, and these points have been

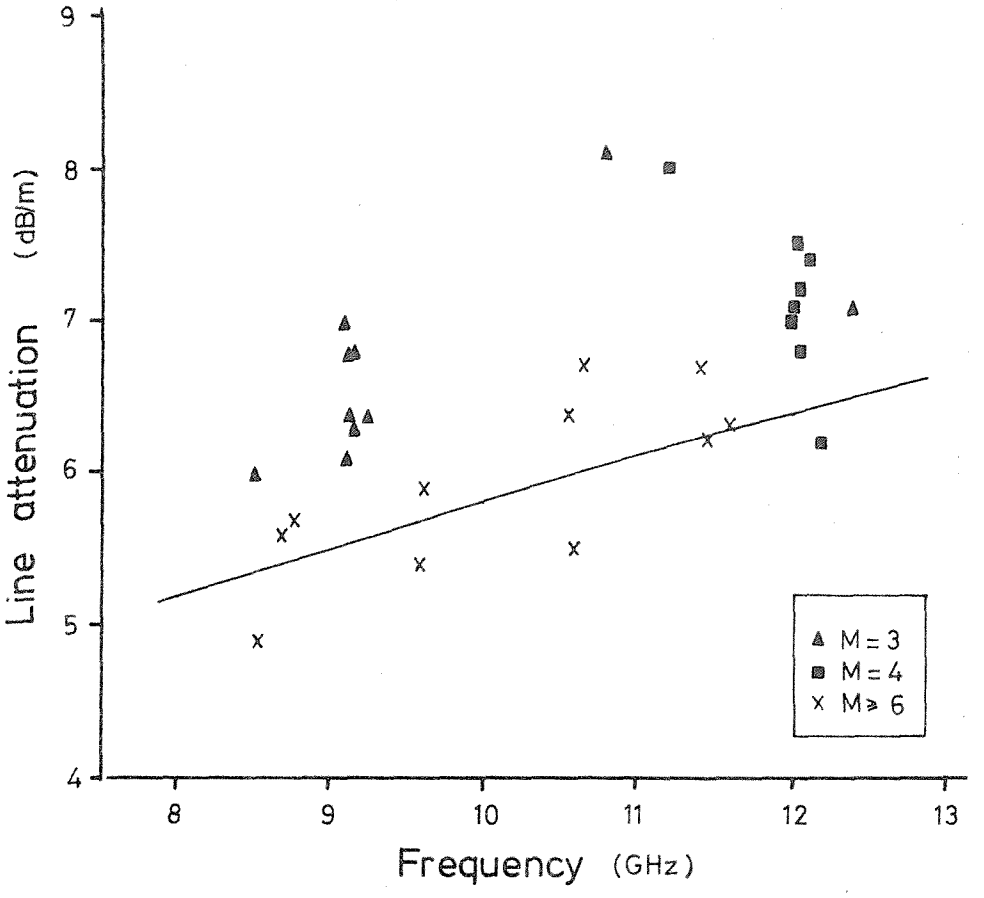

FIGURE 34. Attenuation vs. frequency for nominal 50Ω lines on alumina (MRC Superstrate), from Q measurements on ring resonators.

(For clarity error bars of ± 5% have been omitted).

The curve is calculated attenuation based on equations 21 and 25 and includes a surface roughness factor of 1.05.

w = 0.65mm, h = 0.68mm, tan $\delta = 6 \times 10^{-5}$.

M is the number of wavelengths on the ring at resonance.

singled out as they are consistently higher than other points. The reason for this lies mainly with the fact that these rings were only about 13mm in diameter and this led to direct coupling between the coaxial probes which affected the Q factor. There is the additional factor that, as Roberts[44] has shown, radiation from small rings may not be entirely negligible, but using Roberts' figure of 0.01% for the radiated power fraction from a 3 λ_g ring on alumina, the change in α is found to be less than 0.5%. The remaining points on Figure 34 are seen to be scattered around the curve based on Caulton's expression.

The effect of conductor thickness on line attenuation has been investigated by making measurements on a number of 50 ohm open-circuit line resonators of the same length plated up to different thicknesses. Both the d.c. conductivity and the Q factor at X-band were measured, and because radiation loss from each line was the same, the difference in Q was due almost entirely to a change in conductor loss. (In fact a plated line spreads as its thickness increases and the thick lines were slightly wider than the thin lines, which led to a corresponding increase in Q. No allowance for this has been made in the results). Figure 35 shows the measured Q and the d.c. conductivity as a function of line thickness. It can be seen immediately that the d.c. conductivity increases with line thickness, and that the bulk value is not attained until the line is approximately 10μm thick (~12 skin depths). The change in conductivity is such that it would mask any change in Q factor due to skin effect (see section 4.2), with the result that up to a line thickness of 10μ m

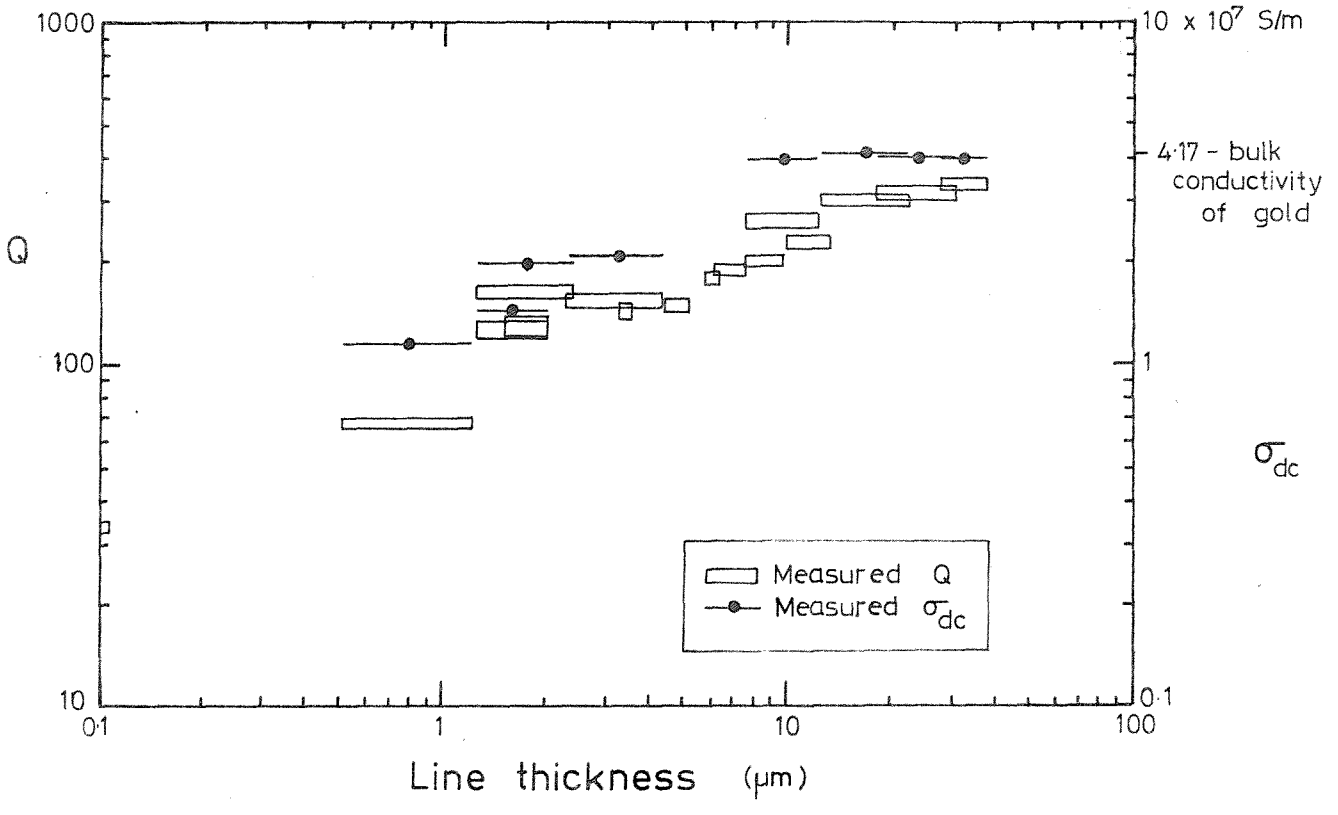

FIGURE 35. MEASURED Q FACTOR AND D.C. CONDUCTIVITY OF PLATED-UP 50Ω LINES ON ALUMINA (COORS ADS 995) AS A FUNCTION OF LINE THICKNESS

line attenuation appears to bear a constant relationship to line thickness. The tolerances on the line thicknesses shown in Figure 35 were due to the non-uniform cross-section of the plated lines, and were determined from Tallysurf measurements made at two positions on each line. The results include measurements on substrates with surface finishes of 0.25μm and 0.6μm, and in fact those lines on the smoother substrate exhibited more non-uniformity in thickness.

Discussion of line attenuation has centred on conductor loss which is the predominant factor. In calculating the dielectric loss for the Coors substrates in Figure 33, the value of tan δ at 100 MHz of 10^{-4} was used, but because dielectric loss is only a small percentage of the total loss even quite a large error in tan δ does not seriously affect the theoretical curves. Experimental results have tended to agree with Caulton's model for conductor loss, but it is felt that with high quality lines losses nearer the value predicted by Pucel could be achieved.

8.4 Open-circuit Radiation Loss

Radiation from an open-circuit termination was analysed by Lewin[42], as mentioned in section 4.3. In discussing radiation from microstrip line resonators, Lewin assumed that the length of the structure would be sufficient for the radiation from the two ends to be considered separately, the total power radiated being just twice that from a single termination. The experimental determination of open-circuit radiation loss has been based on this assumption, in that the five lines on a substrate were assumed to radiate equally at their common resonant frequency, in spite of being of different lengths. Easter and Roberts[43] have pointed out that this assumption

is unlikely to hold for half-wavelength X-band resonators on alumina when the length of the structure is only about $\lambda_o/6$, and their method predicts a radiated power fraction approximately twice that of Lewin's for a half wavelength resonator on alumina.

The radiated power fraction was calculated from Q measurements on open microstrip, and as already described, the reflection coefficient of the open circuit was found graphically from the intercept on the N/Q vs L' graphs. Any variation of radiated power with line length would be revealed as a curvature of this linear graph. Two of these graphs ('good' and 'bad' examples in relation to the scatter of experimental points) are shown in Figure 36; no such curvature is evident. The shortest lines used were λ_g long and thus Lewin's assumption appears justified for open circuit resonators of this length on alumina.

The results are shown in Figure 37, the ordinate being the total power fraction radiated from a 50 ohm open circuit resonator. $200(1 - \rho^2)$ %. The vertical bars are the errors given by $\pm$ one standard deviation of the intercept of the N/Q vs L' graphs. The results exceed Lewin's value at the lower end of the frequency range, but are all well below Easter's prediction for a half wavelength resonator which, for these substrates, gives a radiated power fraction of 3½% at 10 GHz. It is difficult to be more specific; as before the spread in results is due primarily to differences in conductor losses, since the intercept is sensitive to small errors in gradient. Measurements of open-circuit radiation loss by a different method - that of measuring the Q of a resonator inside and outside a shielding enclosure - do however show a comparable spread in measured values[43].

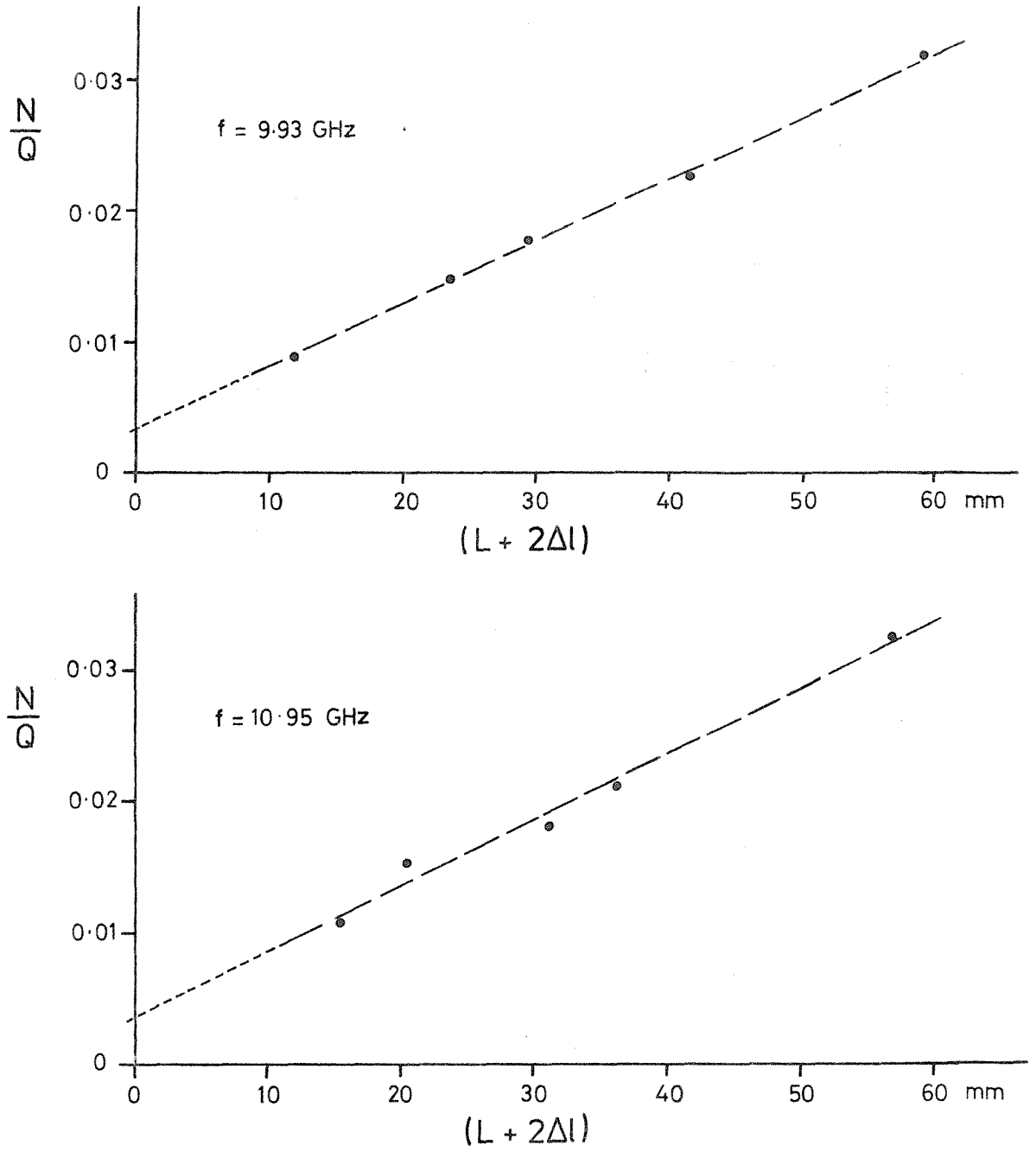

FIGURE 36. TWO EXAMPLES OF THE TWELVE GRAPHS OF N/Q vs. ELECTRICAL LENGTH (L +2Δℓ) USED IN THE CALCULATION OF LOSSES

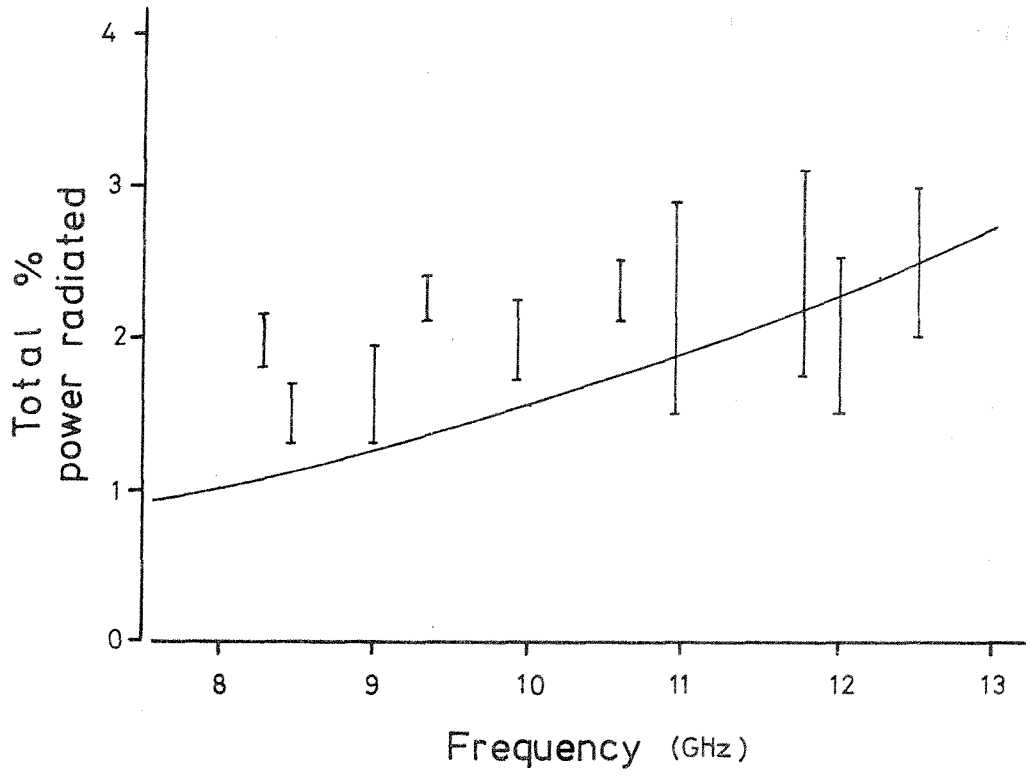

FIGURE 37. PERCENTAGE POWER RADIATED FROM OPEN-CIRCUIT 50 ohm MICROSTRIP RESONATOR, $\{200(1 - \rho^2)\}$ AS A FUNCTION OF FREQUENCY. The vertical bars are $\pm$ one standard deviation of the 5 experimental values at each frequency.

Curve is calculated according to Lewin (reference 42)

w = 0.61mm, h = 0.65mm.

Another theoretical approach to open-circuit radiation loss has been given by Sobol[55] who considers the end of the microstrip line as a radiating aperture, but his results are presented in terms of the ratio of radiation loss to distributed loss in a quarter wave stub, and without an accurate set of Q measurements information on radiation loss alone cannot be extracted.

8.5 Open-circuit end effect

Work with the standing wave indicator had shown considerable fringing field at the end of open-circuited lines. The capacitance of this fringing field causes an apparent increase in the length of the line, and this extension provides a convenient means of characterising the end effect. Accurate determination of the end-correction is important since the open-circuit stub is widely used in filter sections, but both measurement and calculation of the end-correction can be limited in accuracy as they rely on the difference of two large quantities. Benedek and Silvester[56] recognised this and have made a direct calculation of the fringing capacitance at an open-circuit; the calculation is complex, but a reasonably straightforward expression for the capacitance is found which accurately fits the computed results. Their paper presents a useful review of other discussions of the microstrip end-effect.

The experimental method used here was a graphical method involving the fifty five lines on the set of substrates used for loss measurements. The resonant condition for an open-circuited line resonator can be written

$$L + 2\Delta\ell = \frac{Nv}{2f} \qquad (36)$$

where $\Delta\ell$ is the end correction at the open circuit. The five lines on each substrate had a common resonant frequency, and it was intended to plot L vs N for each substrate. There were, however, small variations in the nominally identical frequencies, and it was necessary to determine the frequency dependence of the phase velocity in order to normalise to one particular frequency. The shortest of the five lines only resonated at a single frequency, and this was taken as the normalising frequency for that substrate. In adjusting the other frequencies, use was made of the linear decrease in phase velocity with frequency for 50 ohm lines on alumina; examination of equation 36 shows that this requires a corresponding decrease in f/N for a given line, and thus by measuring all the resonant frequencies of a line and plotting f/N vs f for the line it was possible to calculate a value of N at the new frequency (N'). Once the value of N for each line had been normalised a least squares technique was used to establish the best fit straight line to a graph of L vs N' for each substrate. This graph has a negative intercept of $2\Delta\ell$.

This procedure was carried out for each substrate, and the resulting value of $\Delta\ell$ were then further corrected for small differences in linewidth between substrates, by assuming from the data of Napoli and Hughes[27] that $\Delta\ell$ was proportional to w over the small range of widths involved. The results are given in Figure 38, which shows the end-correction for a 50 ohm open-circuited line as a function of frequency; the error bars indicate $\pm$ one standard deviation in the calculated value. The dotted line is a best least squares fit to the experimental points, and it can be seen that the end-correction is virtually constant over X-band, between

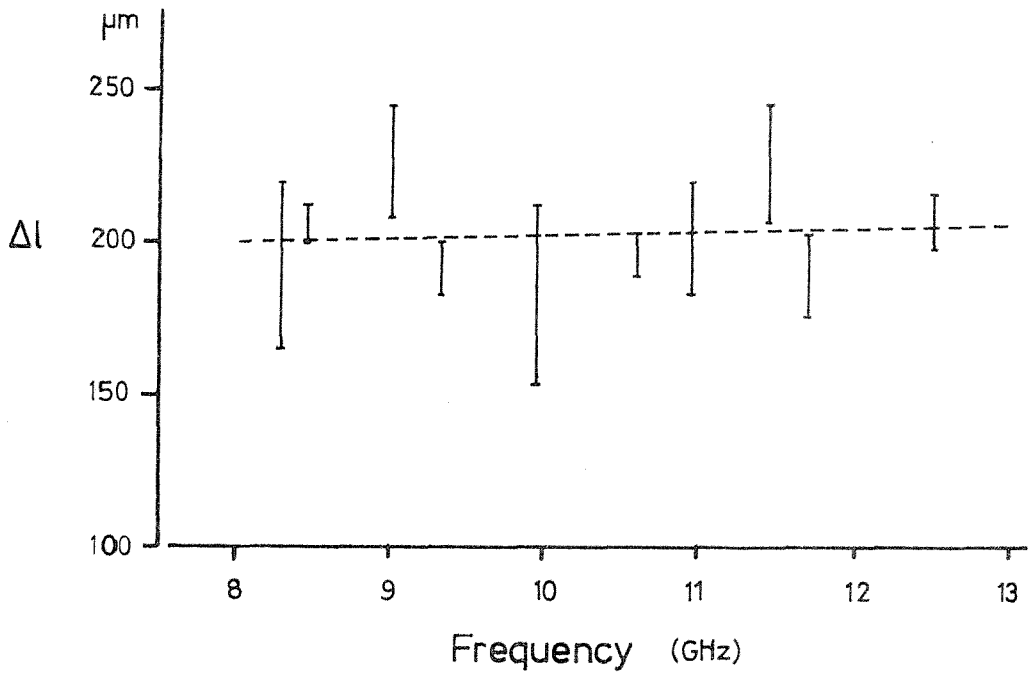

FIGURE 38. MEASURED OPEN CIRCUIT END CORRECTION FOR 50Ω LINES, AS A FUNCTION OF FREQUENCY. The vertical bars indicate ± one standard deviation of the 5 experimental values at each frequency. The dotted line is a best fit to the measured points. w = 0.61, h = 0.65 mm.

200 and 205μm. The average deviation from the best fit is 12μm.

It is interesting to make a comparison between open circuit end-correction in microstrip and in balanced stripline. For a high permittivity dielectric like alumina the microstrip field is largely confined to the substrate, and closely resembles the field in one half of an alumina filled balanced stripline. For balanced stripline it can be shown rigorously[57] that the end-correction for an infinitely wide line with plate separation 'a' is given by

$$\frac{\Delta\ell}{a} = \frac{\ell n 2}{\pi} \quad \text{as } w \to \infty \qquad (37)$$

$$= .221$$

The variation of the end correction in balanced stripline as a function of w/a has been studied by Altschuler and Oliner[48] who give a semi-empirical formula for $\Delta\ell$ as a function of w and λ_g, together with experimental results. Jain et al[58] have applied this formula directly to microstrip, but a more general approach is possible once it is recognised that Altschuler and Oliner's results are reducible to linear form by plotting instead $\Delta\ell/a$ versus $Z_o \sqrt{\varepsilon_r}$ (the impedance of an air-spaced line of the same geometry)[33]. In order to identify microstrip with balanced stripline it is necessary to put a = 2h, and then, to preserve the same capacitance per unit length for both structures, to double the microstrip permittivity to $2\,\varepsilon_{eff}$. The parameters plotted are thus $\Delta\ell/2h$ vs $Z_o \sqrt{2\,\varepsilon_{eff}}$, using the experimental value of $\Delta\ell$ at $Z_o = 50\Omega$, and the theoretical value at $Z_o = 0$ ($w \to \infty$). Reliance on a single experimental value like this is only justified by the accuracy attributed to this value resulting from the large number of measurements involved. The graph is shown in Figure 39, and allows $\Delta\ell$

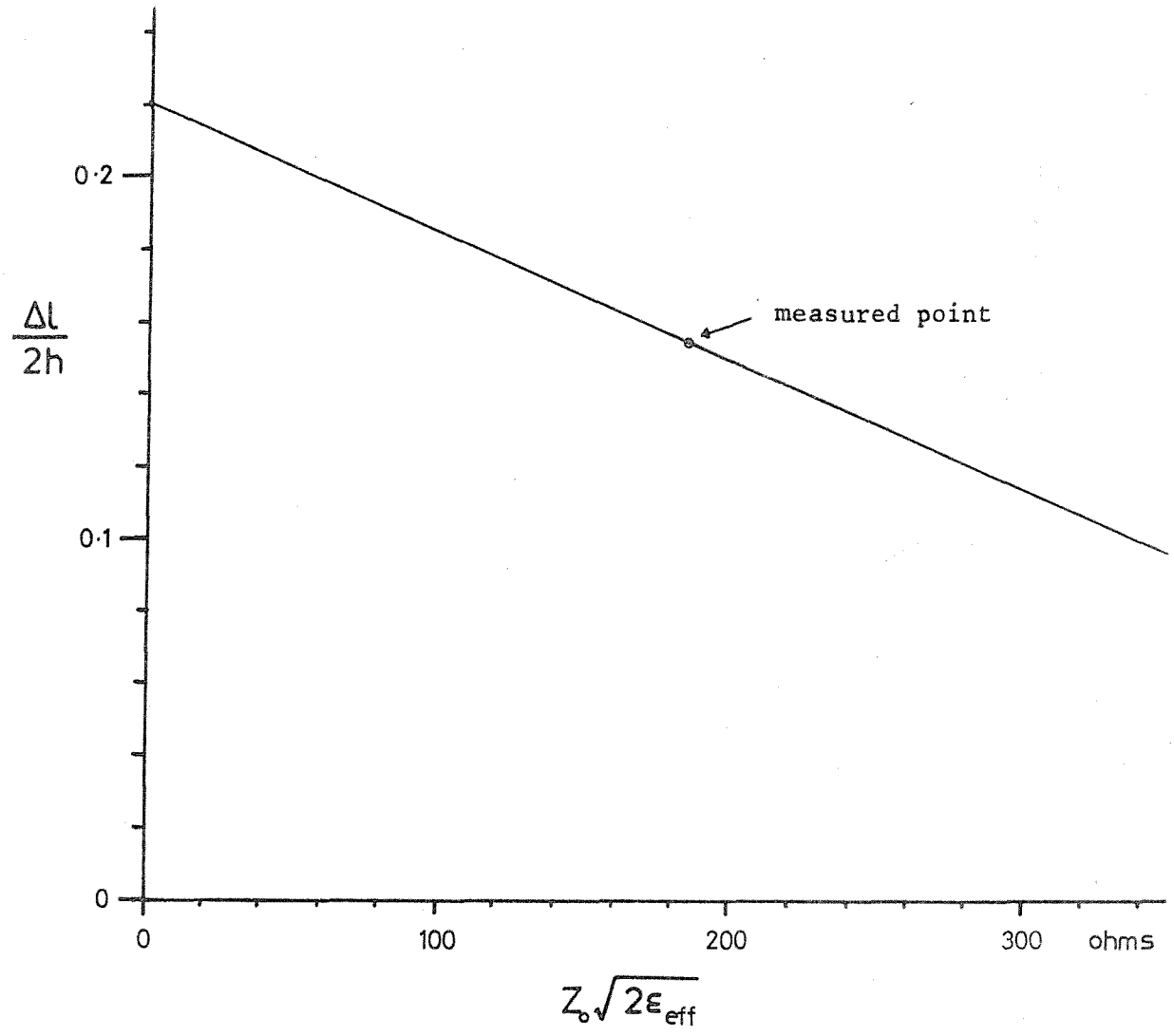

FIGURE 39. GRAPH USED FOR THE DETERMINATION OF END CORRECTION ($\Delta\ell$) BASED ON A THEORETICAL VALUE OF $\Delta\ell$ FOR STRIPLINE AT Z_o = 0, AND A MEASURED VALUE ON MICROSTRIP AT Z_o = 50 ohms.

to be predicted for a wide range of impedances. It is difficult to assess the accuracy of this graph since the error in taking $\{\Delta\ell / 2h\}_{w \to \infty}$ as 0.221 is unknown, and the linear dependence will cease for narrow linewidths as the corner fields become significant. Values of $\Delta\ell$ given by this graph can, however, be compared to those given by the direct calculation of Silvester and Benedek[56], and the two curves are shown in Figure 40, for $\varepsilon_r = 9.6$; the agreement is remarkably good.

It appears therefore that this linear graph enables the end-correction for microstrip to be calculated with reasonable accuracy over a wide range of w/h, and it is both comprehensive and simple.

8.6 Line environment

The field distribution in microstrip had previously been observed using the standing wave indicator, and it was found that the field could be detected for a considerable distance either side of the line. This has implications in circuit design since it is related to the packing density of circuits - a point which is becoming increasingly important in computer technology where microstrip is finding applications as a transmission line for fast pulses.

A quantitative assessment of the effect of the environment of a microstrip line on its transmission qualities has been made, by both decreasing the width of substrate supporting the line and also by allowing a grounded conductor to encroach upon the top of the substrate. The resonant frequency and Q factor of a line are sensitive indicators of any extraneous coupling or losses, as well as being convenient to measure. In the first experiment a 50 ohm open-circuit line 32 mm long on a substrate 15 mm wide was placed on a large sheet of microwave

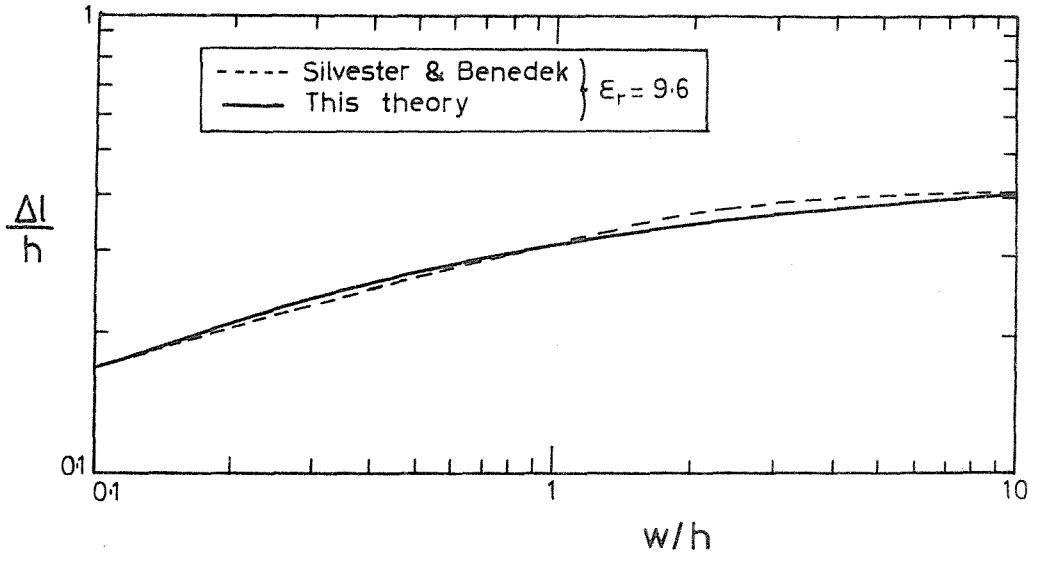

FIGURE 40. COMPARISON OF END CORRECTION AS A FUNCTION OF w/h, BETWEEN THE VALUES CALCULATED FROM FIGURE 39 AND VALUES GIVEN BY SILVESTER & BENEDEK (reference 56) $\varepsilon_r = 9.6$

absorbent material, and its resonant frequency and Q factor were measured as the width of the substrate was gradually reduced. The results are shown in Figure 41, from which it can be concluded that the substrate ought to extend about 10 linewidths either side of a 50 Ω line to ensure no deterioration in performance.

The second experiment involved a 25 x 75mm substrate with a 50 Ω line, 65 mm long positioned centrally. Using conducting silver paint grounded conducting areas were gradually brought up parallel to the line while its resonant frequency and Q factor were measured. The results were not as uniform as those of the previous experiment and only the change in Q factor has been plotted (Figure 42). It can be seen from Figure 42 that the Q drops markedly for values of p/w less than about eight, and that as before an undisturbed width of alumina of approximately ten linewidths either side of the line appears advisable. This value is somewhat greater than the four linewidths suggested by Caulton and Sobol[41].

8.7 Coupled Microstrip Lines

Parallel-coupled microstrip lines exhibit quasi TEM propagation characteristics just as single microstrip, but in this case there are two solutions depending on the relative polarity of the top conductors. If both conductors are of the same polarity the mode is said to be 'even', and if they are of opposite polarity the mode is 'odd'. Figure 43 is a sketch of the field lines for the two modes, and it can be seen that in both configurations there is symmetry about a vertical plane midway between the lines. The two modes have different impedances and phase velocities, with $v_p(\text{odd}) > v_p > v_p(\text{even})$ where v_p is the phase velocity of a single microstrip line of the same width.

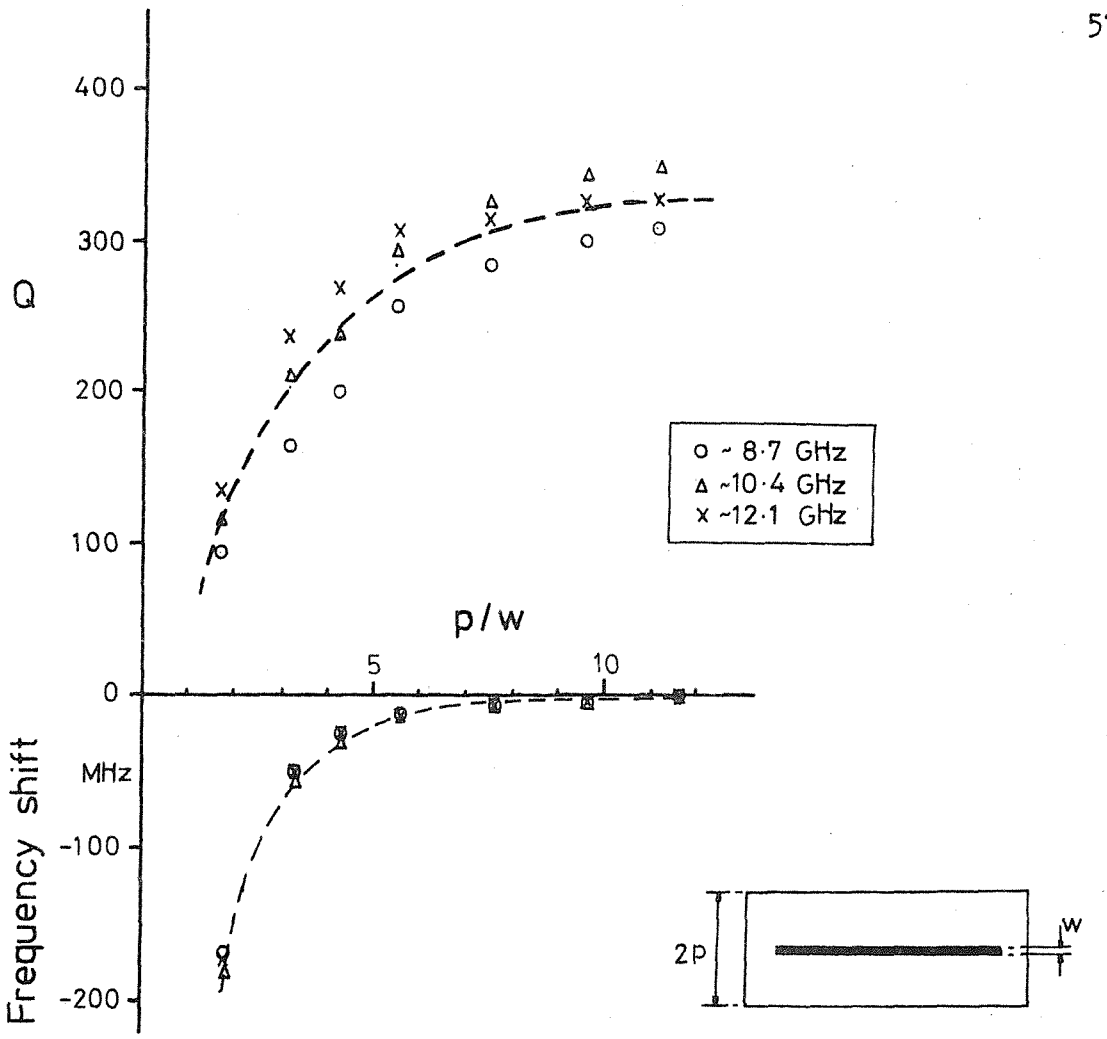

FIGURE 41. CHANGE IN Q AND RESONANT FREQUENCY FOR A 51 ohm LINE, 32mm LONG, AS THE ALUMINA SUBSTRATE WAS REDUCED IN WIDTH

(The 5% error in Q is not shown)

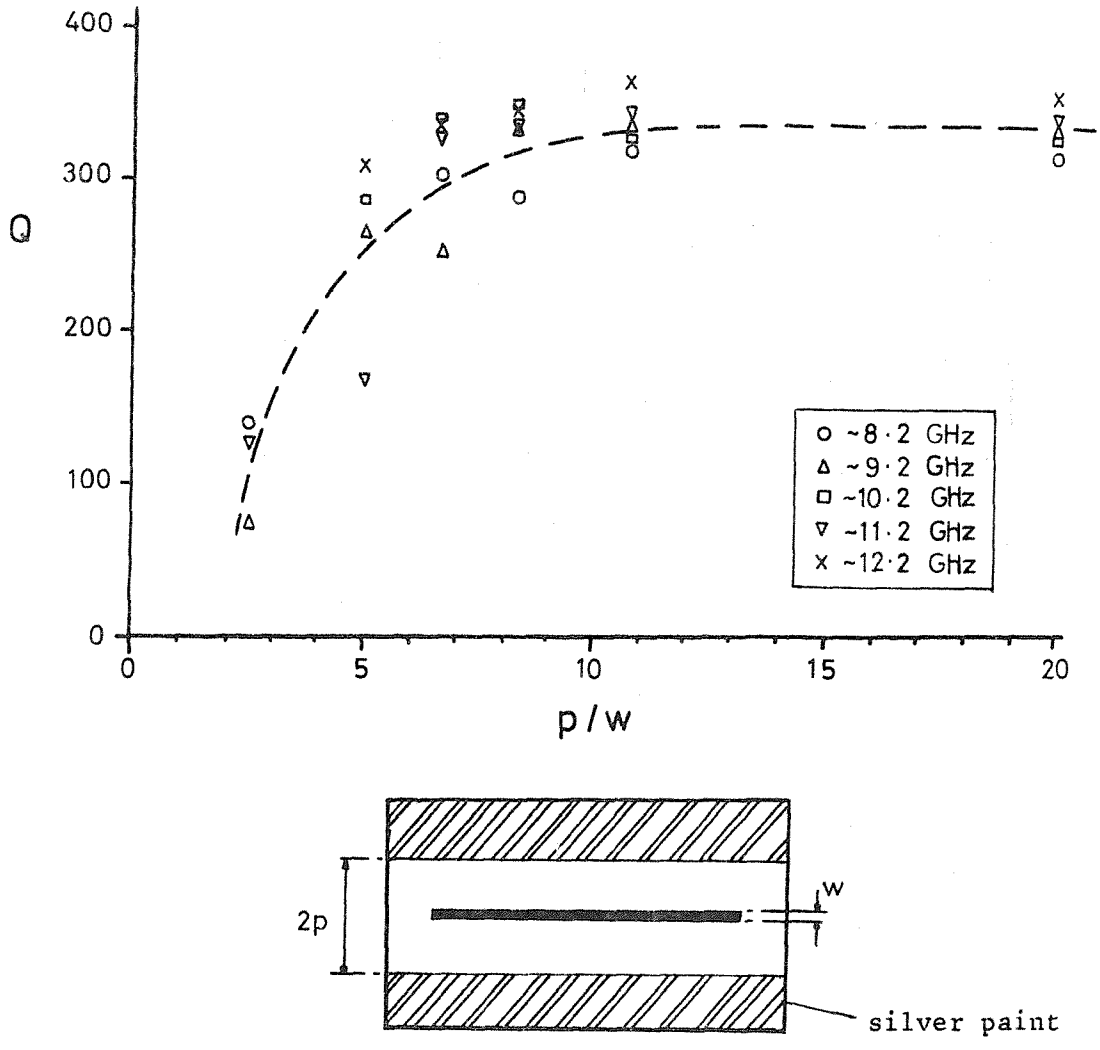

FIGURE 42. CHANGE IN Q FACTOR FOR A 50 Ω LINE, 65mm LONG, AS GROUNDED AREAS WERE ALLOWED TO ENCROACH UPON THE TOP CONDUCTOR

(The 5% error in Q is not shown)

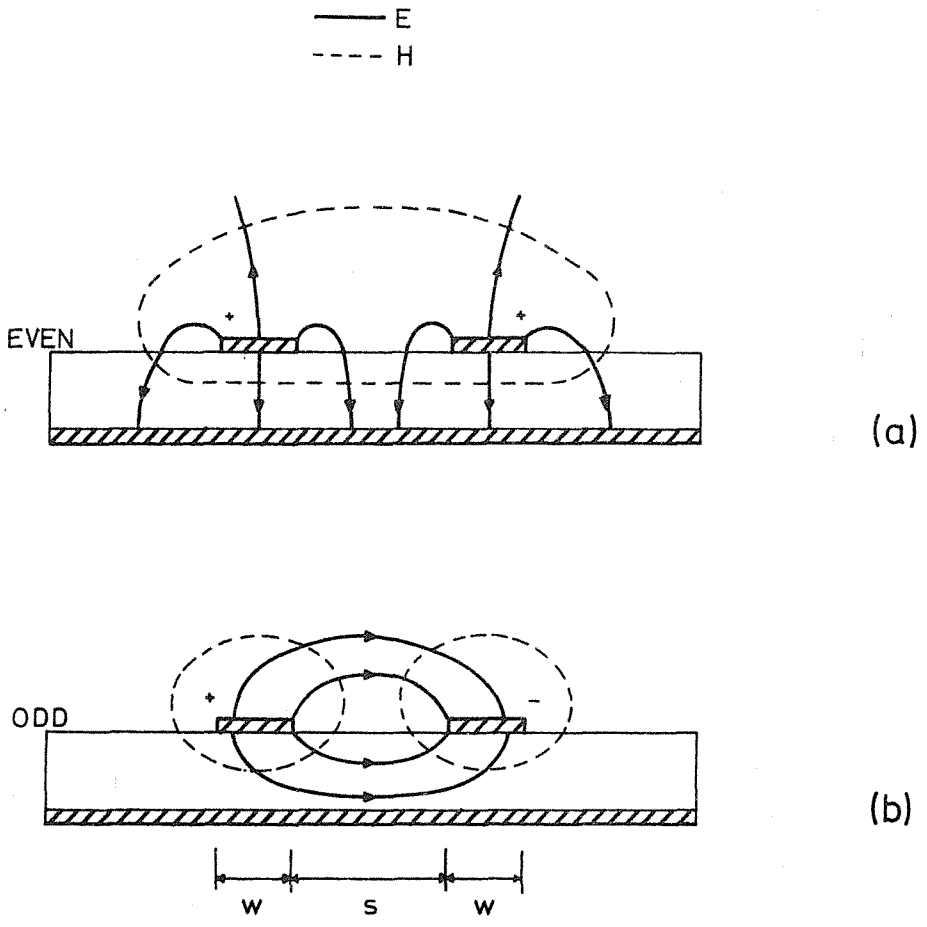

FIGURE 43. STATIC FIELD CONFIGURATION IN PARALLEL COUPLED MICROSTRIP

(a) even mode (b) odd mode

As the spacing, s, between the strips decreases, v_p (odd) and v_p (even) both tend to v_p. Parallel coupled strips are used in filters,[59] and knowledge of the impedance and phase velocity of each mode is important. Bryant and Weiss[19] were the first to present comprehensive results on coupled microstrip, but subsequent experimental work has shown that their results slightly overestimate the phase velocities, especially for the even mode[60,61].

Ring resonators are the most suitable means of determining phase velocity, but with coupled concentric rings difficulty arises in exciting the even and odd modes separately. Various methods have been described: in reference 62 a microstrip probe is end-coupled to the rings and a short piece of shellac-insulated wire laid across the gap to increase the coupling to the inside ring; this caused both resonances to be excited, but by shorting the two rings at various points the odd resonance was attenuated. In reference 61 parallel coupled microstrip probes are used for the odd resonance, and a probe above the substrate, presumably coaxial, used to excite the even resonance.

It was found in this project that the coaxial probes would satisfactorily excite even and odd modes on line and ring resonators, and that an optimum position for the probes could be found for any particular resonance. Measurement of the phase velocities of the even and odd modes on coupled open-circuit lines with $w \simeq h \simeq s$ have been undertaken, but no attempt at a comprehensive series of measurements has been made since with the additional parameter of line spacing, s, a large number of measurements are necessary to cover a reasonable range of variables. In the course of these measurements, limited data on end-correction and line attenuation has also been

acquired. The measurement technique was similar to that previously described for single lines: six coupled pairs of line resonators of different lengths were deposited on two 76 x 25 mm substrates. All the resonant frequencies and Q factors of each line were measured, and graphs plotted for f/N vs f for the even and odd modes on each substrate. These were found to be linear, showing that the dependence of phase velocity with frequency is also linear. From these graphs a value of N for a particular line may be found at any frequency, and in this way graphs of L vs N were plotted at a number of frequencies; the phase velocity was found from the gradient of the graph and the end correction from the intercept. Figure 44 (a) shows the wavelength ratios for the even and odd modes to the free space wavelength, as a function of frequency, calculated from these measurements.

Losses in coupled microstrip differ between the two modes, owing to the different current distributions. In the odd mode there is a high current at the inside edges of each strip, and the losses in this mode exceed those in the even mode. The few measurements made show that line attenuation in the even mode is approximately twice that for a single line of the same width, and for the odd mode is half as much again (Figure 44 (b)).

The difficulty in measuring the end-correction has been encountered already and the results obtained for these coupled lines were not sufficiently accurate to enable the behaviour of the end-correction with frequency to be assessed. One reason for this was that the linelengths were not specifically designed for this measurement and the shortest was around 36 mm long; as a result very small errors in the experimental points can lead to very large changes in the intercept.

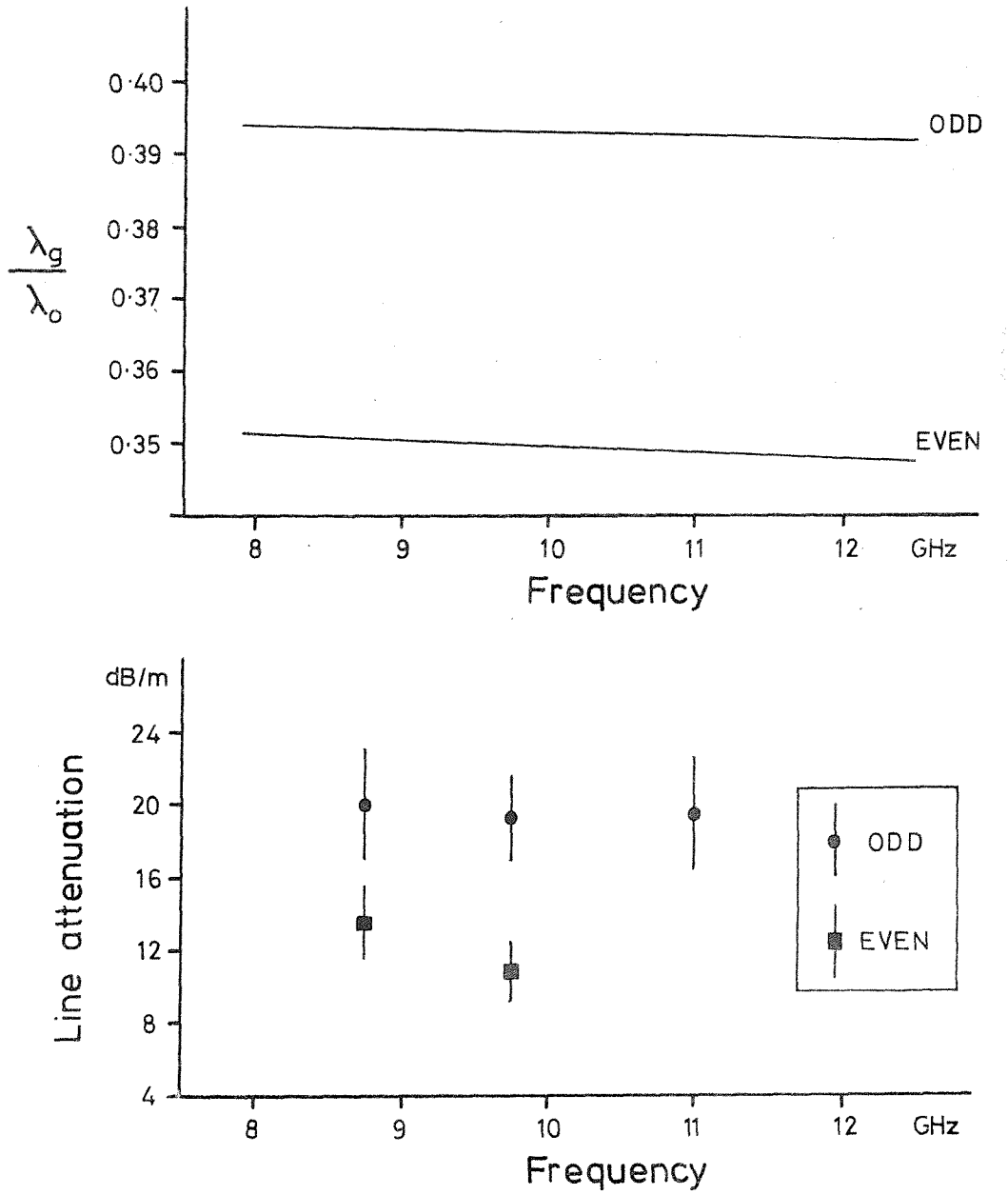

FIGURE 44. (a) Even and odd mode wavelengths in coupled microstrip, based on measurements on line resonators.

(b) Measured line attenuation in the even and odd modes.

w = 0.67mm, h = 0.64mm, s = 0.60mm.

The calculated end-corrections were $0.10 \pm .06$ mm for the even mode, and 0.33 ± 0.10 mm for the odd mode.

9. RING RESONATORS

Ring resonators have been used in the study of two forms of microstrip discontinuity - the mitred right angle bend and the abrupt step in width of the top conductor. As with open-circuit end-correction the quantities to be measured are small, and the advantage of ring resonator techniques is that both frequency and physical length are capable of being measured to a high degree of accuracy (typically $\pm$ 0.1%). A ring resonator is here simply defined as a closed resonator.

9.1 Discontinuities in Microstrip

Discontinuities in conventional forms of transmission line such as waveguide and coaxial line are well documented,[63] and it is possible to make use of this information in dealing with discontinuities in microstrip. It is assumed that the microstrip line supports a TEM mode and that any discontinuities are lossless. This is not strictly true, but the radiation loss from microstrip discontinuities is small and will not invalidate the consequences of the assumption.

At a discontinuity higher order modes are excited, but they are local to the discontinuity and in their effect on any one mode on the line can be represented in terms of lumped components in an equivalent circuit. A discontinuity in any transmission line can be represented by a two-port network, which in general requires six constants to completely characterise it; T and Π networks are two common forms. In microwave networks it is often possible to simplify the equivalent circuit if, for example, the discontinuity region is small with respect to the wavelength, or by taking the symmetry of the structure into consideration.

Calculation of the values of equivalent circuit components requires analysis of the electric and magnetic fields at the discontinuity. A rigorous solution of Maxwell's equations is often impossible and in fact unnecessary, since it is only the effect of the discontinuity on the line's propagating wave that is of importance, and approximate solutions are sufficient. If the discontinuity region is small with respect to the line wavelength, voltage across it is continuous and the discontinuity can be represented by a single shunt admittance, whose value can be calculated from simple electrostatic theory. If necessary, a closer approximation can be obtained by using the variational techniques developed by Schwinger[64], in which an expression for the discontinuity admittance is formulated in such a way that a first order error in the assumed field distribution gives only a second order error in the admittance. This is a powerful technique which has found applications in a wide range of microwave discontinuity problems[65].

A huge amount of work has been devoted to waveguide discontinuities, and there is some work on balanced stripline, notably that of Altschuler and Oliner[48], but the work on microstrip discontinuities is sparse indeed, and most of it has concerned the open-circuit end correction.

9.2 Measurement Method for Microstrip Discontinuities

The method of measuring microstrip discontinuities used here is based on observation of the disturbance caused by incorporating the discontinuity in an otherwise uniform ring resonator. In some cases more than one discontinuity is introduced, but for the purposes of analysis a uniform ring with a single point discontinuity, represented by a shunt admittance, is considered. The effect of the input and output probes is ignored initially. To the incident signal the ring, in both directions, appears to be a semi-infinite line with shunt admittances

periodically spaced along its length. In the absence of attenuation all the incident energy is ultimately reflected, and as Slater[66] has shown for the case of a periodically loaded waveguide, the steady state solution can be considered in terms of two standing waves , $\pi/2$ out of phase. It is convenient to label these two standing waves as being of sine and cosine form;the cosine form has a voltage antinode at the discontinuity, while the sine form has a voltage null there. The electrical length of the ring differs for the two waves, since the shunt admittance contributes electrical length to only one wave; a capacitive discontinuity, for example, only affects the cosine form of standing wave. The result is that the ring exhibits two sets of resonances, one set coinciding with the resonances of an identical undisturbed ring, and the other set shifted in frequency according to the nature and magnitude of the discontinuity. This result is just a special case of a general property of periodically loaded structures, namely the existence of pass- and stop-bands. The situation occurs in many branches of physics, but for a periodically loaded transmission line may be described by the equation

$$\text{Cos } \theta = \cos \beta L - \frac{b}{2} . \sin \beta L \qquad (38)$$

where θ = the electrical length of the periodic structure

β = the phase constant of the undisturbed line

L = the length of line in the 'period'

b = the normalised susceptance of the shunt admittance

This equation is readily derived from the cascaded matrices of the two port network obtained by breaking the ring at one point, and is given in the Appendix (Section 12.31). An alternative form of

equation 38 is

$$\cos \theta = \Phi \cos (\beta L + \phi) \qquad (39)$$

where $\Phi = \{ 1 + (b/2)^2 \}^{\frac{1}{2}}$

$$\phi = \tan^{-1}(b/2)$$

It can be seen that solutions to equation 39 exist for positive and negative values of $(\beta L + \phi)$, corresponding to the positive and negative travelling waves on the structure which together comprise the two standing waves. The pass- and stop-band nature of the structure is also seen more readily from this equation: as $(\beta L + \phi)$ increases from zero, β is real until the right hand side of equation 39 becomes equal to one, when β must become imaginary implying attenuation; with further increase in $(\beta L + \phi)$, β becomes real again and thereafter alternates between imaginary and real. In the case of the ring resonator there is the additional constraint that $\theta = 2\pi M$, where M is the number of wavelengths on the ring at resonance. Thus the pass band is limited to the two frequencies for which the right hand side of equation 39 is equal to one.

Solving equation 38 or 39 for b in terms of the two resonant frequencies of the ring f_1, f_2 gives

$$b = 2 \tan\left[\frac{f_1 - f_2}{f_1} \cdot M\right] \qquad (40)$$

where f_1 is the frequency at which an undisturbed ring would resonate. For a ring with a single discontinuity, the two standing waves are aligned in relation to the position of the discontinuity, and this is still the case when the input and output probes are present, provided the coupling is loose. Which resonant frequency is observed depends on the position of the output probe relative to the discontinuity.

The input probe merely couples into either the sine or cosine form of standing wave to a greater or lesser extent. Even for a perfectly uniform ring, the necessity to couple into the ring introduces a discontinuity at the probes and this will lead to some resonance splitting (which may not be measurable). In practice most gold rings on alumina exhibit small non-uniformities in the line whose effect exceeds that of the probes, and resonance splitting becomes detectable. This resonance splitting has been observed by several workers[67,68,69], and it has an associated effect which can lead to erroneous results in Q measurements. This arises if the probe coupling is loose, when discontinuities on the ring determine the positions of the standing waves; if the output probe is positioned such that it coupled into both the sine and cosine forms of standing wave a low-Q resonance is observed. This effect can be demonstrated by using the coaxial probes, when it is a simple matter either to rotate the substrate or to move the probes to reveal different resonances. Figure 45(a) shows two resonance curves corresponding to the sine and cosine forms of standing wave on a particular ring; these curves were obtained for positions of the output probe $\lambda_g/4$ apart. At an intermediate position of the output probe the resonance of Figure 45(b) was observed which, although apparently normal, has a Q factor significantly lower than either of the true resonance curves. This is one possible cause of the anomalously low Q values that have been reported[70].

9.3 Right Angle Corners in Microstrip

A matched right angle corner allows microwave integrated circuit components such as circulators to be realised in rectilinear form, which leads to more compact circuitry and may simplify the generation of artwork, especially if automatic drafting equipment is available.

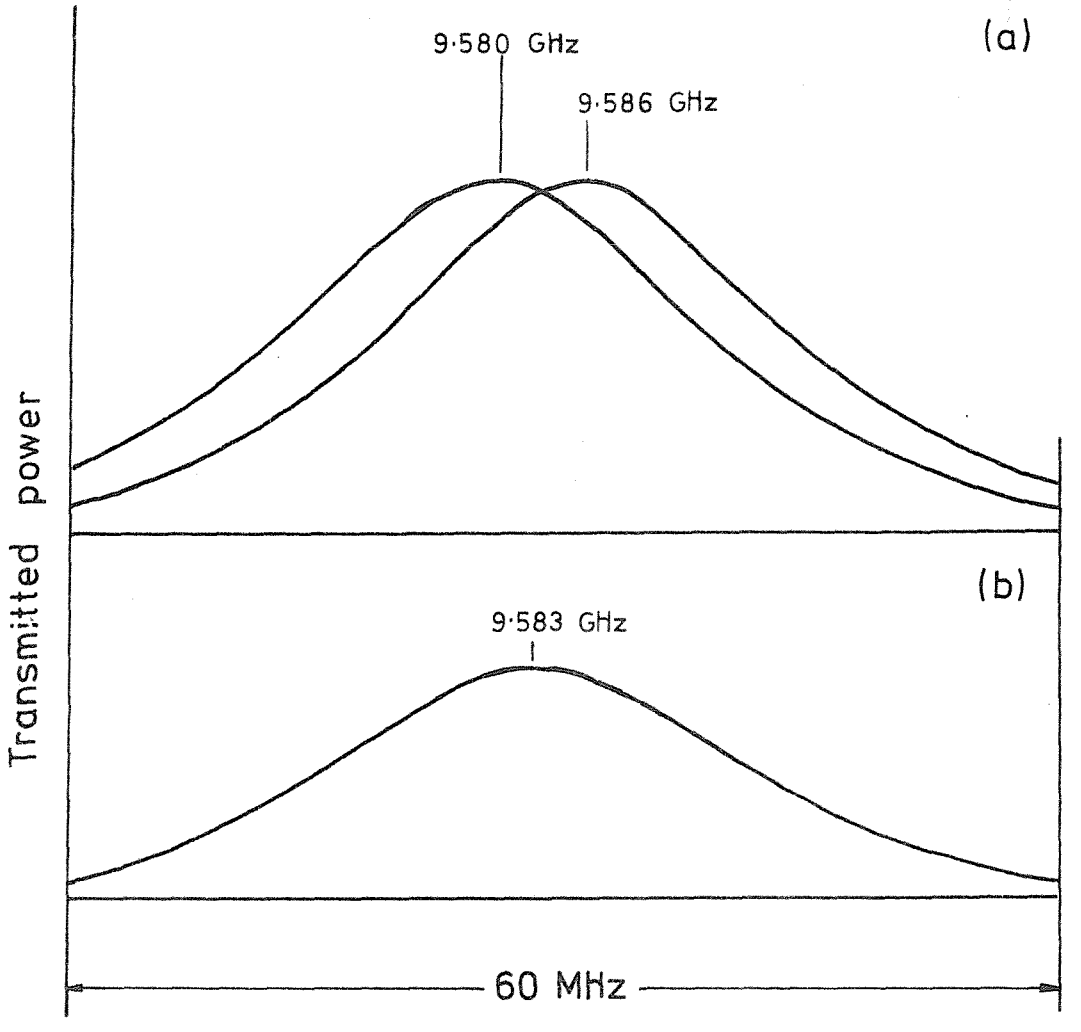

FIGURE 45. RESONANCE CURVES OF A RING RESONATOR

(a) two curves obtained for positions of the output probe $\lambda_g/4$ apart.

(b) curve with output probe placed midway between the two positions in (a).

One of the commonest methods of matching right angle corners in many types of transmission line is the 45° mitre. In waveguide, matching can be achieved using either two 45° corners quarter of a wavelength apart, or a right-angle corner with a 45° mitre. The former is the easier to construct and more commonly used; design data on the latter variety appears to be limited to empirical results[71]. In balanced stripline work has been carried out on different types of right angle corner[72], and the 45° mitre was found to be most effective. Measurements have also been made of the depth of 45° mitre required to give a match in dielectric supported stripline, using line resonators[73].

In microstrip, mitred right angle corners (presumably matched) are evident in commercial M.I.C's, but the only published work is that of Arditi[74] in 1955 on different angles of mitre, and of Stephenson et al[75] in 1971 on mitred corners in 50 ohm microstrip.

The mismatch at an unmitred microstrip corner is due to the fringing field at the corner which introduces excess capacitance, and the effect of a mitre is to reduce the total capacitance at the corner. In view of the quasi TEM nature of the microstrip propagating mode, it appeared feasible to use simple static capacitances to calculate the depth of mitre required to give a match. This approach will be valid provided the dimensions of the corner are small with respect to the microstrip wavelength. In common with Stephenson et al the depth of mitre is defined as the proportion of the corner diagonal removed expressed as a percentage (Figure 46(b)).

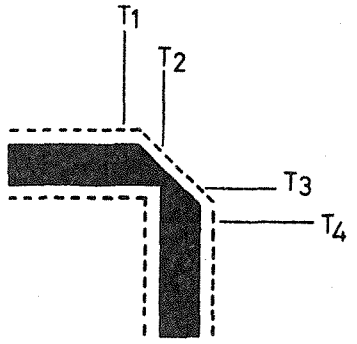

(a)

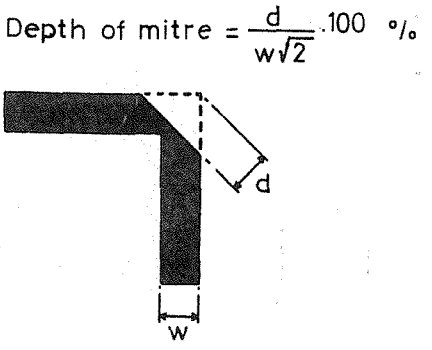

(b)

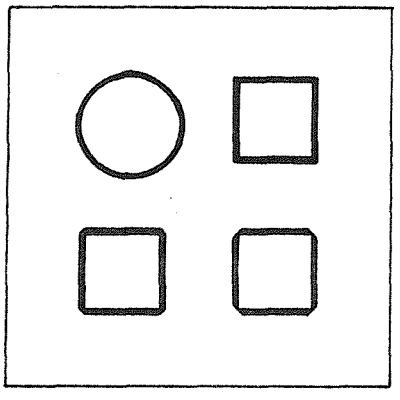

(c)

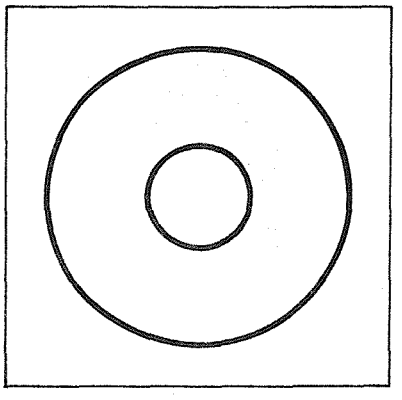

(d)

FIGURE 46. (a) Reference planes for a mitred corner. The dotted line indicates the effective width of the fringing field.

(b) Definition of depth of mitre.

(c) Layout of rings on 51 x 51mm substrates used for measurements on corners.

(d) Layout of rings used to determine influence of curvature.

Figure 46(a) shows the mitred corner with the fringing field represented by a dashed line parallel to the conductors; it is assumed that the fringing field extends for the same distance all round the corner. The reference planes T_1 T_4 are taken a distance w back from the inside edge of the corner (which is as far back as 100% mitre extends). For a matched corner, it is assumed that the total capacitance of the line between planes T_1 and T_4 must equal the capacitance of an equivalent length of undisturbed line. In calculating the total capacitance, the fringing fields on either side of the line are represented by ideal parallel plate capacitors of width 0.44h. This value is derived from that for the fringing field at the edge of an infinitely wide balanced stripline, and is based on the results for open-circuit end correction given in Section 8.4.

The resulting equation for capacitances may equally well be written in terms of area. Thus, for a depth of mitre m, we have

$$\text{Area of conductor } \{3w^2 - 2m^2w^2\}$$

$$+$$

$$\text{Effective area of fringing field } \{(2w\Delta F - \Delta F^2) + 4w\Delta F(1-m) + 2.8\, mw\Delta F + 0.7\, \Delta F^2\}$$

$$=$$

$$\text{Area of undisturbed line of length } (2w + u) \quad \{(2w + u)(w + 2\Delta F)\}$$

where $\Delta F = 0.44h$ = equivalent width of fringing field

u = effective distance between planes T_2 and T_3

Rearranging,

$$m^2(2w^2) + m(1.172w\Delta F) - w^2 + uw - 2w\Delta F + 2u\Delta F + .293\Delta F^2 = 0 \qquad (41)$$

which can be solved for m.

This expression for m includes the effective length of the corner, u, which must be determined experimentally, and thus it remains a semi-empirical technique. Examination of equation 41 reveals that m is insensitive to changes in ΔF but very sensitive to any changes in u.

In verifying this expression for m experimentally, it was also intended to verify the assumption, implicit in the above derivation, that the mitre provides a broadband match. The unmatched corner is represented by a shunt susceptance, and by taking reference planes at T_2 and T_3 the full equivalent circuit includes two transmission lines u/2 long, as below.

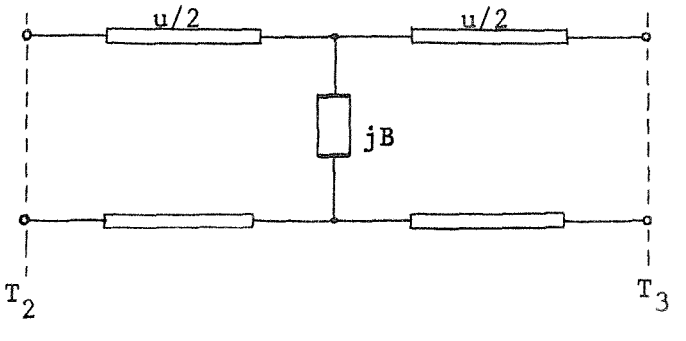

A resonance method was used to determine u and B which differed somewhat from methods used by other workers. In work on dielectric supported stripline Cooper[73] had used two line resonators of length λ_g and $3\lambda_g/2$ at 1 GHz, with corners at their midpoints; the matched condition was found by adjusting the depth of mitre until

both lines resonated at the same frequency. Stephenson et al,[75] working on alumina, used a ring resonator comprising two circular arcs intersecting at right angles, with microstrip coupling probes midway between the corners. From the previous discussion on discontinuities in ring resonators, it will be appreciated that if the number of wavelengths (M) on the ring was even, the microstrip probes would couple into the cosine form of standing wave and the resonant frequency was shifted; with M odd, coupling was to the sine form of standing wave, and no shift occurred. Using this technique only half the full number of resonances are measured.

In this investigation the method used was to incorporate four corners into a square ring resonator, and using the coaxial probes it was possible to couple into either the sine or the cosine forms of standing wave and thus to measure both frequencies at each resonance. The linear form of these square rings allowed accurate measurement of geometric length. Owing to the practical difficulties of successively altering the corners on one ring, a number of rings were used covering a range of mitres, viz. 0, 33, 55, 70, 80, 90%. Using two 51 x 51 mm substrates, three square rings and one circular ring were placed on each substrate. All the mitres on one square ring were identical, but each square ring was different.

Figure 46(c) shows the layout of a typical substrate. The circular ring was used for a phase velocity determination on the substrate. In order to ensure that the curvature of the ring had no effect, a ring of this diameter and a larger ring of the same linewidth were deposited on one substrate (Figure 46(d)), and their

resonant frequencies measured. No difference in phase velocity between the two rings was noted. The square rings resonated at approximately 8 GHz (M = 4), 10.5 GHz (M = 5), 12 GHz (M = 6), but only the even resonances are useful since identical voltage conditions are required at each corner. A second pair of substrates was therefore fabricated with a 4 λ_g resonance at 10.5 GHz. In all, three sets of four substrates were fabricated, for lines of 36, 50 and 70 ohms impedance.

An expression for the excess capacitance, C_x, at the corner may be found from the theory of ring resonators, as given in the appendix (section 12.3.2.)

The expression is

$$\frac{C_x}{C'} \simeq S. \frac{f_1 - f_2}{f_2} \qquad (42)$$

where C' is the capacitance per unit length of the line (Fm^{-1})

$S = Mv/4f_1$ is the length of one side of the square (measured to the inside edge of the corner).

$$\text{Also } u = \frac{1}{4} \cdot \left[\frac{Mv}{4f_1} - S \right] \qquad (43)$$

The ratio C_x/C', and the length of the corner u are shown in Figures 47, 48, and 49 for the 36, 50, 70 ohm lines respectively. The quantity C_x/C' is found to be approximately proportional to the square of the depth of mitre, and thus to the area of the triangular piece of conductor removed by the mitre, as the quasi-static theory would suggest. (The proportionality is approximate because there is also a small change in area of the fringing field when the mitre is removed).

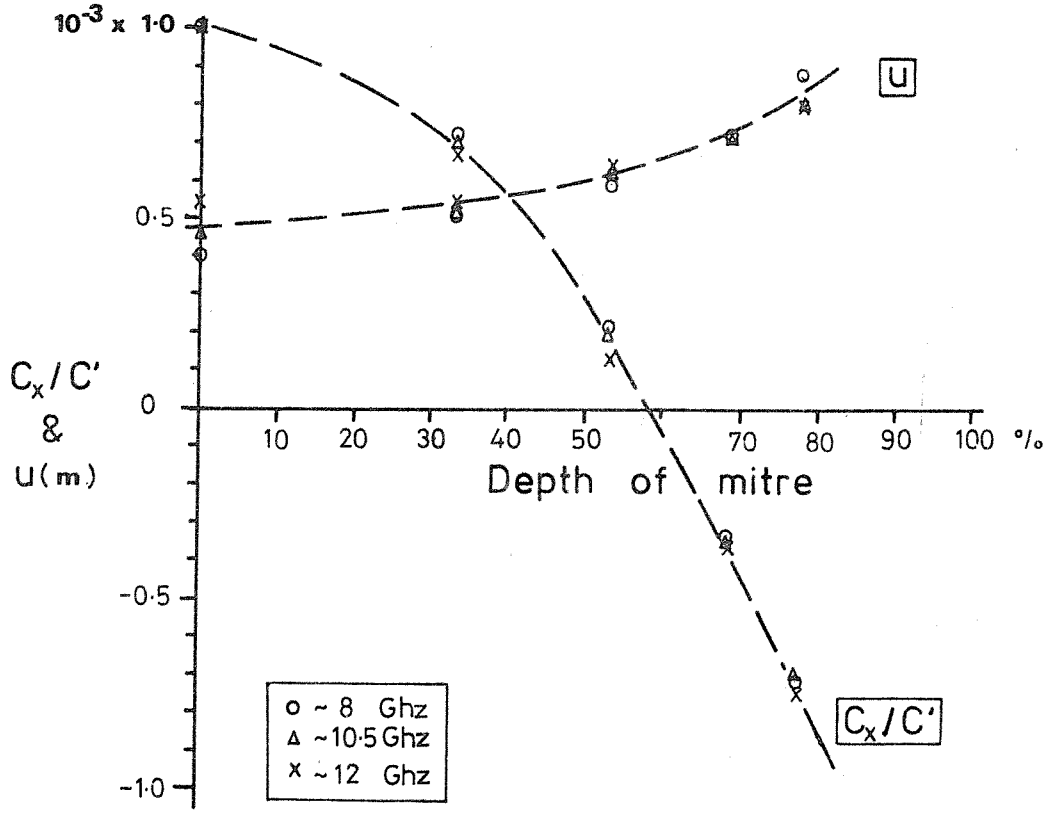

FIGURE 47. EXCESS CAPACITANCE AT CORNER C_x/C', AND EFFECTIVE LENGTH OF CORNER, u, AS A FUNCTION OF DEPTH OF MITRE FOR

$Z_o \simeq 36$ ohms (w = 1.32 mm h = 0.68mm)

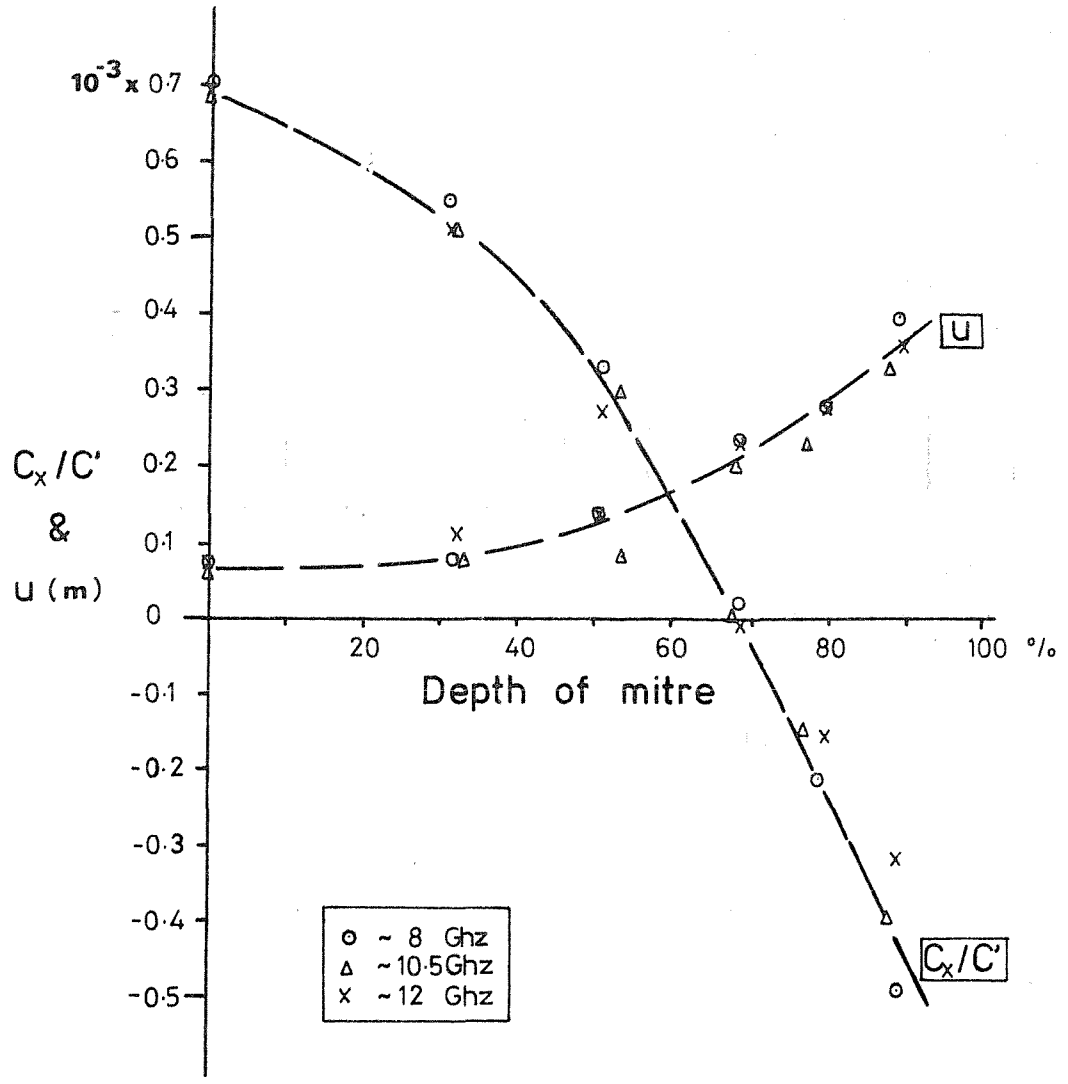

FIGURE 48. EXCESS CAPACITANCE AT CORNER C_x/C', AND EFFECTIVE LENGTH OF CORNER, u, AS A FUNCTION OF DEPTH OF MITRE, FOR

$Z_o \simeq 50$ ohms (w = 0.68mm h = 0.69mm)

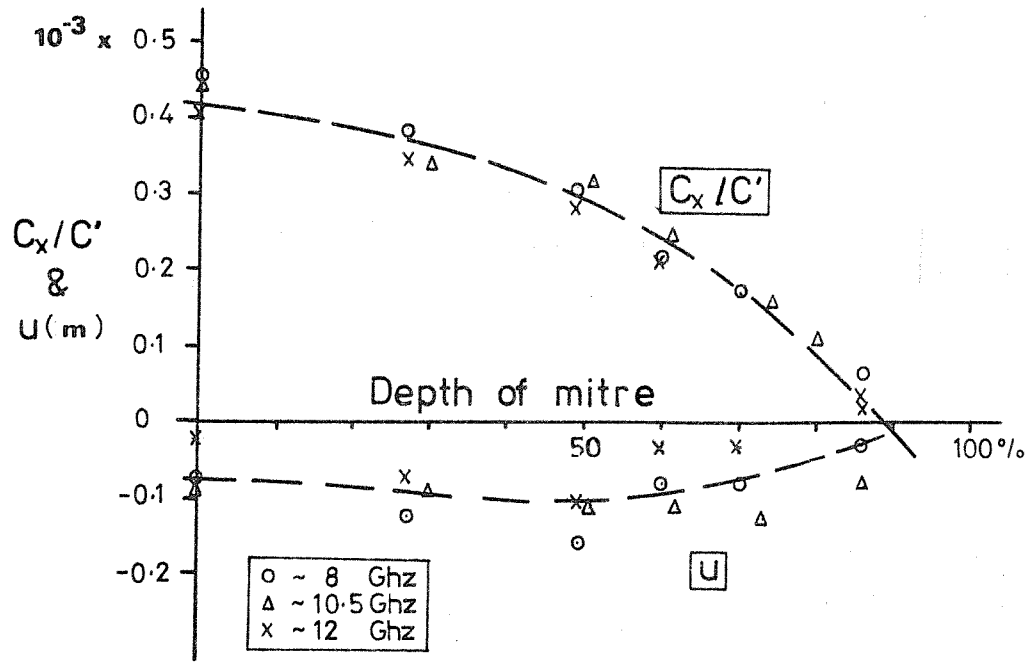

FIGURE 49. EXCESS CAPACITANCE AT CORNER C_x/C', AND EFFECTIVE LENGTH OF CORNER, u, AS A FUNCTION OF DEPTH OF MITRE, FOR $Z_o \simeq 70$ ohms (w = 0.32mm h = 0.68mm)

The capacitance shows little frequency dependence for any of the lines, but the quality of some of the 70 ohm rings was poor, and this was the reason for the erratic behaviour of u, which is the difference between relatively large calculated and measured lengths, in Figure 49. The effective length of a matched corner is found to increase linearly with w/h between 36 and 70Ω , as shown in Figure 50. Cooper had noted similar behaviour with dielectric supported stripline.[73] Using values of u from Figure 50 in equation 41, the depth of mitre required for a match as a function of w/h can be calculated. This curve is shown in Figure 51, together with the experimentally determined points from Figures 47, 48 and 49.The agreement is reasonably good; the curve becomes less accurate for low impedances as the line dimensions become significant fractions of a wavelength, but for lines between 70 ohms and 36 ohms the prediction appears to be accurate to within a few percent. One fact which does emerge from this graph is the impossibility of using a 45^{o} mitre to match a line of impedance >70 ohms on alumina.

It has been assumed throughout that the corner is lossless, but in fact it does radiate a small amount. This does not affect the analysis, but does appear as a difference in Q factor of the sine and cosine forms of standing wave on the square rings if M is even. (If M is odd only one resonance curve is obtained, with intermediate Q factor). The Q factor was independent of the depth of mitre of the corners. A guide to the power fraction radiated by the corner can be obtained by assuming that the high Q factor of the sine form of standing wave (with voltage nodes at the corners) represents the Q due solely to conductor (and dielectric) loss. Then

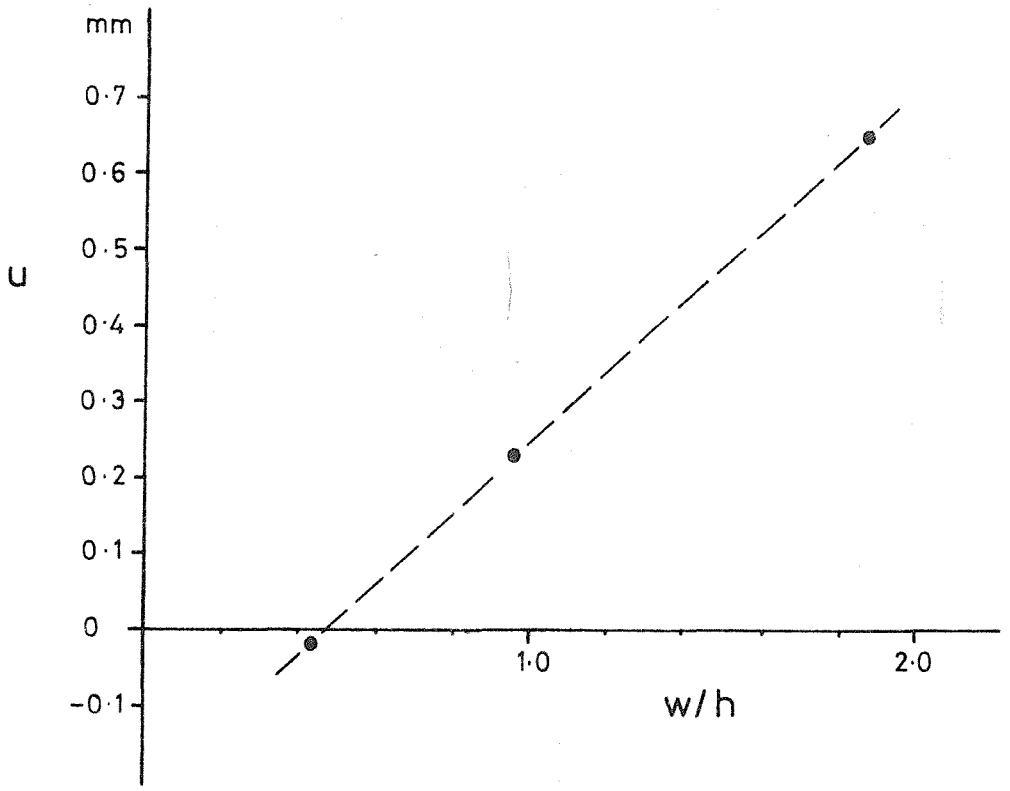

FIGURE 50. EFFECTIVE LENGTH OF A MATCHED CORNER AS A FUNCTION OF w/h, TAKEN FROM FIGURES 47, 48, 49 with $C_x = 0$.

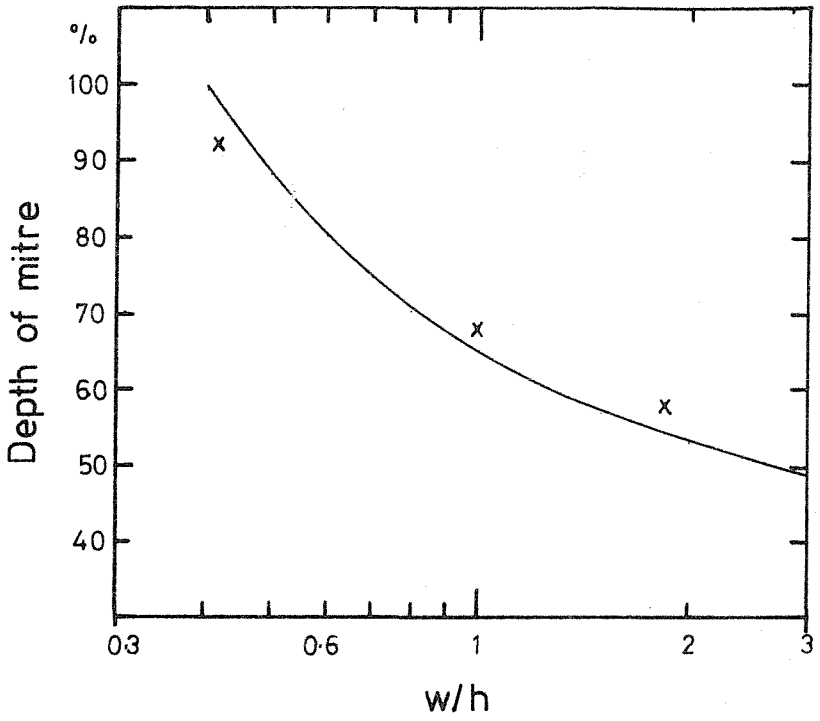

FIGURE 51. CALCULATED DEPTH OF MITRE AS A FUNCTION OF w/h

MEASURED POINTS ARE SHOWN ×

$$\frac{P_{rad}}{P_{inc}} = (1 - \rho^2) \times 100\% \qquad (44)$$

where ρ is the reflection coefficient of the radiation conductance at a corner, and is found from equations 31 - 34. Thus

$$-\ell n\, \rho = \frac{\pi}{2} \cdot \frac{Q_c - Q_o}{Q_c Q_o} \qquad (45)$$

The radiated power fraction calculated in this way shows definite anomalies, giving maximum radiation at 10.5 GHz and minimum at 12 GHz. It was suspected that this behaviour was due to interaction between radiation from the four corners since the squares had a diagonal length $\sim \lambda_o/2$, and further Q measurements on larger square rings supported this theory. Figure 52 shows the measured Q factors of five square rings of side approximately 30 mm as a function of frequency. The power fraction radiated was calculated from these Q factors and equation 45, and then divided by a factor of 4 to allow comparison to be made with Lewin's results[42] (since Lewin's theory is based on unidirectional current flow, but the square rings support standing waves). Considering the very rough approximations used, agreement is reasonable and the results are of a similar order of magnitude to Lewin's figures. Were the initial assumption correct, that there was no radiation for one of the resonances, the high Q values would lie on a $\sqrt{f}$ gradient line, and it can be seen that this is not the case. What this experiment did show was that it is necessary to exercise caution in calculating the radiation loss from microstrip components in close physical proximity to each other. Easter[45]

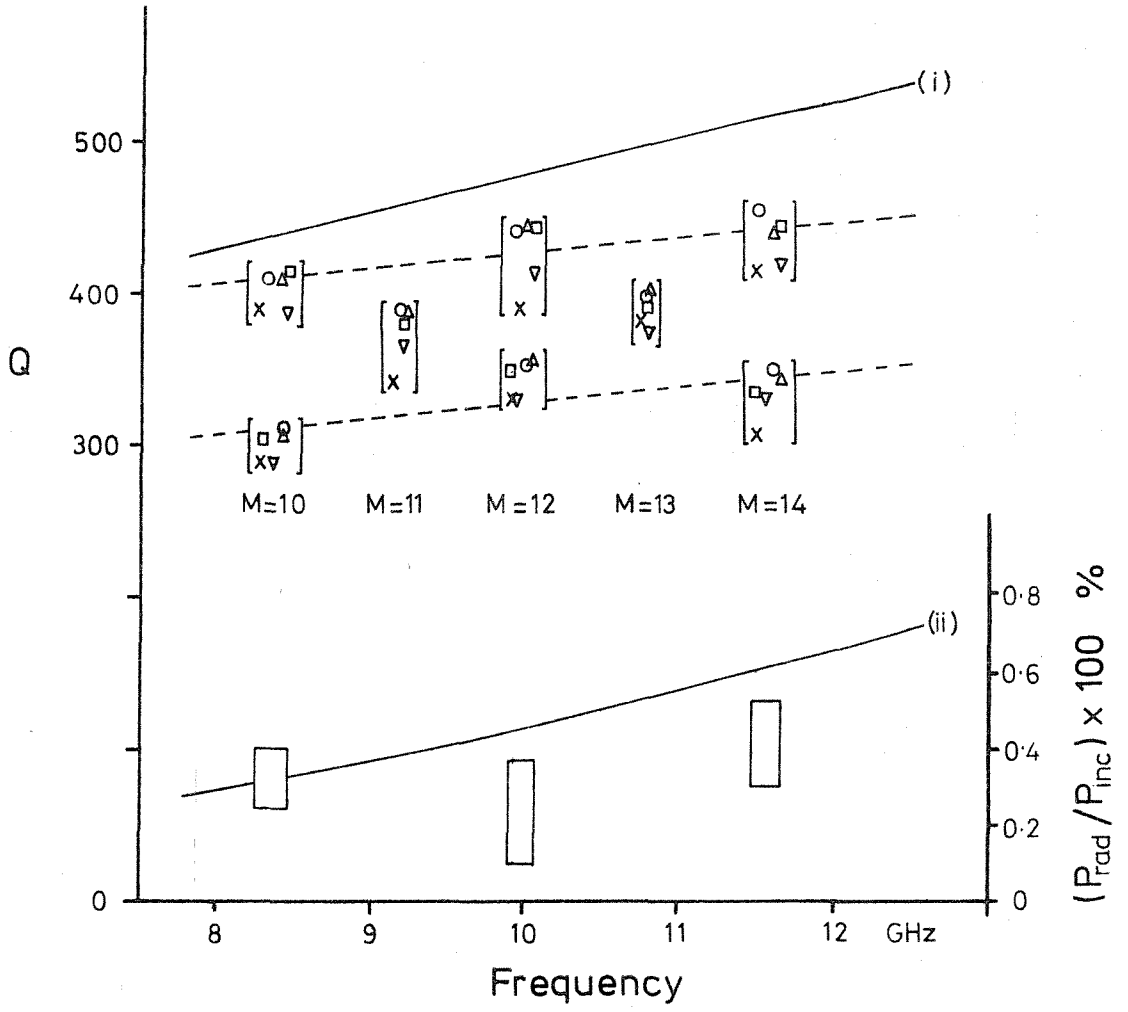

FIGURE 52. Q FACTOR AND RADIATION LOSS FROM 50Ω SQUARE RING RESONATORS OF SIDE ~30mm

(The square brackets are to emphasise the grouping of the Q measurements, and have no other significance).

Curve (i) is an arbitrary line of slope $\sqrt{f}$; the dotted line indicates the slope of the measured points.

Curve (ii) is calculated from Lewin's expression for radiation from a right angle corner (reference 42). The rectangles indicate values calculated from the Q measurements above (and include the effect of a 5% error in Q).

has noticed a similar phenomenon with parallel-coupled half wavelength filter sections.

9.4 Impedance Steps

Changes in line impedance are required in filters, circulators, and quarter wavelength transformers, and in microstrip are most easily realised by an abrupt step in width of the top conductor.

In balanced stripline, the effect of a step in width of the centre conductor has been studied by Altschuler and Oliner[48], and more recently by Nalbandian[76]. Altschuler and Oliner showed that the stripline step in width was the Babinet equivalent of a step in height of a parallel plate guide, whose solution is known, and Nalbandian uses the same technique. The Babinet equivalence procedure, derived from optics, may be expressed as follows:- if the equivalent circuit of a given discontinuity is known, then the dual equivalent circuit represents that structure obtained by interchanging electric and magnetic fields and boundaries in the original discontinuity structure. Quantities are replaced by their duals in any equations, but numerical values remain unaltered. The procedure is best explained by carrying it through for the microstrip step.

The known solution for a step in height of a parallel plate guide has been given by Marcuvitz[63]

The equivalent circuit is

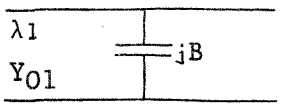

and $\frac{B}{Y_{O_1}} = \frac{2\,r_1}{\lambda_1} \cdot G$ (46)

$$G = \ell n \left[\left(\frac{1 - \xi^2}{4\xi} \right) \left[\frac{1 + \xi}{1 - \xi} \right]^{\frac{1}{2}\left(\xi + \frac{1}{\xi}\right)} \right] + \frac{2}{K} \qquad \xi = \frac{r_2}{r_1} < 1$$

$$K = \left[\frac{1 + \xi}{1 - \xi} \right]^{2\xi} \cdot \left[\frac{1 + \{1 - (r_1/\lambda_1)^2\}^{\frac{1}{2}}}{1 - \{1 - (r_1/\lambda_1)^2\}^{\frac{1}{2}}} \right] - \frac{1 + 3\xi^2}{1 - \xi^2}$$

$r_{1,2}$ is the height of the guide with impedance $Y_{O_{1,2}}$ and wavelength $\lambda_{1,2}$. K is a small frequency correction term, and the expression is correct to within 3% for $r_1/\lambda_1 < 0.07$.

The field distribution at the step in height of a parallel plate guide is sketched in Figure 53(a), with the field in the narrow part of the guide being only slightly disturbed.

The distribution of electric field lines closely resembles that of the magnetic field lines seen looking down on a microstrip step, except that magnetic field lines in microstrip disappear into the substrate either side of the top conductor, and the electric field lines bow out at the edges of the top conductor. Complete equivalence is achieved by constructing a parallel plate model of microstrip with no fringing field, and with magnetic field lines parallel to the conductors, as in Figure 53(c).

The new structure is required to have the same capacitance per unit length and phase velocity as the original microstrip line, and thus it is assumed to be filled with a material of relative permittivity ε_{eff}; its width is given by

$$W_{eff} = \frac{h}{\varepsilon_o \sqrt{\varepsilon_{eff}} Z_o v_o} \qquad (47)$$

A change in width of this model is now the exact equivalent of a change in height of a parallel plate guide. The microstrip equivalent circuit is thus a series reactance.

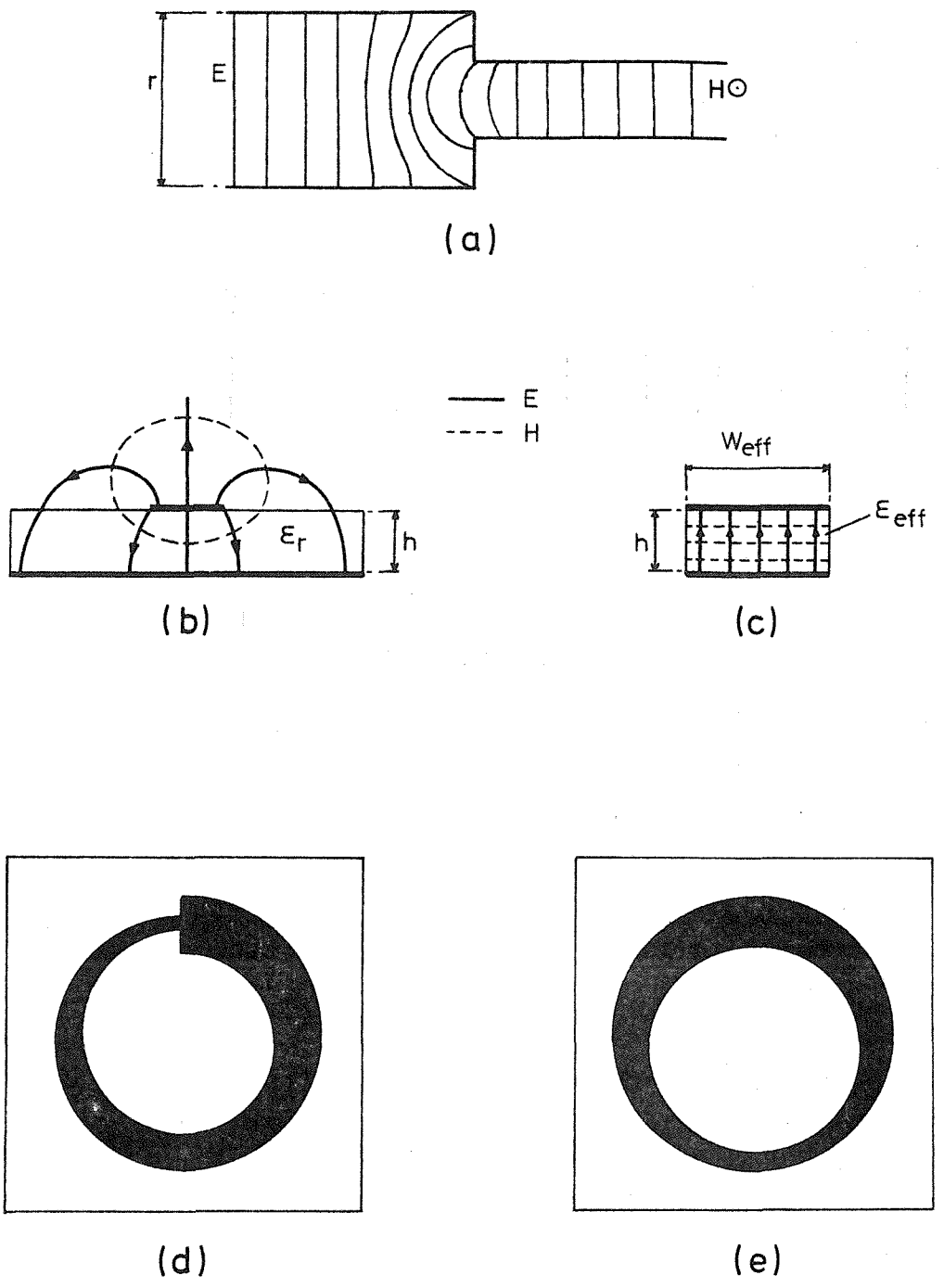

FIGURE 53

(a) Side view of step in parallel plate waveguide, showing electric field lines.

(b) Microstrip field configuration.

(c) Parallel plate model of the microstrip line in (b).

(d) Form of the tapered ring resonator containing abrupt step (exaggerated).

(e) Form of the taped ring resonator used to assess the effect of the taper.

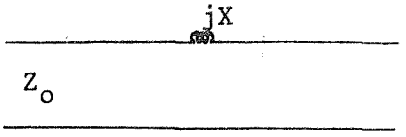

Thus $$\frac{X}{Z_o} = \frac{2\,W_{eff}}{\lambda} \cdot G \qquad \text{[the dual of eqn. 46]} \qquad (48)$$

where Z_o, W_{eff} and λ refer to the line on the low impedance side of the step.

Combining equations 47 and 48 gives the inductance I of the series reactance

$$I = 4\,h\,G \quad nH \quad \text{[h in cm]} \qquad (49)$$

Figure 54 shows I as a function of W_{eff_1}/W_{eff_2} for a 0.65 mm thick substrate. The inductance is very slightly frequency dependent through G, but for a 50 ohm line on alumina the variation over X-band is negligible.

Experimental determination of the reactance at a microstrip step in width was carried out using ring resonators. The resonator was in fact a long smooth tapered line turned back on itself to form a circular resonator with an abrupt, symmetrical step, as sketched in an exaggerated manner in Figure 53 (d).

The ring was about 36 mm in diameter and the reflection coefficient of the taper was calculated to be less than 0.01 in magnitude, which allowed its effect to be neglected. This was confirmed by measurements on a ring of the form shown in Figure 53 (e), which exhibited only a single resonance peak. The step is assumed to be lossless and is represented by a series reactance.

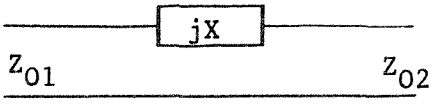

The effect of the taper is to provide a reflectionless match between the impedance Z_{0_2} on one side of the step and the impedance Z_{0_1}

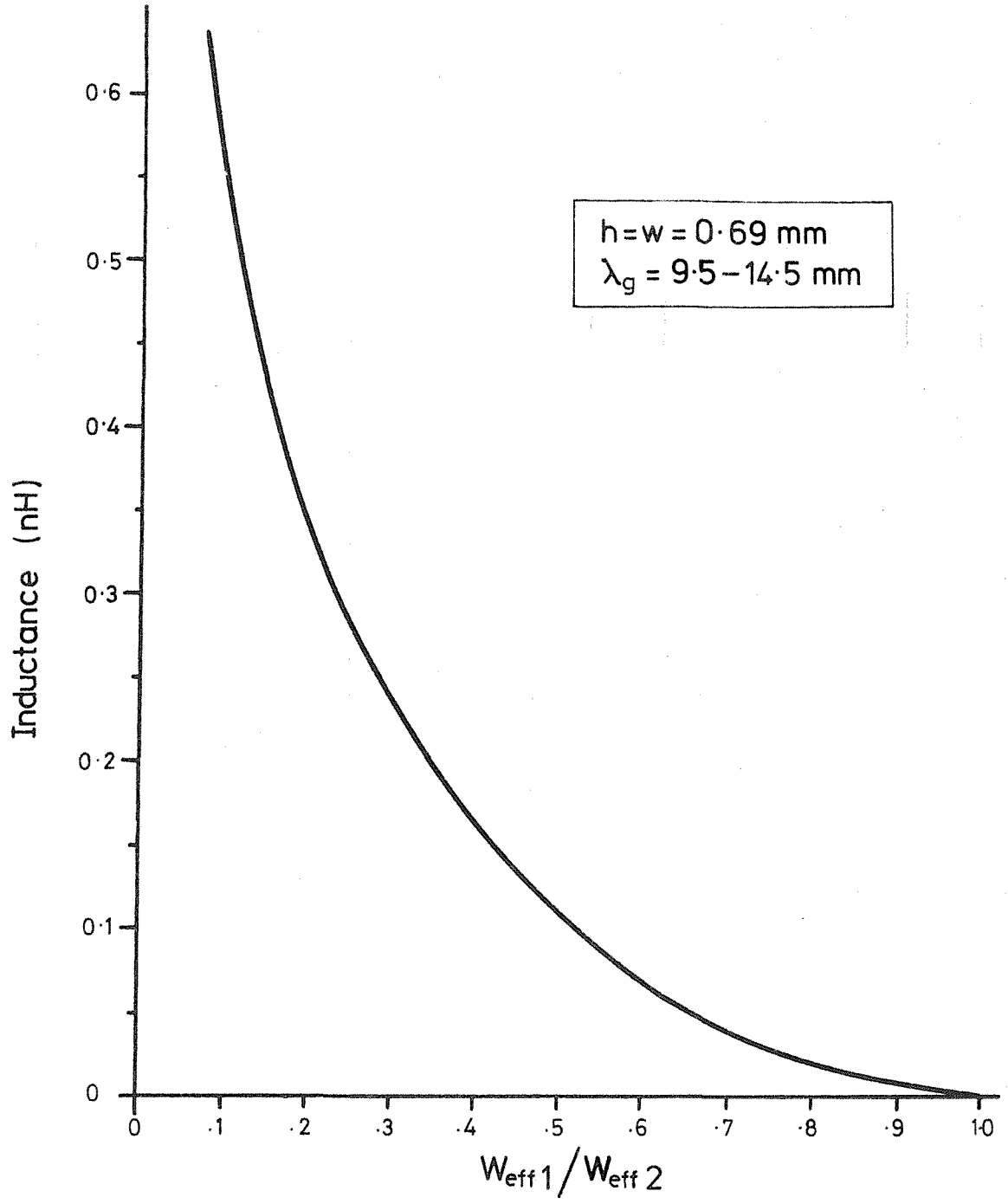

FIGURE 54. CALCULATED INDUCTANCE AT AN ABRUPT STEP IN MICROSTRIP AS A FUNCTION OF THE RATIO OF EFFECTIVE LINEWIDTHS ON EITHER SIDE

on the other side. It is assumed to be lossless and to have constant phase velocity along its length. (In fact for a 25/50 ohm taper the phase velocity changes by 7%).

Analysis of a ring resonator containing an impedance step is given in the appendix, section 12.3.3, where the following equations are derived for the series reactance at the step, X", as a function of the two measured resonant frequencies f_1, f_2 ($f_2 < f_1$):

$$X'' = \frac{X}{Z_{01}} = \frac{(1 + n^2) - 2n}{2 \tan \phi} - \left[\frac{(1 + n^2) + 2n}{2}\right] \tan \phi \qquad (50)$$

$$\phi = \frac{1}{2} \cdot \frac{f_2}{f_1} \left[2M\pi + \cos^{-1}\left(\frac{2n}{1+n^2}\right)\right]; \quad n^2 = \frac{Z_{02}}{Z_{01}} > 1$$

Experiments were carried out on rings containing abrupt symmetrical steps of 28/48 ohms, 30/42 ohms and 46/60 ohms. Each ring resonated at four pairs of frequencies in X-band, and in two cases a pair of rings of different diameters but with the same step ratio were fabricated. The Q factors of the resonances in a pair were equal to within the 5% measurement accuracy, indicating little radiation from the step. The calculated series reactances, normalised to the low impedance lines, are shown in Figure 55 (a), (b) and (c), together with theoretical curves predicted from the Babinet equivalence theory.

The error bars only show the relative accuracy of each point, and indicate the effect of a 1 MHz error in both the resonant frequencies. The absolute accuracy of the experimental points is found to be strongly dependent on the impedance ratio, n^2, as a result

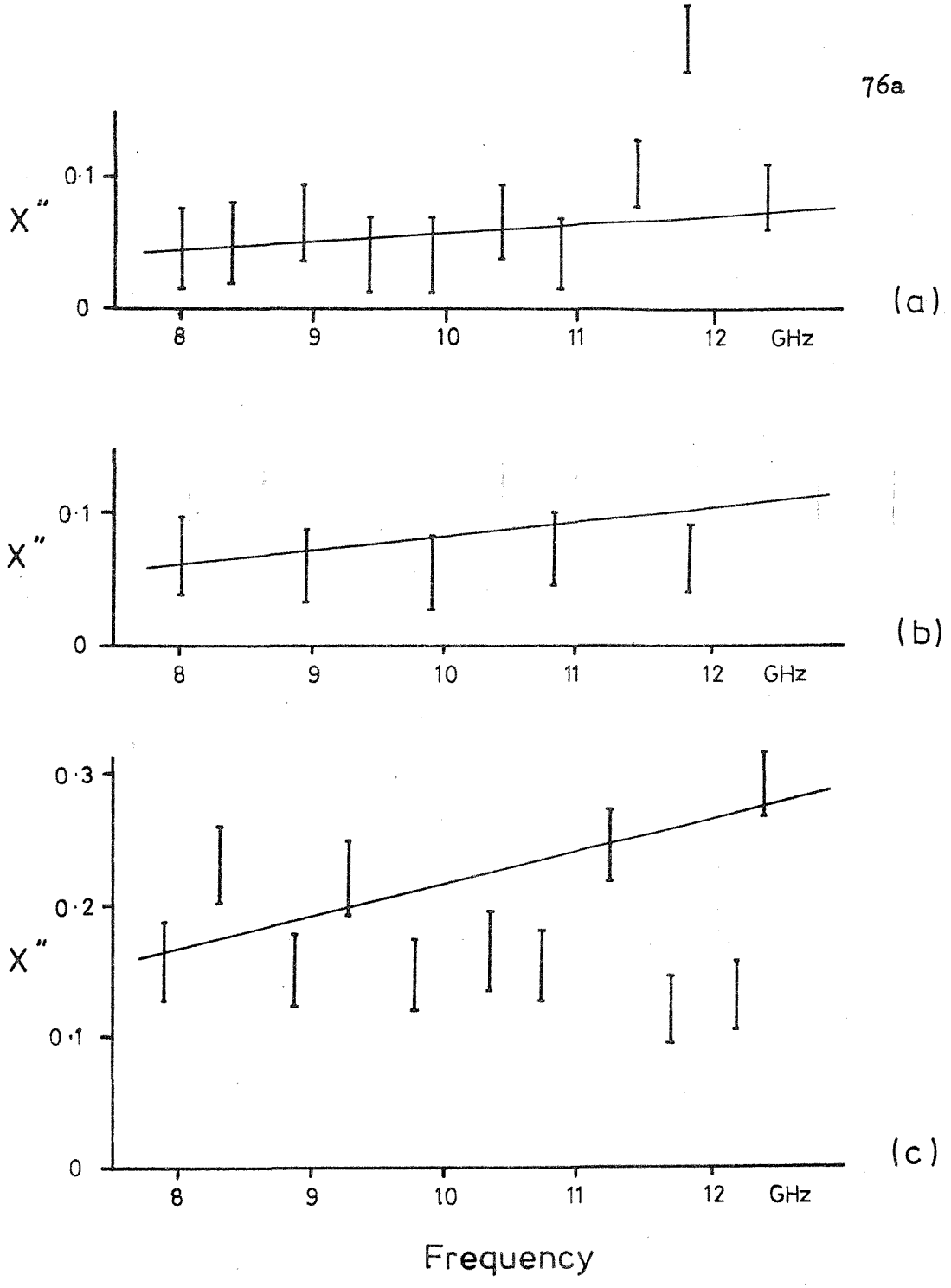

FIGURE 55. NORMALISED REACTANCE AT ABRUPT STEP IN MICROSTRIP

THE ERROR BARS INDICATE RELATIVE ERROR (SEE TEXT)

(a) 46/60 ohm step

(b) 30/42 ohm step

(c) 28/48 ohm step

I experimental points; —— Babinet theory

of the form of equation 50. Accurate determination of microstrip impedance is possible to within approximately $\pm$ 1%, but an error of this magnitude is sufficient to double the size of the error bars in Figure 55. In fact Time Domain Reflectrometry was used for impedance measurement in this experiment, and the accuracy of this method was approximately $\pm$ 1 ohm. (The technique was to measure the impedance of a number of lines of different widths deposited on a substrate from the same batch, from which a graph of Z_o vs. w/h was drawn up and used for subsequent impedance determinations).

Thus the overall error in the experimental points in Figure 55 may amount to $\pm$ 100% at worst. In view of this the neglect of other sources of error in the analysis, such as the variation in phase velicity along the taper, is quite reasonable. Some slight improvement in the experimental accuracy could be achieved by re-processing the substrates and measuring their properties individually, but it is felt that these results as they stand are sufficiently good to establish the validity of the Babinet equivalence procedure when applied to impedance steps in microstrip. The procedure enables the reactance at an abrupt step between any two microstriplines to be accurately determined (with the proviso that the linewidth is small with respect to the microstrip wavelength). It yields no information as to the precise location of the electrical plane defining the step, but consideration of the fringing field around the microstrip line shows that this plane will be on the high impedance side of the step, displaced a distance equal to the fringing field at the end of the low impedance line, i.e.$\simeq$ 0.44h. Experiments with the coaxial probes have confirmed this approximate position.

Wolff[77] has worked on impedance steps in microstrip lines on

'Polyguide' substrates ($\varepsilon_r = 2.3$), and has noted severely non-linear behaviour below 12 GHz. This was due to higher-order modes which are present at these frequencies on low permittivity substrates. The frequency at which higher-order modes on alumina become significant is much higher, and the inductance at an impedance step can be expected to remain approximately constant up to $\sim$ 20 GHz on typical alumina substrates.

9.5 Slot line

Slot line is a type of planar transmission line comprising a narrow slot in a metallic layer on one side of a dielectric sheet (Figure 1(e)). It was proposed by Cohn[78] in 1968, who later analysed this configuration by treating it as a waveguide problem. Results of Cohn's analysis have been presented graphically[79]. Another, numerical approach is that of Itoh[80] which appears to be in agreement with Cohn's results.

The electric field in slot line extends across the width of the slot, while the magnetic field forms longitudinal loops perpendicular to the slot. This gives rise to regions of elliptical polarisation which Cohn has suggested may be useful for non-reciprocal ferrite devices; another advantage of slot line is the ease with which shunt components may be mounted. Like microstrip, slot line has zero cut-off frequency; it is more dispersive than microstrip and because propagation is not TEM its impedance varies more strongly with frequency. There is no exact definition of impedance for a non-TEM mode; Cohn defined it in terms of the voltage across the slot and the power transmitted, but this gives a predicted value higher than the measured impedance.

Experimental work with slot line suffers from the lack of a good transition, but using the coaxial probes it has been found possible to couple in to a slot line ring resonator, and hence to determine wavelength and attenuation. A small number of measurements have been made, mainly to determine the effectiveness of this method. Slot line rings 0.13 mm wide and ~30 mm in diameter were deposited on two alumina substrates, and each resonated at five frequencies in X-band. Their impedance according to Cohn was 75 ohms, the value suggested to give a 50 ohm match. Normally for slot line, a substrate with higher permittivity than alumina (ε_r=10) would be used; it was found with these alumina substrates that any metallic surface underneath the substrate gave rise to spurious resonances, and measurements were therefore made with the substrates suspended in air. Wavelength measurements are shown in Figure 56 as a function of frequency, together with Cohn's predicted curve for this width of slot. Agreement between theory and experiment is good. The Q values of the resonances are also shown in Figure 56, and they are found to increase with $\sqrt{f}$, as they would for a microstrip ring.

These measurements demonstrate the versatility of the coaxial probe method of resonator coupling, and there is clearly scope here for further study.

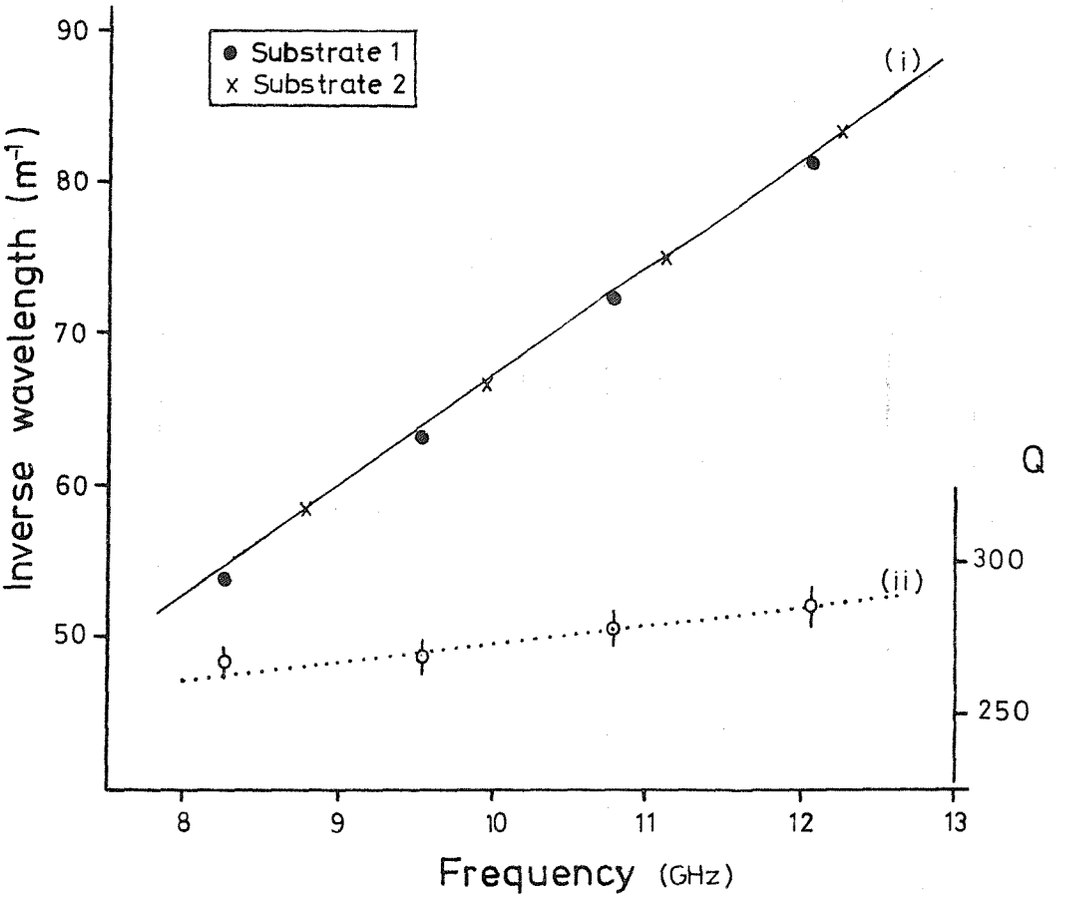

FIGURE 56. INVERSE WAVELENGTH, AND Q FACTOR OF SLOT LINE RING RESONATORS, AS A FUNCTION OF FREQUENCY

Substrate (i) w = 0.14mm h = 0.68mm

Substrate (ii) w = 0.12mm h = 0.68mm

Curve (i) is based on the theory given by Mariani, Cohn et al (reference 79).

Curve (ii) is a line of slope $\sqrt{f}$, fitted to measured Q values.

10. CONCLUSION

The aim of the project was to study some of the basic characteristics of microstrip, and to derive data to aid the design of components for microwave integrated circuits.

In the search for suitable measurement techniques a microstrip standing wave indicator was developed, but, having overcome the problem of radiation from the launcher, it was found that substrate quality was a limiting factor on the performance of the instrument, and this prevented meaningful measurement of standing wave ratio. The instrument was used however for accurate wavelength determination, where the fact that measurements could be made at all frequencies without the need for specially fabricated structures was an advantage.

Most of the quantitative results presented have been obtained using microstrip resonators, in conjunction with coaxial coupling probes above the substrate. This leads to a very versatile measurement technique which is well suited to the study of discontinuities in microstrip. One drawback of using coaxial probes, namely the direct coupling between them, does preclude measurements on small size resonators, but this is not a severe limitation.

Measurements on line resonators have yielded data on line attenuation and open-circuit radiation loss. It has been found that the quality of the plated gold layer forming the conductors is a major factor in the discrepancy noted between theoretical and experimental results for line attenuation, and that it is important to make the conductors at least twelve skindepths thick in order to ensure that the conductivity reaches the bulk value. Results for radiation loss from an open-circuit

resonator have slightly exceeded the theoretical value predicted by Lewin, but they do show that the radiation loss at X-band is independent of the resonator length for lines > λg long on alumina. The end correction for an open-circuit has also been measured using line resonators, and it was found that the extension to microstrip of results applicable to balanced stripline provides values for the microstrip end-correction very close to those of a much more exact analysis, for $\varepsilon_r = 9{\cdot}6$.

Measurements on ring resonators have been used in the study of microstrip discontinuities, utilising the theory of periodically-loaded structures to analyse the situation. The effect of a 45° mitre on a right-angle corner has been treated using straightforward electrostatic theory, and experiments have shown that this approximation appears reasonably accurate for lines between 36 and 70 ohms impedance. The theory is not confined to corners matched by means of a 45° mitre, although the experimental work has been carried out only on this type of corner. In studying the effect of an abrupt step in width of the top microstrip conductor, the Babinet equivalence procedure was used to identify the problem with the corresponding impedance step in parallel-plate waveguide, and results calculated on this basis have been confirmed experimentally. Despite the precision of resonator measurements, it has been found that quantitative determination of some forms of microstrip discontinuity requires an experimental accuracy bordering on the limits of what is currently possible with this technique.

In addition to the work on standard microstrip, it has been demonstrated that the measurement methods evolved here are also

suitable for both coupled microstrip lines and for slotline; either of these structures could merit an extended investigation. As it is, work has concentrated on standard microstrip lines on alumina substrates. It has been found possible to give reasonably comprehensive data on a number of common microstrip discontinuities, thereby alleviating some of the difficulties in microstrip circuit design.

11. REFERENCES

1. BARRETT R.M. "Etched sheets serve as microwave components" Electronics, vol.25, no. 6 , June 1952, pp 114-118.
2. WHEELER H.A. "Transmission line properties of parallel strips separated by a dielectric sheet" IEEE Trans. Microwave Theory Tech. vol MTT-13 no.3, March 1965, pp 172-185.
3. SCHNEIDER M.V. "Microstrip lines for microwave integrated circuits" Bell Syst.Tech.J. vol.48, no.5, May-June 1969, pp 1421-1444.
4. CAULTON M.,HUGHES J.J.,SOBOL H. "Measurements on the properties of microstrip transmission lines for microwave integrated circuits", RCA Review, vol.27, September 1966, pp 377-391.
5. HARTWIG C.P., MASSÉ D., PUCEL R.A. "Frequency dependent behaviour of microstrip" 1968 International G-MTT Symposium Digest, pp 110-116.
6. PUCEL R.A., MASSÉ D., HARTWIG C.P. "Losses in microstrip" IEEE Trans. Microwave Theory Tech. vol.MTT-16, no.6, June 1968, pp 342-350. Correction: MTT-16,no.12,Dec '68,p1064
7. ARNOLD S., "Dispersive effects in microstrip on alumina substrates", Electron.Lett.,vol.5, no.26, 25 December 1969, pp 673-674.
8. GUNSTON M.A.R. "Microwave transmission-line impedance data" Van Nostrand-Rheinhold, London 1972.
9. MARCH S. "Microwave micromin bibliography" Microwaves vol.8, no.12, December 1969, and vol.9, no.1, January 1970.

10. EAVES R.E., BOLLE D.M. "Guided waves in limit cases of microstrip" IEEE Trans. Microwave Theory Tech., vol.MTT-18, no.4, April 1970, pp 231-232.

11. MITTRA R., ITOH T. "A new technique for the analysis of dispersion characteristics of microstrip transmission lines" IEEE Trans. Microwave Theory Tech., vol.MTT-19, no. 1, January 1971, pp 47-56.

12. SOBOL H. "Applications of integrated circuit technology to microwave frequencies" Proc. IEEE, vol.59, no.8, August 1971, pp 1200-1211.

13. CAULTON M. "Film technology in microwave integrated circuits" Proc.IEEE vol.59, no.10, October 1971, pp 1481-1489.

14. CORR D.G., DAVIES J.B. "Computer analysis of the fundamental and higher order modes in single and coupled microstrip" IEEE Trans. Microwave Theory Tech., vol MTT-20, no.10, October 1972, pp 669-678.

15. KRAGE M.K., HADDAD G.I. "Frequency dependent characteristics of microstrip transmission lines" IEEE Trans.Microwave Theory Tech., vol.MTT-20, No.10, October 1972, pp 678-688.

16. ASSADOURIAN F., RIMAI E. "Simplified theory of microstrip transmission systems" Proc. IRE, vol.40, no.12, December 1952, pp 1651-1657.

17. WHEELER H.A. "Transmission line properties of parallel wide strips by a conformal mapping approximation" IEEE Trans. Microwave Theory Tech., vol.MTT-12, no.5, May 1964, pp 280-289.

18. SILVESTER P. "TEM wave properties of microstrip transmission lines" Proc.IEE, vol.115, no.1, January 1968, pp 43-48.

19. BRYANT T.G., WEISS J.A. "Parameters of microstrip transmission lines and of coupled pairs of microstriplines" IEEE Trans. Microwave Theory Tech., vol.MTT-16, no.12, December 1968, pp 1021-1027.

20. SCHNEIDER M.V. "Computation of impedance and attenuation of TEM lines by finite difference methods" IEEE Trans. Microwave Theory Tech., vol.MTT-13, no. 11, November 1965, pp 793-800.

21. JUDD S.V., WHITELEY I., CLOWES R.J., RICKARD D.C. "An analytic method for calculating microstrip transmission line parameters" IEEE Trans. Microwave Theory Tech., vol.MTT-18, no.2, February 1970, pp 78-87.

22. DENLINGER E.J. "A frequency dependent solution for microstrip transmission lines" IEEE Trans.Microwave Theory Tech., vol.MTT-19, no.1, January 1971, pp 30-39.

23. BARLOW H.E.M., BROWN J. "Radio surface waves", Clarendon Press, Oxford 1962.

24. DALY P. "Hybrid-mode analysis of microstrip by finite-element methods", IEEE Trans.Microwave Theory Tech., vol.MTT-19, no.1, January 1971, pp 19-29.

25. JAIN O.P., MAKIOS V., CHUDOBIAK W.J. "Coupled mode model of dispersion in microstrip", Electron.Lett, vol.7, no.14, 15 July 1971, pp 405-407.

26. CHUDOBIAK W.J., JAIN O.P., MAKIOS V. "Dispersion in microstrip" IEEE Trans. Microwave Theory Tech. vol. MTT-19, no.9, September 1971, pp 783-784.

27. NAPOLI L.S., HUGHES J.J. "Foreshortening of microstrip open-circuits on alumina substrates" IEEE Trans.Microwave Theory Tech., vol.MTT-18, no.6, June 1971, pp 559-561.

28. SCHILLING W., LEHRFIELD S.S. "The real world of micromin substrates - part 2" Microwaves, vol.8, no.1, January 1969.

29. DENISON E., SPILLING J.F. "Developments of an X-band microwave integrated circuit marine radar beacon" A.S.W.E.Laboratory Note, XRA-69-9.

30. RICKARD D.C., CLOWES R.J. "Microwave microstrip design from 12-20 GHz" Plessey Company Report, March 1971.

31. KEISTER F.Z. "An evaluation of materials and processes for integrated microwave circuits" IEEE Trans. Microwave Theory Tech., vol.MTT-16, no.7, July 1968, pp 476-477.

32. TROUGHTON P. "The evaluation of alumina substrates for use in microstrip microwave integrated circuits" European Microwave Conference, London, September 1969.

33. JUDD S.V., RICKARD D.C., CLOWES R.J., WHITELEY I. "Fourth stage report on the design of microwave components in strip transmission lines" Plessey Company report 1970.

34. SUNDAHL R.C., SEDORA E.J. "Effects of alumina substrate surface defects on thin-film interconnect patterns" Proc.IEEE, vol.59, no.10, October 1971, pp 1462-1467.

35. WELCH J.D., PRATT H.J. "Losses in microstrip transmission systems for integrated microwave circuits" IEEE NEREM record (Boston) vol.8, November 1966, pp 100-101.

36. RAMO S., WHINNERY J.R., Van DUZER T. "Fields and waves in communication electronics" Wiley, New York, 1965.

37. HORTON R., EASTER B., GOPINATH A. "Variation of microstrip losses with thickness of strip" Electron.Lett., vol.7, no.17, 26 August 1971, pp 490-491.

38. GOPINATH A., HORTON R., EASTER B. "Microstrip loss calculations" Electron.Lett., vol.6, no.2, 22 January 1970, pp 40-41.

39. MORGAN S.P. "Effects of surface roughness on eddy current losses" J.Appl.Physics, vol.20, no.4, April 1949, pp 352-362.

40. SANDERSON A.E. "Effects of surface roughness on propagation of the TEM mode" Advances in Microwaves, vol.7, Academic Press, New York 1971.

41. CAULTON M., SOBOL H. "Microwave integrated circuit technology - a survey" IEEE J.Solid State ccts., vol.SC-5, no.6, December 1970, pp 292-303.

42. LEWIN L. "Radiation from discontinuities in stripline" Proc.IEE, vol.107, pt.c. February 1960, pp 163-170.

43. EASTER B., ROBERTS R.J. "Radiation from half-wavelength open-circuit microstrip resonators", Electron.Lett., vol.6, no.18, 3 September 1970, pp 573-574.

44. ROBERTS R.J., EASTER B. "Microstrip resonators having reduced radiation loss", Electron.Lett., vol.7, no.8, 22 April 1971, pp 191-192.

45. EASTER B., RICHINGS J.G. "Effects associated with radiation in coupled half-wave open-circuit microstrip resonators" Electron.Lett, vol.8, no.12, 15 June 1972, pp 298-299.

46. KOSTRIZA J.A. "Microstrip components" Proc.IRE, vol.40. no.12, December 1952, pp 1658-1663.

47. BOWNESS C. "Strip transmission lines" Electronic Engineering, vol.28, no.335, January 1956, pp 1-7.

48. ALTSCHULER H.M., OLINER A.A. "Discontintuities in the centre conductor of symmetric strip transmission line" IRE Trans. Microwave Theory Tech., vol.MTT-8, no.5, May 1960, pp 328-339.

49. FINCH P.J. "Microstrip; propagation, manufacture, and measurement" M.Sc. Thesis, Southampton University, December 1969.

50. GRÜNEBERGER G.K., KEINE V., MEINKE H.H. "Longitudinal field components and frequency dependent phase velocity in the microstrip transmission line" Electron.Lett., vol.6, no.21, 15 October 1970, pp 683-685.

51. ARDITI M. "Experimental determination of the properties of microstrip" Convention record of the IRE, 23 March 1953, pp 27-37. Reprinted in Electrical Communication, vol.30, December 1953, pp 283-293.

52. TROUGHTON P. "Measurement techniques in microstrip" Electron.Lett., vol.5, no.2, 23 January 1969, pp 25-26.

53. TROUGHTON P. "High Q-factor resonators in microstrip" Electron.Lett., vol.4, no.24, 29 November 1968, pp 520-522.

54. GINZTON E.L. "Microwave measurements" McGraw-Hill, New York, London 1957.

55. SOBOL H. "Radiation conductance of open-circuit microstrip" IEEE Trans. Microwave Theory Tech., vol.MTT-19, no.11, November 1971, pp 885-887.

56. BENEDEK P., SILVESTER P. "Equivalent capacitances for microstrip gaps and steps" IEEE Trans. Microwave Theory Tech., vol.MTT-20, no.11, November 1972, pp 729-733.

57. SMYTHE W.R. "Static and Dynamic electricity" McGraw-Hill, New York, 1939.

58. JAIN O.P., MAKIOS V., CHUDOBIAK W.J. "Open end and edge effect in microstrip transmission lines" IEEE Trans.Microwave Theory Tech., vol.MTT-20, no.9, September 1972, pp 626-628.

59. COHN S.B. "Parallel-coupled transmission line resonator filters" IRE Trans.Microwave Theory Tech., vol.MTT-6, no.4, April 1958, pp 223-231.

60. NAPOLI L.S., HUGHES J.J. "Characteristics of coupled microstrip lines" RCA Review, vol.31, 1970, pp 479-498.

61. GOULD J.W., TALLBOYS E.C. "Even and odd mode guide wavelengths for coupled lines in microstrip" Electron.Lett.vol.8, no.5, 9 March 1972, pp 121-122.

62. MAESEL M. "A theoretical and experimental investigation of coupled microstrip lines" Norwegian Institute of Technology, ELAB report TE-168, April 1971.

63. MARCUVITZ N. "Waveguide Handbook" MIT Radiation Laboratory Series, McGraw-Hill, New York 1951.

64. SCHWINGER J., SAXON D.S. "Discontinuities in waveguides" Gordon and Breach, New York 1968.

65. COLLIN R.E. "Field theory of guided waves" McGraw-Hill, New York, 1962.

66. SLATER J.C. "Microwave Electronics" Van Nostrand, New York 1957

67. KELL R.C. et al. "Novel temperature stable ceramics for microwave dielectric resonators and microstrip substrates" Electron Lett. vol.6, no.19, 17 September 1970, pp 614-616.

68. WESTED J., ANDERSON E. "Resonance splitting in non-uniform ring resonators" Electron.Lett. vol.8, no.12, 15 June 1972, pp 301-302.

69. WOLFF I. "Microstrip bandpass filters using degenerate modes of a microstrip ring resonator" Electron Lett. vol,8, no.12, 15 June 1970, pp 302-303.

70. PATEL R.N. "Microwave conductivity of thick-film conductors" Electron.Lett., vol.6, no.15, 23 July 1970, pp 455-456.

71. ELSON N. "Rectangular waveguide systems" Wireless Engineer, vol 24, no.281, February 1947, pp 44-54.

72. FROST A.D., MINGINS C.R. "Microwave strip circuit research at Tufts College" IRE Trans.Microwave Theory Tech., vol.MTT-3, no.2, March 1955, pp 10-12.

73. COOPER H.W., RINGENBACH M.E. "Measurements of attenuation and phase velocity of various laminate materials at L-band" IRE Trans.Microwave Theory Tech., vol.MTT-3, no.2, March 1955, pp 87-92.

74. ARDITI M. "Characteristics and applications of microstrip for microwave wiring" IRE Trans. Microwave Theory Tech., vol.MTT-3, no.2, March 1955, pp 31-56.

75. STEPHENSON I.M., EASTER B. "Resonant techniques for establishing the equivalent circuits of small discontinuities in microstrip" Electron.Lett., vol.7, no.19, 23 September 1971, pp 582-584.

76. NALBANDIAN V., STEENAART W. "Discontinuities in symmetric striplines due to impedance steps and their compensations" IEEE Trans. Microwave Theory Tech., vol.MTT-20, no.9, September 1972, pp 573-578.

77. WOLFF I., KOMPA G., MEHRAN R. "Calculation method for microstrip discontinuities and T-junctions" Electron.Lett. vol.8, no.7, 6 April 1972, pp 177-179.

78. COHN S.B. "Slotline - an alternative transmission medium for integrated circuits" 1968 IEEE G-MTT International microwave Symposium Digest, pp 104-109.

79. MARIANI E.A., HEINZMAN C.P., AGRIOS J.P., COHN S.B. "Slot line characteristics" IEEE Trans. Microwave Theory Tech., vol.MTT-17, no.12, December 1969, pp 1091-1096.

80. ITOH T., MITTRA R. "Dispersion characteristics of slot lines" Electron.Lett., vol.7, no.13, 1 July 1971, pp 364-365.

81. QURESHI M.S., NICHOLS K.G. "A laser machining system for making integrated circuit masks" Radio and Electronic Engineer, vol.40, no.5, November 1970, pp 233-240.

82. DURNEY C.H., JOHNSON C.C. "Introduction to modern electromagnetics" McGraw-Hill, New York 1969.

12. APPENDIX

12.1 Microstrip Circuit Manufacture

Cleanliness is important in the manufacture of microstrip, and after evaporation all operations on the substrate except plating are performed in clean-air cabinets.

The substrates are first degreased and washed ultrasonically. Mechanical abrasion of alumina substrates is to be avoided since it degrades adhesion to the surface. The substrates are transferred to a vacuum set where nichrome is evaporated to a resistivity of 200 ohms/square with the substrates at 320^{o}C; the temperature is dropped to 120^{o}C, and nichrome and gold are deposited simultaneously for 30 seconds, after which the nichrome is phased out; gold deposition is continued until the resistivity is down to < 2 ohms/square (measured on a separate glass monitor strip). Both sides are coated in this way. At the next stage the top of the substrate (distinguished on alumina by its superior surface finish) is coated with negative photoresist (KPR2) on a spinner; after drying and baking the substrate is placed in a jig in contact with a positive glass photomaster and exposed; development and, if required, dyeing follow. The substrate is now plated, when the whole of the underside and the unprotected areas on top of the substrate become plated-up. A neutral gold cyanide solution is used with a platinised titanium anode; the temperature is maintained at 63^{o}C and the solution stirred mechanically. After plating the negative resist is removed, and a second, positive, resist stage (Shipley AZ1350) is used to protect the plated-up conductors while unwanted

metal is etched away (with potassium iodide for the gold and ceric sulphate for the nichrome). Removal of the positive resist and a final wash complete the process.

12.1.1 Photomaster Preparation

Glass photographic plates make the most suitable photomasters, being convenient to handle and stable with temperature and humidity changes. The plates require to be of high definition and good contrast; those used were Agfa 10E56, 90 x 120 mm, with a resolution of 1000 lines/mm. Three methods have been used in their preparation:

(i) reduction from a large scale taped-up original

(ii) reduction from a large scale cut'n'strip original

(iii) direct use, or enlargement, of a laser-cut mask.

A taped-up original takes the form of opaque, precision width adhesive tapes laid on a transparent film, and is suitable for most linear structures. For circular structures cut'n'strip has been used; it is found to be more suitable than the related scribing methods since it allows large areas of film to be easily removed. Negative cut'n'strip originals usually involve less effort than positive, although both are possible. Taped-up and cut'n'strip originals were reduced by a factor of ten to form the photomaster, using a custom-built reduction camera. At an earlier stage, photomasters were prepared using numerically controlled laser machining equipment, which evaporated areas as required on an antimony-coated slide[81]. This method is highly accurate and it was possible to enlarge the mask produced by a factor of three while maintaining the required accuracy of $\pm$ 10μm in linewidth

on the photomaster. The antimony film is fragile, however, and it was necessary to make a contact print of the slide before use. The method was only used for rectilinear structures, although as the beam stepped only 3μm a good approximation to a smooth curve was possible.

12.2 Q factor of an open-circuited microstrip line resonator

An open-circuit termination can be represented as a complex shunt admittance at the end of the line; alternatively the reactive part may be represented as a small additional length of line, $\Delta\ell$, and the admittance is then entirely real. The equivalent circuit of an open-circuited resonator of geometrical length L and attenuation α np.m^{-1} is shown below.

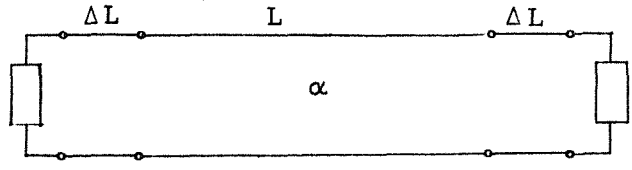

Q factor may be defined as $\frac{\text{energy stored} \cdot \omega}{\text{Average power dissipated}}$ and since this resonator is symmetrical it is sufficient to consider a wave travelling once along the line. TEM propagation is assumed.

If, at one end, the power density incident down the line is P Wm^{-2}, then the power reflected at the other end of the line

$$= P \rho^2 \exp(-2\alpha L') \quad \text{Wm}^{-2} \qquad \text{A2.1}$$

where $L' = L + 2\Delta\ell$, and ρ is the reflection coefficient of the terminating conductance. The energy stored on an ideal TEM line per unit volume $U = \varepsilon E^2$.

But $P = \frac{E^2}{\eta}$, and therefore $U = \frac{P}{v}$ Jm^{-1} where v is the phase velocity. This approximation suffices for the purpose of this derivation.

The power dissipated

$$= \{P - P\rho^2 \exp(-2\alpha L')\}/L' \quad Wm^{-3}$$

Therefore $$Q = \frac{\omega L'}{2v\{1 - \rho^2 \exp(-2\alpha L')\}}$$

$$\simeq \frac{\omega L'}{v\{2\alpha L' - 2\ \ell n\rho\}} \qquad A2.3$$

Hence

$$Q \simeq \frac{\beta L'}{2\alpha L' - 2\ell n\rho} \qquad A2.4$$

12.3 Analysis of discontinuities in microstrip ring resonators

12.3.1 Uniform ring resonator with a single point discontinuity

It is assumed that both the ring and the discontinuity are lossless, and that the loading of the coupling probes is negligible. To the input signal, a ring resonator containing a point discontinuity appears as a semi-infinite transmission line periodically loaded with shunt admittances

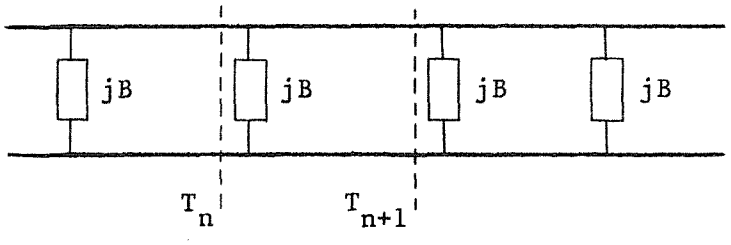

The 'period' of this structure between planes T_n and T_{n+1}, is one revolution of the ring resonator, and can be represented by a two-port network.

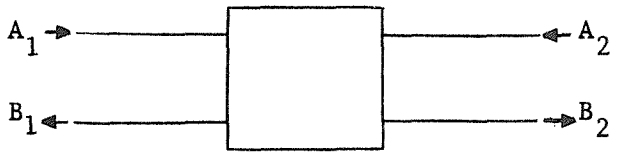

Applying Floquet's theorem for periodic structures to this network gives

$$B_2 = A_1 e^{-j\theta}$$

$$B_1 = A_2 e^{-j\theta}$$

and thus

$$\begin{bmatrix} B_2 \\ A_2 \end{bmatrix} = \begin{bmatrix} e^{-j\theta} & 0 \\ 0 & e^{+j\theta} \end{bmatrix} \begin{bmatrix} A_1 \\ B_1 \end{bmatrix} \qquad \text{A3.1}$$

where θ is the electrical length of the network.

The actual network is (neglecting attenuation) —

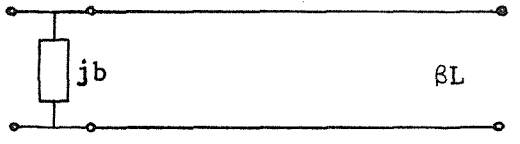

where L is the mean circumference of the ring and b is the normalised susceptance of the discontinuity (B/Y_o). The cascaded matrices for this network can be written down directly, and their product equated to the transfer matrix of equation A3.1

Thus

$$\begin{bmatrix} e^{-j\beta L} & 0 \\ 0 & e^{+j\beta L} \end{bmatrix} \begin{bmatrix} 1-\frac{jb}{2} & -\frac{jb}{2} \\ +\frac{jb}{2} & 1+\frac{jb}{2} \end{bmatrix} = \begin{bmatrix} e^{-j\theta} & 0 \\ 0 & e^{+j\theta} \end{bmatrix} \qquad \text{A3.2}$$

Multiplying out the left hand side and adding the resulting equations gives

$$(1 - \tfrac{jb}{2})e^{-j\beta L} + (1 + \tfrac{jb}{2})e^{+j\beta L} = e^{-j\theta} + e^{+j\theta}$$

$$\cos\beta L - \frac{b}{2}\sin\beta L = \cos\theta \qquad \text{A3.3}$$

For a ring at resonance $\Theta = 2\pi M$ where M is the number of wavelengths on the ring, and thus

$$\cos \beta L - \frac{b}{2} \cdot \sin \beta L = \cos 2\pi M = 1 \qquad \text{A3.4}$$

There are solutions to this equation for two values of β, hereafter denoted as β_1 and β_2.

One solution, corresponding to the value of an undisturbed ring, is

$$\beta_1 L = \pm 2\pi M \qquad \text{A3.5}$$

The other solution is found by expanding equation A3.4 in terms of the half angles:

$$\cos^2 \frac{\beta_2 L}{2} - \sin^2 \frac{\beta_2 L}{2} - \frac{b}{2} \cdot \left[2 \sin \frac{\beta_2 L}{2} \cos \frac{\beta_2 L}{2} \right] = \sin^2 \frac{\beta_2 L}{2} + \cos^2 \frac{\beta_2 L}{2}$$

which gives $$\tan \frac{\beta_2 L}{2} = -\frac{b}{2} \qquad \text{A3.6}$$

It is now possible to express b in terms of the two resonant frequencies f_1, f_2 corresponding to β_1, β_2. In doing so it is assumed that the phase velocity is the same at frequencies f_1 and f_2. (This is a good approximation, since typically $f_1 - f_2 \simeq 200$ MHz and the phase velocity is only decreasing at 0.3% per GHz).

Thus eliminating L from equations A3.5 and A3.6 gives

$$b = \mp 2 \tan \left(\frac{f_1 - f_2}{f_1} \cdot \pi M \right) \qquad \text{A3.7}$$

$$\simeq \mp 2\pi M \frac{f_1 - f_2}{f_1} \qquad \text{A3.8}$$

$$\text{for } f_1 - f_2 \ll f_1$$

12.3.2 Square ring resonators containing four identical mitred corners

The analysis of this problem is based on the discussion in section 12.3.1. The square ring are in fact periodic over one side of the square, but it is more general to retain one revolution of the ring as the 'period'.

Two distinct situations are possible, depending on the number of wavelengths (M) supported by the ring at resonance: if M is even, standing wave voltage maxima can exist at all four corners together, and the total shunt susceptance in the 'period' is 4b, where b is the normalised susceptance at one corner; if M is odd, voltage maxima can only exist simultaneously at two diagonally opposite corners, and the total shunt susceptance in the period is 2b. Two examples are sketched below.

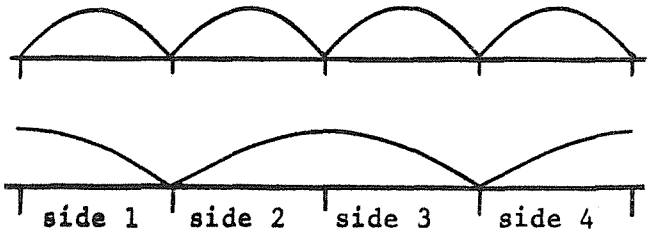

Thus for M even, equation A3.7 becomes

$$4b = 2\tan_{\pi}M \frac{f_1 - f_2}{f_1} \qquad \text{A3.9}$$

and for M odd

$$2b = 2 \tan \pi M \frac{f_1 - f_2}{f_1} \qquad \text{A3.10}$$

In practice only even resonances were measured, and therefore for each pair of resonances

$$b = \frac{1}{2} \tan\left(\pi M \frac{f_1 - f_2}{f_1}\right) \qquad \text{A3.11}$$

If the excess capacitance at the corner, C_x, is small, equation A3.11 becomes

$$\frac{2\pi f_2 C_x}{Y_o} = \frac{\pi M}{2} \cdot \frac{f_1 - f_2}{f_1}$$

and since for TEM propagation $Y_o = vC'$, where C' is the capacitance per unit length of the line, then

$$\frac{C_x}{C'} = \frac{Mv}{4} \cdot \frac{f_1 - f_2}{f_1 f_2} \qquad \text{A3.12}$$

The effective length of one corner, u, (between planes T_2 and T_3 in Figure 46a) is found from equation A3.5 since the length of the ring, L, is equal to $4(S + u)$, where S is the length of one side of the square measured to the inside of the corner.

Thus

$$\left[\frac{2\pi f_1}{v}\right] \cdot 4(S + u) = 2\pi M$$

$$u = \frac{Mv}{4f_1} - S \qquad \text{A3.13}$$

12.3.3 Tapered ring resonator containing an abrupt step in width of the line

The analysis is similar to that discussed in Section 12.3.1. of this appendix.

The equivalent circuit of the structure is

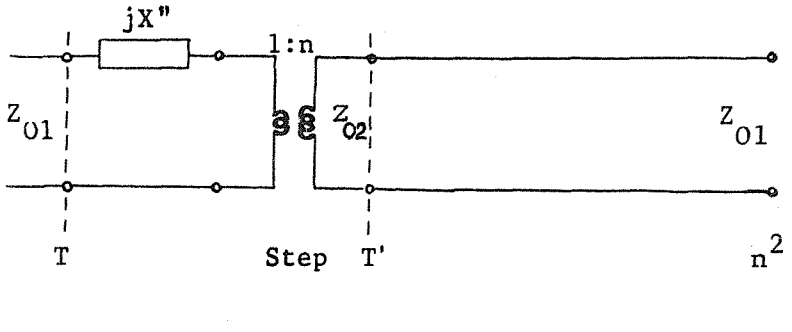

The taper is assumed to provide a reflectionless match from the impedance Z_{0_1} on one side of the step to the impedance Z_{0_2} on the other side of the step, and thus behaves as just a length of transmission line. The reflection coefficient of the taper is given by[82]

$$\Gamma = \frac{j}{4\beta_1 L} \left[\frac{Z_{01} - Z_{02}}{Z_{01}} \right] \cdot \frac{Z_{01}}{Z_{02}} \{ \exp(-2j\beta_1 L) - 1 \} \qquad \text{A3.14}$$

where Z_{0_1}, Z_{0_2} are the characteristic impedances either side of the step, L is the geometrical length of the taper, and β_1 is the phase constant at Z_{0_1}.

If $Z_{0_1} = 50\Omega$ and $Z_{0_2} = 20\Omega$, then $\beta_1/\beta_2 \simeq .92$; it is thus reasonable to assume that β is constant along the length of the taper, and for a typical value of L of 110 mm,

$$\Gamma < 0.01j$$

which is negligible in relation to the reflection coefficient of the step.

As in Section 12.3.1, analysis of the structure is dealt with by writing down the cascaded matrices of the ring, and equating their product to the matrix equation A3.1, which for a ring is equal to the unit matrix.

Thus
$$\begin{bmatrix} 1 - \frac{jX''}{2} & \frac{jX''}{2} \\ -\frac{jX''}{2} & 1+\frac{jX''}{2} \end{bmatrix} \frac{1}{2n} \begin{bmatrix} n^2+1 & n^2-1 \\ n^2-1 & n^2+1 \end{bmatrix} \begin{bmatrix} e^{-j\beta L} & 0 \\ 0 & e^{+j\beta L} \end{bmatrix} = \begin{bmatrix} e^{-j\theta} & 0 \\ 0 & e^{+j\theta} \end{bmatrix}$$

$$= \begin{bmatrix} 1 & 0 \\ 0 & 1 \end{bmatrix} \quad \text{since } \theta = 2M\pi$$

giving $(1 + n^2)\cos\beta L - X'' \sin\beta L = 2n$ A3.15

where $n^2 = Z_{0_2}/Z_{0_1} > 1$ and $X'' = X/Z_{0_1}$ is the normalised reactance of the step.

The two measured resonant frequencies of the ring represent solutions of this equation. For the cosine form of standing wave with a voltage antinode at the plane of the step the reactance is ineffective (i.e. X=0), and the solution to equation A3.15 is

$$\cos \beta_1 L = \frac{2n}{(1 + n^2)} \qquad \text{A3.16}$$

Denoting the resonant frequency corresponding to this solution as f_1, it is found that

$$L = \left[2\pi M \pm \cos^{-1} \left(\frac{2n}{1 + n^2} \right) \right] \cdot \frac{v_p}{2\pi f_1} \qquad \text{A3.17}$$

Selecting the positive sign in A3.17, and using this equation to solve equation A3.15 for X" gives

$$X'' = \frac{(1 + n^2) - 2n}{2 \tan \phi} - \left[\frac{(1 + n^2) + 2n}{2}\right] . \tan \phi \qquad \text{A3.18}$$

$$\phi = \frac{1}{2} \cdot \frac{f_2}{f_1} \cdot \left[2\pi M + \cos^{-1} \left(\frac{2n}{1 + n^2}\right)\right]$$

where $f_2 (< f_1)$ is the second resonant frequency on the ring.